ABSTRACT

ALMOUSA, NOUF MOUSA A. Modeling Electrothermal Plasma with Boundary Layer Effects. (Under the direction of Dr. Mohamed Bourham and Dr. John Gilligan.)

Electrothermal plasma sources produce high-density (10^{23}-10^{28} /m^3) and high temperature (1-5 eV) plasmas that are of interest for a variety of applications such as hypervelocity launch devices, fusion reactor pellet injectors, and pulsed thrusters for small satellites. Also, the high heat flux (up to 100 GW/m^2) and high pressure (100s MPa) of electrothermal (ET) plasmas allow for the use of such facilities as a source of high heat flux to simulate off-normal events in Tokamak fusion reactors. Off-normal events like disruptions, thermal and current quenches, are the perfect recipes for damage of plasma facing components (PFC). Successful operation of a fusion reactor requires comprehensive understanding of material erosion behavior. The extremely high heat fluxes deposited in PFCs melt and evaporate or directly sublime the exposed surfaces, which results in a thick vapor/melt boundary layer adjacent to the solid wall structure. The accumulating boundary layers provide a self-protecting nature by attenuating the radiant energy transport to the PFCs. The ultimate goal of this study is to develop a reliable tool to adequately simulate the effect of the boundary layers on the formation and flow of the energetic ET plasma and its impact on exposed surfaces erosion under disruption like conditions.

This dissertation is a series of published journals/conferences papers. The first paper verified the existence of the vapor shield that evolved at the boundary layer under the typical operational conditions of the NC State University ET plasma facilities PIPE and SIRENS. Upon the verification of the vapor shield, the second paper proposed novel model to simulate the evolution of the boundary layer and its effectiveness in providing a self-protecting nature for the exposed plasma facing surfaces. The developed models simulate the radiant heat flux

attenuation through an optically thick boundary layer. The models were validated by comparing the simulation results to experimental data taken from the ET plasma facilities. Upon validation of the boundary layer models, computational experiments were conducted with the purpose of evaluation the PFCs' erosion during plasma disruption in Tokamak fusion reactors. Erosion of a set of selected low-Z and high-Z materials were analyzed and discussed. For metallic plasma facing materials under the impact of hard and long time-scale disruption events, melting and melt-layer splashing become dominate erosion mechanisms during plasma-material interaction. In order to realistically assess the erosion of the metallic fusion reactor components, the fourth paper accounts for the various mechanisms by which material evolved from PFCs due to melting and vaporization, with a developed melting and splattering/splashing model incorporated in the ET plasma code. Also, the shielding effect associated with melt-layer and vapor-layer is investigated.

The quantitative results of material erosion with the boundary layer effects including a vapor layer, melt layer and splashing effects is a new model and an important step towards achieving a better understanding of plasma-material interactions under exposure to such high heat flux conditions.

Modeling Electrothermal Plasma with Boundary Layer Effects

by
Nouf Mousa A AlMousa

A dissertation submitted to the Graduate Faculty of
North Carolina State University
in partial fulfillment of the
requirements for the degree of
Doctor of Philosophy

Nuclear Engineering

Raleigh, North Carolina

2016

APPROVED BY:

Dr. Mohamed Bourham Committee Co-Chair	Dr. John Gilligan Committee Co-Chair
Dr. Sharon Lubkin	Dr. K. Linga Murty

DEDICATION

To my mom Nourah

To my dad Mousa

To my husband Solaiman

To my children Rakan, Reema, Ragad, and Abdullah

To my sisters Nuha, Lamya, May, and Afnan

Who represent the single greatest influence on my life

I dedicate my PhD … and all of my success to you!

BIOGRAPHY

Nouf AlMousa was born on June 10, 1980, in Riyadh, Kingdom of Saudi Arabia where she attended government schools. She received quality education and graduated from high school in 1998. She obtained a Bachelor of Science degree in Physics in 2002 and a Master of Science degree in Plasma Physics in 2007 both with honors from Princess Nourah bint Abdulrahman University in Riyadh. After earning her master's degree, Nouf spent a couple of years teaching at the physics department at Princess Nourah bint Abdulrahman University. In 2010, she entered the nuclear engineering program at North Carolina State University and has been conducting her research on ET plasmas since that time.

ACKNOWLEDGMENTS

In the name of Allah the most gracious, the most merciful.

"And if you should count the favors of Allah you could not enumerate them. Indeed, Allah is forgiving and merciful"

Quran 16:18

All praise and thanks be to my lord "Allah" for all blessings he has given me.

For my great parents … who were always there in every step of my life to guide me to where I am today!

For my wonderful husband …who stood by me and gave me all that I needed to chase my dreams and to make them come true!

For my adorable kids … who given me strength and taught me how to be a better me every single day!

For my beloved sisters … who gave me the ultimate love and support in my ups and downs!

For my teachers … from my caring first grade teacher to my knowledgeable PhD committee members and my PhD dissertation advisors … and for all my teachers in between who taught me and inspired me to dream the most impossible!

Pursuing a PhD is a dream that could not have come true without all these blessings in my life.

In pursuing my PhD, the sincere advice and guidance of my committee have helped to make this a rewarding experience. The effort and the time that Dr. Sharon Lubkin and Dr. K. Linga Murty put into reviewing my work throughout the development of this dissertation are invaluable and appreciated. The scientific guidance and expertise of Dr. John Gilligan

have shaped the theoretical background behind my dissertation. Along this journey, the insightful academic guidance and encouragement I have received from Dr. Mohamed Bourham have shaped my academic and personal expertise. I am deeply grateful for Dr. Mohamed Bourham for all the research skills I have developed during my time at NCSU that will carry me through my academic life.

I am honored to have been supported over the many years to pursue my graduate studies by the Kingdom of Saudi Arabia represented by Princess Nourah bint Abdulrahman University. Now, it is my turn to give back to my beloved country. I am not completely moving back to my home country though, as part of me will always be here. God Bless America, land that I love!

TABLE OF CONTENTS

LIST OF TABLES

LIST OF FIGURES

CHAPTER 1

INTRODUCTION

1.1 Background

Over the past three decades, there has been increasing interest on the subject of electrothermal (ET) plasma sources and their applications in advanced launch systems, space thrusters, fusion reactor fueling, high heat flux sources for materials studies, and several other applications such as deposition and coating techniques [1-7]. Plasma produced by ET capillary source has high densities ($10^{23} - 10^{28}/\mathrm{m}^3$), relatively low temperature ($1 - 5$ eV), high pressure (several MPa), and high velocity (several km/s). The name ET plasma refers to the production of thermal plasma by electric current. Plasma, which is a quasi-neutral gas of charged and neutral particles, is classified as "*thermal*" when its particles are in thermal equilibrium with each other such that the condition for local thermodynamic equilibrium (LTE) is applicable. The thermal plasma can be generated electrically in many ways, some of which are: direct current, alternating current, and radio-frequency discharges. These types of electric discharges are typically confined high current discharges where an internal high current density arc converts the stored electrical energy into the generation of ET plasma. This happens through surface ablation of the capillary due to the arc radiant energy deposited on the inner wall of the capillary [8-12].

In ET plasma source, the mechanism from which the ET plasma is generated is known as an ablation controlled arc (ACA). This type of ACA-driven plasma is known for its high current density ($10\mathrm{s\ of\ kA}/\mathrm{cm}^2$). The high current density corresponds to a high-

temperature arc (10,000s of K°) that ohmically heats and ablates the source wall material which leads to dissociation and ionization, thus forming plasma [8-12].

Figure 1.1 shows a simple description of the basic processes in ACAs. The arc is ignited between the two electrodes in the confined cylindrical capillary. The extended arc can be initiated in the capillary in high vacuum conditions or at atmospheric pressure conditions with a thin wire fuse inserted in the capillary to initiate the arc. The radiant energy from the high-temperature arc is transported to the ablative capillary wall material and ablates the wall. The ablated material accumulates adjacent to the capillary wall, forming a thin boundary layer. The arc radiant energy is high enough to dissociate, excite and ionize the ablated material and forms plasma at a high core temperature. The plasma flows axially through the capillary core and toward the open end where the plasma is allowed to expand and exit the capillary. The continuing energy deposition in the arc by Ohmic heating results in increased radiative heat flux that ablates additional wall material. The continual ablation and the subsequent process feed the plasma at the capillary core, which results in high pressure and high density plasma that balances the flow of the plasma out of the capillary [8-12].

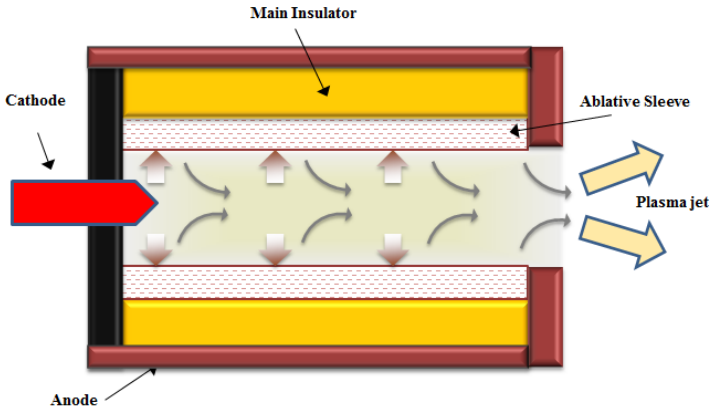

Figure 1.1: A schematic description of the ablation controlled arc in a capillary discharge.

The arc-driven plasma jet is of great interest for different purposes in various types of applications. Continued advances have progressed the applications of arc-driven plasmas for ET launchers, plasma-driven pellet accelerators, satellite thrusters, and electrothermal–chemical launchers [1-16]. Also, due to their extremely high heat flux, ET plasma sources are adequate to simulate high heat flux exposure of the interior components of future fusion large tokamaks reactors during hard disruption [12, 17]. Additionally, ET plasma sources with larger aspect ratios can be used to generate metal and carbon plasma vapors. The exhausted plasma vapors jet at the source exit can be used in material synthesis where the plasma vapor may then interact with controlled gas to produce novel nanomaterials, surface coating with powder injection, and coating from ablated multi-species multi-phase segmented ET plasma source [6, 7, 18-20].

1.2 Literature Review

Since the 1970s, great efforts have been made to study ET plasma sources that work under ACAs. A search of the literature emphasizes the increasing interest of modeling ET

plasma sources due to their subsequent applications in launch technologies. Also, a great deal of interest has been shown in the use of ET plasma sources to study plasma-material interactions (PMI) in fusion devices. This review will cover a wide range of published papers on this topic.

Several theoretical studies appear in the literature on the subject of modeling ACAs in ET plasma sources to determine the parameters of the generated plasma. The determination of the basic plasma parameters has attracted the attention of a group of Russian scientists, Ogurzowa et. al., who have conducted extensive studies on an optically thick pulsed capillary discharge [8, 21]. In their research, Ogurzowa el. al. conducted comparative theoretical studies to evaluate the plasma pressure and temperature based on the magnitude of the discharge current and the capillary geometry. Their studies were based on the single-zone discharge theory where the capillary discharge is fully occupied by a hot core region that radiates as a perfect blackbody towards the capillary wall material. In the single zone discharge, the input joule energy into the capillary is totally dissipated into the ablation process, which is followed by plasma generation. Later, experimental studies by Ogurzowa et. al. revealed discrepancies between the experimental and theoretical plasma core temperatures. An increase of 50% in the plasma core temperature suggests the existence of the boundary-sheath zone that surrounds the hot core region and reradiates a fraction of the black body radiation.

The two-zone discharge theory has been adopted by Ibrahim in his investigations on ACAs [9]. The main purpose of Ibrahim's work is to experimentally and theoretically analyze the ACAs in a capillary discharge. Through his extensive studies he developed an

analytical model and semi-empirical scaling laws to evaluate plasma temperature and pressure based on the current density.

The theory of two-zone discharge was proposed by Ibrahim when he calculated the energy balance between the input Ohmic power and the radiant energy from the equivalent blackbody radiation. An imbalance was reported because the Ohmic power was greater than the radiated power. Findings of Ibrahim's research suggest that a cooler sheath surrounds the hot core and part of the radiated power is absorbed in the developed boundary region [9].

Valuable studies on ACAs in capillary discharge carried out by Ruchti and Niemeyer experimentally proved the existence of a vapor boundary sheath due to photoablation of the capillary wall material [10]. Their experimental data support their proposed model in regards to the cylindrical isothermal arc being separated from the capillary wall material by a vapor shield layer. Ruchti and Niemeyer assumed that the energy is transferred from the arc toward the capillary wall via radiant heat transport. In an attempt to quantify the transmitted energy through the boundary layer, a one-dimensional transparency factor that relates the power flux toward the wall to the total arc power has been defined by [10]. However, a quantification of this factor was difficult due to the presence of multiple physical phenomena that affect the radiative transfer.

The radiant heat transport assumption has also been applied to the analytical model of Loeb and Kaplan [11]. In their model the discharge was divided into two regions, a central optically thick, hot plasma region and a thin, colder peripheral region that surrounds the cylindrical wall surface. However, due to the low sublimation energy of wall material, the power emitted from and into the plasma at the interface between the two regions is equal.

Consequently, radiation losses through the boundary region were negligible, and their model did not consider the boundary layer attenuation effect [11].

The unexplored areas of research related to the nature of energy transport within the boundary layer region drove Bourham and Gilligan to further investigate the fundamental mechanisms during PMI within this boundary region [22-24]. They reported that the main mechanism that dominates the PMI in capillary discharges is the injection of the vapor into the boundary region adjacent to the solid wall. Because this vapor shields the walls from the incoming radiant heat flux, the name vapor shield was coined to describe the crucial role of the evolving boundary layer in limiting surface erosion [22-24].

The authors attempt to measure the influence of the boundary layer by defining a distinguished transmission factor within which the vapor cloud shields the wall. The transmission factor specifies the fraction at which the radiant heat flux is transmitted through the vapor shield to the wall material. As the eroded material was the only indication of the thermal radiation reaching the eroded surfaces, Gilligan and Bourham teamed to carry out a series of experiments on two ET plasma sources, named SIRENS and PIPE designed and constructed at NC State University [22-26]. The collected measured erosion data were compared to the numerical predicted ones with the purpose of determining the exact energy transmission through the vapor shield for each specific material under a definite value of the incident heat flux.

An additional set of experiments were conducted using graphite, insulators, metals, alloys, and specially coated materials, and the energy transmission factor was chosen to get agreement with the experimental erosion data [22-24]. The experimental results suggest that

the net radiant heat flux transmitted through the vapor shield could be reduced by as much as 90% for some insulators and carbon materials.

The first approach Gilligan and Bourham tried towards modeling the vapor shield effect was to define the transmission factor as the ratio between the incident radiant heat flux reaching the wall to the total heat flux emitted by the plasma. Continuing on their efforts, the dissertation author (Nouf AlMousa) has applied new models to achieve accurate approaches that look specifically at the thickness of the boundary layer and how it changes with time. The developed models are presented and discussed in Chapter 3 and are applied for the rest of this dissertation.

1.3 NCSU Electrothermal Plasma Sources

NC State University Department of Nuclear Engineering has designed, constructed and operated two ET plasma sources for studying the high-density plasmas, the generation and evolution of plasma as a propelling mechanisms for hypervelocity launches, the use of these devices as high heat flux facilities for surface studies, and the use as an ignition system for solid propellants for the electrothermal-chemical launch applications [3-5, 12, 14, 17, 22-26]. The SIRENS facility was built in 1987 and has fulfilled over 1,200 successful experimental shots. Figure 1.2 shows a schematic of the SIRENS facility, the source, the pulse power system, the high voltage spark gap switch and a picture of the source and the main discharge chamber [22, 23].

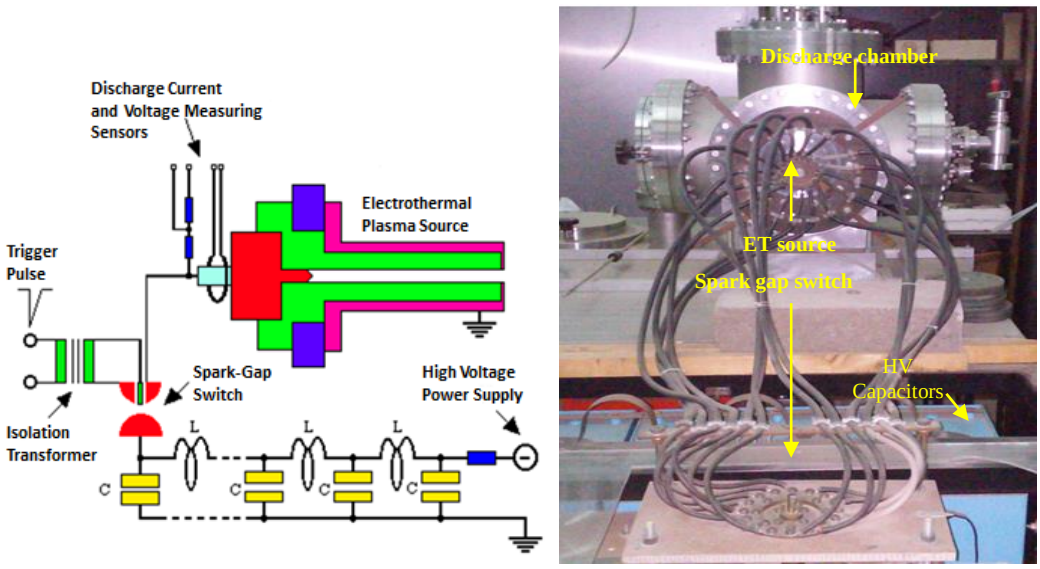

Figure 1.2: Schematic of SIRENS facility and a picture of the source and the chamber.

The second device is the ET plasma source facility PIPE, which was constructed and operated in 1993 to study the plasma-propellant interactions and has successfully completed over 450 experimental shots [25]. PIPE was constructed on the same design features of SIRENS with some modifications in the source and the discharge chamber. Figure 1.3 illustrates a schematic drawing of PIPE showing the source, the current and voltage monitors, the discharge chamber and the material target (metals, insulators or solid propellants). The external electric pulse power system is used to power the ET plasma source using a pulse forming network (PFN) composed of a Maxwell 340 μF high energy density capacitor connected to a transmission line to provide a pulse length 100-400 μs. The capacitor can store electric energy up to 17 kJ at 10 kV charging voltage, and can, therefore, deliver up to 100 kA current pulse. A Pearson coil is used to measure the discharge current, and a

compensated capacitively-coupled HV probe measures the discharge voltage. Figure 1.4 shows a picture of the PIPE facility with its components.

Experiments conducted on PIPE have been used in this dissertation to accurately validate the developed theoretical models. In addition, experimental data have been compared with data obtained from different numerical models to assess the reliability of the vapor shielding models and to confirm the hypotheses behind these models.

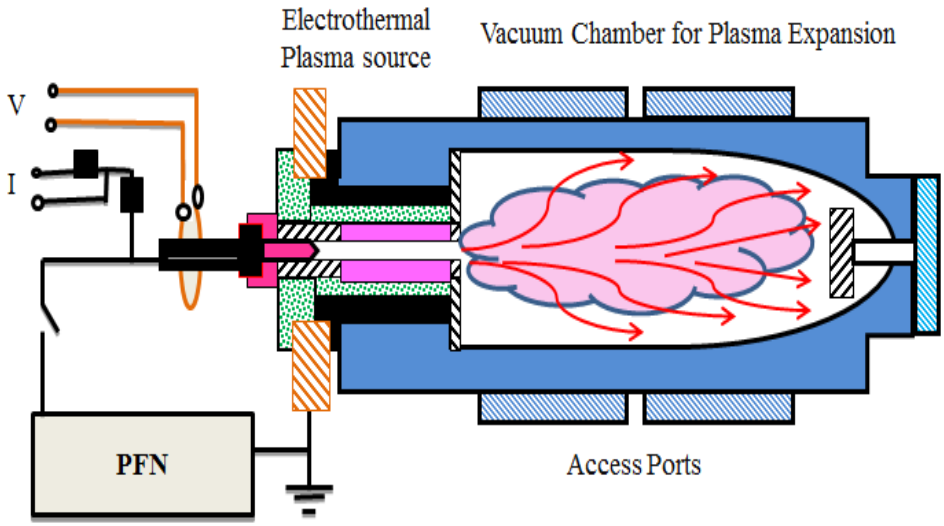

Figure 1.3: A schematic drawing of PIPE facility.

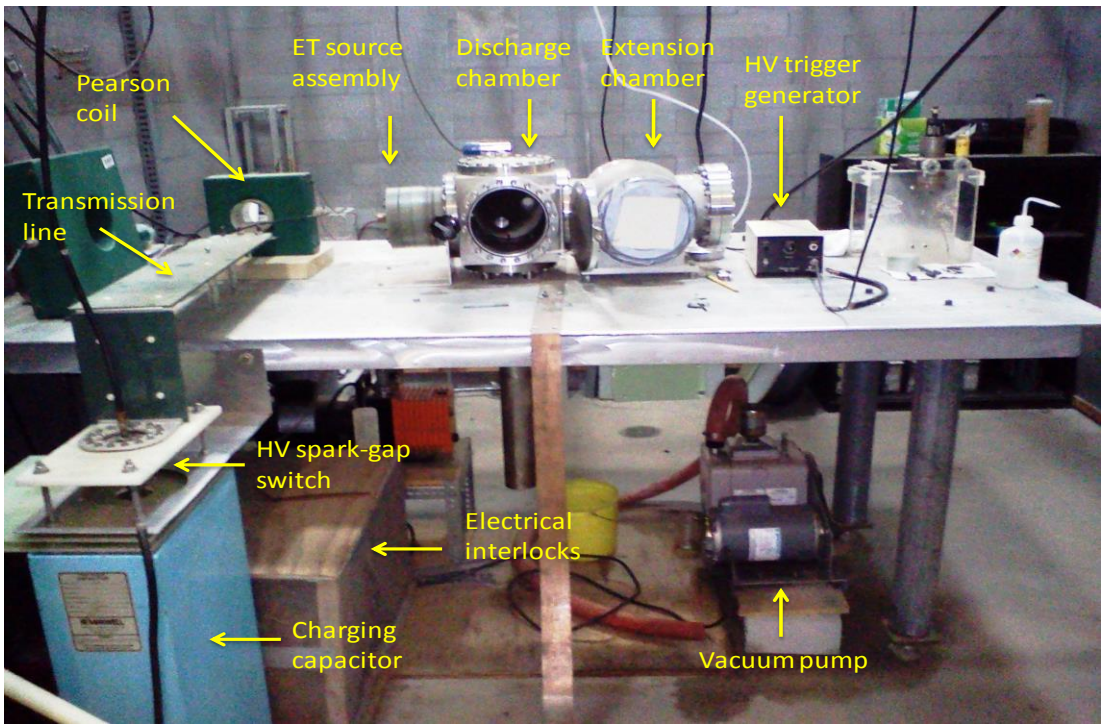

Figure 1.4: A photograph of the PIPE facility.

As shown in Figure 1.5, the ET plasma source section consists of a cathode, Lexan main insulator, and the ablative sleeve. The components are assembled inside a brass outer housing that is connected to the stainless steel expansion chamber and serves as a grounded anode. The ablative sleeve is 9.0 cm long and 2.0 mm inner radius and can be manufactured from any material of interest except adding two small insulating sections at each end if the selected material is metallic. Upon triggering the spark gap switch the arc is initiated inside the sleeve, and its radiant heat flux ablates the wall and forms plasma. The pressure builds up inside the sleeve due to continuous ablation of the wall material during the length of the current pulse and forces the plasma to flow along the sleeve, out of the ET source section, and into the expansion chamber.

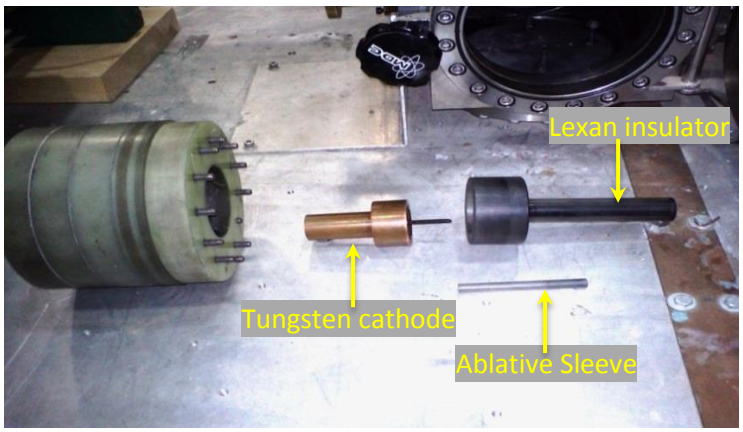

Figure 1.5: The ET source section in PIPE facility.

1.4 Electrothermal Plasma Modeling

Modeling the behavior of ET plasma flow inside the capillary of the ET source section is based upon the fundamental principles that the mass is conserved, Newton's second law of motion is applied, and energy is conserved. Such principles must be applied along with simplifying assumptions in order to derive the basic equations that govern the flow of the plasma fluid. The governing equations that embody these physical principles are the conservation of mass, momentum and energy. Classical assumptions of hydrodynamics along with other assumptions are applied to simplify the governing equations as detailed in various published works [4, 9, 11, 14, 18].

1.4.1 Model Assumptions and Governing Equations

Simplifying assumptions have to be made to model ET plasma with valid approximations. The commonly adopted assumption in the modeling of ET plasma in a

capillary discharge is the one-dimensional coaxial arrangement, which is justified by the small aspect ratio (0.0222) as per the case of R=2.0 mm and L=9.0 cm of the source used in this research. Another key simplifying assumption with respect to the plasma species temperatures and the associated kinetic energy with the plasma species is the condition of LTE, in which the temperatures of electrons and heavy particles (ions and neutrals) are equal. The radiant heat flux from the plasma core is assumed to be transferred in the radial direction towards the capillary wall material while the axial transport of radiation is neglected [14]. The radial radiant heat transport is assumed to be the main energy transfer mechanism that leads to ablation (evaporation/sublimation) of capillary wall material and the generation of the ET plasma [5, 8-11, 14]. It is usually assumed that the ablated wall material is fully dissociated, followed by ionization [8-12]. The generated ET plasma has ions and electrons of nearly equal charge densities throughout the core region and away from the boundary layer. This means that over a large volume of the cell, the plasma is quasi-neutral, and the net charge density is zero. The plasma may deviate from quasi-neutrality over the Debye length λ_d, which has the following numerical value [27]:

$$\lambda_d[m] = 7.434\ X\ 10^3 \left(\frac{\sigma_b T_e[ev]}{n_e[m^{-3}]}\right)^{\frac{1}{2}} \tag{1.1}$$

where σ_b is Stefan-Boltzmann constant, T_e is the temperature of electrons, and n_e is the number density of electrons. However, for ET plasma with electron densities in the range of ($10^{23} - 10^{27}/\mathrm{m}^3$) and temperatures in the range of ($1 - 5$ eV), the characteristic length over which the quasi-neutrality condition is invalid is estimated to range between ($10^{-9} - 10^{-7}$ m), which is much smaller than the scale length of the plasma in the ET source. The

existence of LTE and quasi-neutrality in ET plasma allow the use of single fluid description of the plasma flow which involve the use of particles, momentum, and energy conservation equations. Both ideal and non-ideal plasma models are considered in the present study, as described by previous investigations of ET plasmas [28-30]. The number of particles contained within a sphere of Debye radius, which can be expressed as $N^D = \frac{4}{3}\pi\lambda_D^3 n$, can determine the ideality of the plasma. The number of particles in the Debye sphere is related to the non-ideality parameter Γ by the relationship [27]:

$$N^D = \frac{4}{3}\pi\,\lambda_D^3\,n \;\propto \frac{1}{\Gamma^{3/2}} \tag{1.2}$$

where Γ is given by:

$$\Gamma = \frac{e^2 n^{1/3}}{4\pi\epsilon_\circ T} \tag{1.3}$$

where n $(/\mathrm{m}^3)$ is the number density of the plasma particles. The plasma is considered ideal if $N^D \gg 1$ ($\Gamma \ll 1$), which means the particles are all in the Debye sphere. The plasma tends to behave in a non-ideal way as the plasma parameter increases, meaning fewer particles are screened by the Debye sphere. In general, ET plasmas are cold and dense, which necessitate the consideration of non-ideal treatment of the plasma resistivity [28-30].

The aforementioned physical principles are applied in order to build a model that simulate the moving plasma fluid. In this model, the constant cross section of the cylindrical capillary is divided into a specific number of axial nodes. The governing equations are applied to the plasma fluid inside and through each axial node. The axial nodalization of the

plasma fluid in the capillary is sketched in Figure 1.6. The plasma scalar variables are stored at axial nodes centers, and the plasma fluid velocity is stored at the center of the cell faces.

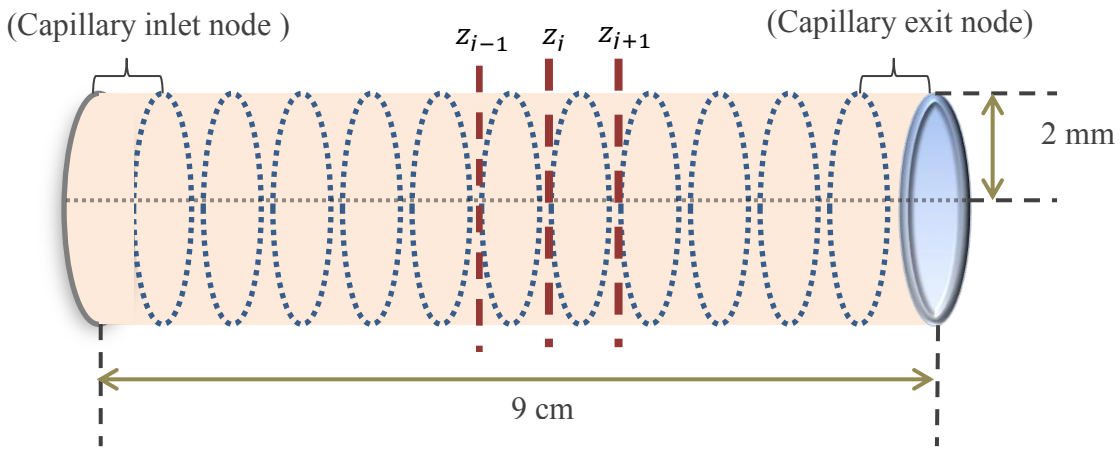

Figure 1.6: The axial nodalization in ETFLOW code.

1.4.1.1. Conservation of Mass

Considering an axial cell of the hollow cylindrical sleeve, the conservation of mass equation represents that the rate of change of particle density is the difference of the rates at which particles flux into the cell and flux out of the cell [14, 20, 30]. The rate of increase of particle density is due to the ablation of the sleeve material. The rate of decrease of particle density is due to the loss of particles as they axially flow out of the cell. Under the above statements, the conservation of mass equation can be easily expressed as the following [14, 30]:

$$\frac{\partial n}{\partial t} = \dot{n}_a - \frac{\partial (nv)}{\partial z} \tag{1.4}$$

where $\dot{n}_a$ $(/\mathrm{m}^3)$ is the time rate of change of the number density of the ablated material entering the plasma from the cell wall, and v $(\mathrm{m/s})$ is the velocity of the plasma. The time rate of ablation of the cell wall material depends on the surface radiation heat flux q''_{rad} $(\mathrm{W/m}^2)$ incident on cell surface of inner radius R (m). The cell material is of a sublimation energy $H_{sub}(\mathrm{J})$ which is the total energy required to dissociate the wall molecules to the constituent plasma atoms of mass A_p $(\mathrm{kg/atom})$. Based on the aforementioned definitions, the rate of ablation can be calculated using [13, 14, 30]:

$$\dot{n}_a = \frac{2q''_{rad}}{R\, H_{sub} A_p} \tag{1.5}$$

where the factor $\frac{2}{R}$ is introduced to $\mathrm{q''_{rad}}$ to transfer from surface into volumetric heat flux q'''_{rad} $(\mathrm{W/m}^3)$. The radiant heat flux is taken from the Stefan-Boltzmann equation for radiation heat transfer $q''_{rad} = \sigma_b \left(T_p^4 - T_v^4\right)$ where T_p is plasma core temperature and T_v is the cell wall surface temperature. Due to the development of the fairly thin boundary layer, a factor *f* must be introduced to account for the vapor shielding effect caused by the boundary layer, and hence the radiant heat flux can be written as $q''_{rad} = f\ \sigma_b \left(T_p^4 - T_v^4\right)$.

1.4.1.2. Conservation of Momentum

The motion of the ET plasma as fluid can be described by the mean velocity of all particles in the axial cell. The total momentum of the plasma fluid moving through the axial cell with mean velocity v can be determined by:

$$p_{tot} = m\, n\, v\ = \rho\, v \tag{1.6}$$

where p_{tot} is the total momentum density and ρ is the mass density. For the total momentum to be conserved, the rate of change of momentum within the cell and the momentum flux across the cell should balance any acting forces within each cell.

The rate of momentum density changes due to the fluid acceleration under the influences of Lorentz force is [27]

$$en(\bar{E} + \bar{v} \times \bar{B}) = \sigma\bar{E} + \bar{J} \times \bar{B} \tag{1.7}$$

where e is the electric charge, $\bar{E}$ is the electric field, $\bar{B}$ is the magnetic field, σ is the charge density, and $\bar{J}$ is the current density. The total momentum loss rate due to the exchange of momentum by plasma particles thermal motion across the axial cell boundary is given by:

$$\nabla P = \frac{\partial}{\partial z} P \tag{1.8}$$

where P is the plasma pressure. The momentum equation for the flowing plasma through an axial cell under the influence of the Lorentz force and the scalar pressure gradient can be written as [27]:

$$\rho \frac{d\bar{v}}{dt} = \sigma\bar{E} + \bar{J} \times \bar{B} - \nabla P \tag{1.9}$$

The quasi-neutrality implies that the plasma charge density is $\sigma \sim 0$, so the contribution from the electric field in the momentum equation is negligible. Also the contribution from the magnetic pressure carried by the plasma's self-induced magnetic field is much less than kinetic pressure carried by kinetic energy of plasma particles, which make the remaining Lorentz magnetic force term go away as well [13, 14, 30].

It is conventional to rewrite the acceleration term in the momentum equation in terms of the convective derivative and to write the axial dependence term in the form of axial rate of change of the kinetic energy:

$$\frac{\partial}{\partial t}(\rho v_z) + \frac{\partial}{\partial z}\left(\frac{1}{2}\rho v_z^2\right) = -\frac{\partial P}{\partial z} \tag{1.10}$$

The wall ablated material entering the plasma flow has a pronounced impact on the total momentum. The increased plasma density due to ablation slows down the plasma flow. Also, as the plasma flows through the cell, the viscous drag force decreases the fluid velocity. Accordingly, the time rate of change of plasma momentum must be corrected to account for all momentum loss terms to get the final form [14, 20, 30]:

$$\frac{\partial}{\partial t}(\rho v \quad) = -\frac{\partial P}{\partial z} - \frac{\partial}{\partial z}\left(\frac{1}{2}\rho v^2\right) - \rho v \quad \frac{\dot{n}_a}{n} - \frac{2\tau_\omega}{R} \tag{1.11}$$

where τ_ω is the viscous drag which is given by ($\tau_\omega = \frac{C_f \rho v^2}{2}$) and where C_f is the friction factor to be calculated according to the flow regime of the plasma fluid [14, 20, 30]. Details of the friction factor for various flow regimes in smooth pipes can be found in literature and published work [14, 20, 30-32].

1.4.1.3. Conservation of Energy

The energy equation describes the time rate of change of internal energy U of the plasma fluid moving with a mean velocity v. The change in the total internal energy in each axial cell results from the net heat flux into the cell and the rate of work done on the moving fluid within the cell [14, 20, 30]. The generated/lost heat in each cell is due to the joule

heating Q_{Joule}, thermal radiation Q_{rad}, and thermal conduction $Q_{conduct}$. The ablation of the cell wall material contributes to the net change of internal energy as the cold ablated species entering the plasma lower the total energy [14, 20, 30]. Also, frictional contributions may affect the energy exchange process between the plasma fluid and the ablated material entering the fluid. Finally, the time rate of change of the internal energy in the cell must account for the net internal energy carried by particles entering and leaving the cell.

The final format of the energy conservation equation can be obtained by combining all contributions that lead to gaining/losing internal energy in the moving plasma occupying each cell at time t, obtaining [14, 20, 30]:

$$n\frac{\partial U}{\partial t} = Q_{Joule} - Q_{rad} + Q_{conduct} + Q_{KE} - Q_{cold\ entry} - Q_{cell\ change} - Q_{flow\ work} \quad (1.12)$$

where $Q_{Joule} = \eta J^2$, $Q_{rad} = \frac{2q''}{R}$, $Q_{conduct} = k_e \nabla T$, $Q_{KE} = \frac{1}{2}\dot{\rho}_a v^2$, $Q_{cold\ entry} = \dot{n}_a U$, $Q_{cell\ change} = v\frac{\partial(nU)}{\partial z}$ and $Q_{flow\ work} = P\frac{\partial v}{\partial z}$ as defined in the published work [14, 20, 30], where η is the plasma resistivity and k_e is the electron thermal conductivity.

The internal energy is attributed to energy associated with ionization $\bar{I}$, heat of sublimation, and thermal motion $3kT\left(\frac{1+\bar{Z}}{2}\right)$, and can be expressed as [14, 20, 30]:

$$U = \bar{I} + H_{sub} + 3kT\left(\frac{1+\bar{Z}}{2}\right) \quad (1.13)$$

where $\bar{Z}$ is the average charge state.

The total resistivity of the plasma is due to the collision of electrons with neutrals and ions and, hence, can be calculated from $\eta = \eta_{en} + \eta_{ei}$ [14, 20, 30].

The resistivity due to collisions between electrons and neutrals η_{en} is written as:

$$\eta_{en} = \frac{m_e}{n_e e^2} \langle \frac{2}{3} n_a v_e \bar{Q}_{en} \rangle \tag{1.14}$$

where m_e is electron mass, v_e is the average thermal velocity averaged over a Maxwellian electron distribution, and $\bar{Q}_{en}$is the average momentum cross section. The resistivity due to the strong Coulomb collisions between unlike charged particles can be calculated based on the Coulomb Logarithm $ln(\Lambda)$ from [27]:

$$\eta_{ei} = \frac{38\ Z\ \ ln(\Lambda)}{\alpha_e T^{3/2}} \tag{1.15}$$

and α_e is the correction factor that accounts for electron-electron collisions. The Coulomb Logarithm for an ideal plasma can be best described by the classical Spitzer model which is given by [27]:

$$ln(\Lambda) = ln\left(\frac{1.23 \times 10^7 T^{3/2}}{n^{1/2} \bar{Z}^{3/2}}\right) \tag{1.16}$$

For the non-ideal plasma, the Coulomb logarithm is expressed by an exact analytical model developed by Zaghloul et. al. which has the following formula [33, 34]:

$$ln(\Lambda) = \frac{\pi}{2} sin\left(\frac{3}{2\Lambda}\right)\left[1 - \frac{2}{\pi}\left(Si\left(\frac{3}{2\Lambda}\right) + \frac{Ci\left(\frac{3}{2\Lambda}\right)}{tan\left(\frac{3}{2\Lambda}\right)}\right)\right] \tag{1.17}$$

where Λ in the Coulomb logarithm is the ratio of the Debye length and the the average thermal impact parameter.

1.5 Dissertation Overview

This chapter presented the ET plasma source concept in which the plasma is generated under ACA regime. An overview of possible useful applications of ET plasmas in modern technology was presented. A survey of distinguished studies from the literature that investigate the modeling of ET plasma sources and their use in various applications was overviewed. Schematics of the experimental setup of NC State University ET facilities were illustrated, and their typical operational parameters were discussed. The developed model to numerically simulate the ET plasma source and its history were presented, as well as the model's basic equations and the adopted simplifying assumptions. An overview of the work presented in this dissertation is briefly presented to conclude chapter one.

In the next chapter, Chapter 2, the concepts of vapor shield (VS) formation and the two zones discharges are discussed. A series of experimental shots taken from actual shots conducted on the PIPE facility are analyzed, and the experimental results are compared to predicted data by ETFLOW code [30]. The main purpose is to investigate the effect of the VS on the erosion of Lexan polycarbonate in ET capillary discharge. The analyzed discharge current ranges between 9.4 to 42.8 kA, and corresponding heat flux ranges between 10 to 50 $\mathrm{Gw/m^2}$. The existence of the VS is verified, and the transmission factor is quantified for the material of interest. Also shown in this chapter is the effect of the transmission factor on the eroded mass, the plasma pressure, temperature, velocity, and radiant heat flux.

Chapter 3 presents the developed models that simulate the VS formation and its effect on PMI using a modification to the ETFLOW code [30] and named ETFLOWVS. One of the

discussed VS models is a modified version from the Hurley et. al. model [14] that defines the transmission factor as the ratio between the radiant heat flux at the eroded wall and the total radiant heat flux by the plasma. The other model developed by the author of this dissertation is a novel model that evaluates the transmission factor based on the optical properties of the developed boundary layer. Comparisons between the VS models are presented with more specific attention paid to how the VS models analyze the temporal variation of the transmission factor and its effect on the material erosion.

Chapter 4 presents the use of the ET plasma sources as a simulator to study the VS effect on material response under tokamak disruption conditions expected in future fusion reactors. The modified code presented in chapter 3 is used to investigate the erosion of candidate plasma facing materials (PFMs) under high heat load deposition, taking into consideration the effect of the VS. Numerical results for the temporal evolution of the transmission factor are presented and compared as well for the different PFMs under study. The total eroded mass of the PFMs are calculated for hard disruption conditions with radiant high heat flux of $55\,\mathrm{GW/m^2}$, along with erosion rate and erosion thickness profiles. Comparisons of the erosion parameters for low-Z and high-Z PFMs conclude the chapter.

Chapter 5 deals with the erosive behavior of metallic PFMs with the inclusion of melting, splashing and splattering due to intense high heat flux from tokamak plasma disruption under the effect of ablation/melting boundary layers. The experimental evidence of metallic PFMs melting that was observed in the experiments is shown and discussed in the beginning of the chapter, along with evidence of melt layer splashing and splattering. An additional modification of the ETFLOW is the inclusion of models for melting and splashing.

Numerical predictions of metallic PFMs' erosion are given for multiple heat flux values and disruption conditions. Comparisons of different material erosion due to the individual and combined effects of the vaporization, melting, and melt layer loss are presented at the end of the chapter.

The last chapter, Chapter 6, concludes the dissertation and provides suggestions of research areas that need further improvements and more in depth investigations.

1.6 References

[1] J. Dyvik, J. Herbig, R. Appleton, J. O'Reilly, J. Shin, "Recent Activities in Electro-thermal Chemical Launcher Technologies at BAE Systems", IEEE Transactions on Magetics, vol. 43, pp. 303-307, 2007.

[2] T. Edamitsu and H. Tahara, "Experimental and Numerical Study of an Electrothermal Pulsed Plasma Thruster for Small Satellites", Vacuum, vol. 80, pp. 1223-1228, 2006.

[3] R. W. Kincaid, M. A. Bourham and J. G. Gilligan, "Plasma Gun Pellet Acceleration Modeling and Experiment", Fusion Technology, vol. 30, pp.834-839, 1996.

[4] A. L. Winfrey, M. A. Abd Al-Halim, J. G. Gilligan, A. V. Saveliev and M. A. Bourham, "Modeling of an Ablation-free Electrothermal Plasma Pellet Accelerator", Fusion Science and Technology, vol. 60, pp. 480-485, 2011.

[5] A. Leigh Winfrey, John G. Gilligan and Mohamed A. Bourham, "Computational Study of a Capillary Discharge Pellet Accelerator Concept for Magnetic Fusion Fueling", Journal of Fusion Energy, vol. 32, pp. 227-234, 2013.

[6] E. Ya. Shcolnikov, A. V. Chebotarev, A. E. Ignatovitch, I. L. Kolensky, Yu. A. Kulikov, A. V. Melnik and S.V. Volkov, "Acceleration of Powder Materials in an Electrothermal Launcher", IEEE Transactions on Magnetics, vol. 31, pp. 758-763, 1995.

[7] D. Zolery, Z. Kaplan and J. Ashkenazy, "Analysis of Powder Particle Acceleration and Heating Processes in a Discharge Capillary–Ablative Pipe Device", Plasma Sources Science Technology, vol. 5, pp. 588–601, 1996.

[8] N. N. Ogurzowa, I. V. Podmoshenskii, and P. N. Rogovtsev, "Calculation of the Parameters of an Optically Dense Plasma Obtained by a Discharge with an Evaporating Wall", High Temperature, vol. 9, pp. 430-435, 1971.

[9] E. Z. Ibrahim, "The Ablation Dominated Polymethylmethacrylate Arc", Journal of Physics D: Applied Physics, vol. 13, pp. 2045-2065, 1980.

[10] C. B. Ruchti and L. Niemeyer, "Ablation Controlled Arcs", IEEE Transactions on Plasma Science, vol. 14, pp. 423 -434, 1986.

[11] A. Loeb and Z. Kaplan, "A Theoretical Model for the Physical Processes in the Confined High Pressure Discharges of Electrothermal Launchers", IEEE Transactions on Magnetics, vol. 25, pp. 342–346, 1989.

[12] M. Bourham, J. Gilligan, O. Hankins, W. Eddy, and J. Hurley, "Electrothermal Plasma Source as a High Heat Flux Simulator for Plasma-Facing Components and Launch Technology Studies", Proc. 9th International Conference on High Power Particle Beams (Beams 92), vol. 3, pp. 1979 -1992, Washington, D.C., 25-29 May 1992.

[13] J. D. Powell and A.E. Zielinski, "Capillary Discharge in the Electrothermal Gun," IEEE Transactions on Magnetics, vol. 29, pp. 591–595, 1993.

[14] J. Hurley, M. Bourham, and J. Gilligan, "Numerical Simulation and Experiment of Plasma Flow in the Electrothermal Launcher SIRENS," IEEE Transactions on Magnetics, vol. 31, pp. 616-621, 1995.

[15] G. L. Katulka, W. F. Oberle, G. P. Wren, J. Okamitsu and N. A. Messina, "Pulsed-Power and High Energy Plasma Simulations for Application to Electrothermal-Chemical Guns", IEEE Transactions on Magnetics, vol. 33, pp. 299-304, 1997.

[16] J. Sun, Y. Lv, Y. Wang, and G. Feng, "Simulation and Research of One-Dimensional Coupling Model of Solid Propellant Electrothermal-Chemical Gun," IEEE Transactions on Magnetics, vol. 41, pp. 360-364, 2005.

[17] J. G. Gilligan and M. A. Bourham, "The Use of an Electrothermal Plasma Gun to Simulate the Extremely High Heat Flux Conditions of a Tokamak Disruption", Journal of Fusion Energy, vol. 12, pp.311-316, 1993.

[18] K. Kim and D. R. Peterson, "A Low Aspect Ratio ET Gun for Metal Plasma Vapor Discharge and Ceramic Nanopowder Production", Journal of Mechanical Science and Technology, vol. 22, pp. 1408-1416, 2008.

[19] E. Ya. Shcolnikov, S. P. Maslennikov, N. N. Netchaev, V. N. Nevolin, and L. A. Sukhanova, "Electrothermal Technology of Coating", IEEE Transactions on Magnetics, vol. 39, pp.314-318, 2003.

[20] A. L. Winfrey, "A Numerical Study of the Non-Ideal Behavior, Parameters, and Novel Applications of an Electrothermal Plasma Source", PhD Dissertation, NC State University, Raleigh, NC, December 2010.

[21] N. N. Ogurtsova, I. V. Podmoshenskii and P. N. Rogoytsev, "Calculation of Parameters of Optically Dense Plasma Obtained by Discharge within an Evaporating Wall". High Temperature, vol. 9, pp. 468-474, l971.

[22] J. Gilligan, O. Auciello, M. Bourham, O. Hankins, B. Wehring, D. Hahn, R. Mohanti and J. Stock, "Theoretical and Experimental Studies of the Vapor Shielding Mechanism

for Surfaces Subjected to High Heat Fluxes", Fusion Technology, vol. 15, pp. 522-527, 1989.

[23] M. Bourham, O. Hankins, O. Auciello, J. Stock, B. Wehring, R. Mohanti and J. Gilligan, "Vapor Shielding and Erosion of Surfaces Exposed to High Heat Load in an Electrothermal Accelerator", IEEE Transactions on Plasma Science, vol. 17, pp. 386-391, 1989.

[24] J. Gilligan, M. Bourham, O. Hankins, W. Eddy, J. Hurley and D. Black, "Vapor Shield Protection of Plasma Facing Components Under Incident High Heat Flux", Journal of Nuclear Materials, vol. 196-198, pp. 596-601, 1992.

[25] C. M. Edwards, M. A. Bourham and J. G. Gilligan, "Experimental Studies of the Plasma-Propellant Interface for Electrothermal-Chemical Launchers", IEEE Transactions on Magnetics, vol. 31, pp.404-409, 1995.

[26] G.E. Dale and M.A. Bourham, "Pulse Power System Characterization of the Plasma Interactions with Propellants Experiment (PIPE) Electrothermal Plasma Gun", IEEE Transactions on Plasma Science, vol. 30, pp. 1852-1857, 2002.

[27] F. F. Chen, Introduction to Plasma Physics and Controlled Fusion, vol.1, Plasma Physics, 2nd Ed., Plenum Press, NY, 1984.

[28] M. R. Zaghloul, M. A. Bourham and J. M. Doster, "Semi-analytical modeling and simulation of the evolution and flow of ohmically-heated non-ideal plasmas in electrothermal guns", Journal of Physics D: Applied Physics, vol. 34, pp.772-786, 2001.

[29] M. R. Zaghloul, M. Al-Naiemy and M. A. Bourham, "Measurement of electrical conductivity of weakly non-ideal ,multi-component plasma mixtures generated from dielectric materials", IEEE Transactions on Plasma Science, vol.37, pp.1626-1631, 2009.

[30] A. L. Winfrey, J. G. Gilligan, A. V. Saveliev, M. Abd Al-Halim and M. A. Bourham "A study of plasma parameters in a capillary discharge with calculations using ideal and non-ideal plasma models for comparison with experiment", IEEE Transactions on Plasma Science, vol. 40, pp. 843-852, 2012.

[31] A. J. Ward-Smith, Internal Fluid Flow: The Fluid Dynamics of Flow in Pipes and Ducts. New York: Oxford Univ. Press, 1980.

[32] I. Shames, Mechanics of Fluids, 2nd ed. New York: McGraw Hill, 1982.

[33] M. R. Zaghloul, M. A. Bourham, J. M. Doster and J. D. Powell, "On the average electron-ion momentum transport cross-section in ideal and nonideal plasmas", Physics Letters A, vol. 262/1, pp. 86-89, 1999.

[34] M. R. Zaghloul, M. A. Bourham and J. M. Doster, "Energy-averaged electron-ion momentum transport cross-section in the Born approximation and Debye-Huckel potential: comparison with the cut-off theory", Physics Letters A, vol. 268/4-6, pp.375-381, 2000.

CHAPTER 2

RADIATIVE HEAT TRANSPORT THROUGH VAPOR SHIELD PLASMA

Published in J Nucl Ene Sci Power Gen. Technol. 2014, 3:1, January 2014, Nouf AlMousa, Leigh Winfrey, John Gilligan and Mohamed Bourham, with the title: "Radiative Heat Transport through Vapor Plasma for Fusion Heat Flux Studies and Electrothermal Plasma Sources Applications", DOI: 10.4172/2325-9809.1000116

Abstract

High heat fluxes of up to 100 GW/m^2 and greater over a discharge period of 100 to 1000 μs can be generated from electrothermal (ET) plasma sources from the confined arc discharge. Sources with input energy of 10 kJ in a miniature capillary (2 mm radius and 9 cm length) are capable of producing 88.33 GW/m^2 heat flux inside the capillary; higher heat fluxes can be generated for higher input energies. Such high heat fluxes are adequate to simulate the energy deposition during hard disruptions in future fusion tokamak reactors, which result in erosion and thermal deformation of the surfaces of the critical internal components of the reactor. Calculation of the eroded mass due to intensive transient radiative heat transport to the surfaces is critical in terms of the determination of the performance, durability, and the life time of these components. Short intense high heat flux causes surface melting and vaporization. The vapor boundary layer absorbs a fraction of the incident heat flux, which results in a reduction of overall erosion. The transmitted fraction has a strong dependence on the energy input to the ET source, which is used as a simulator for high heat

flux deposition of plasma facing materials. The ETFLOW code models the plasma formation and calculates the plasma parameters for corresponding values of the transmission factor. Comparing experimental measurements to the computationally calculated mass erosion of the ET source material has verified the partial deposition of the incident heat flux. The energy transmission factor through the vapor boundary layer is found to be between 20% - 60% for discharge currents above 30 kA and between 60% - 80% for less than 30 kA. The time of peak discharge current is set to be the time at which the transmission factor is evaluated.

2.1 Introduction

There has been great interest in the research on the electrothermal (ET) plasma sources over more than two decades due to the various applications of such sources as mass accelerators, space mini-thrusters, propulsions and as high heat flux sources [1-4]. The heat fluxes generated in ET sources can vary from as low as 5 GW/m^2 to as high as 100 GW/m^2 and greater, making such devices excellent simulators to study high heat flux erosion of plasma facing components in fusion tokamak reactors [4, 5].

The ET plasma sources basically produce high density, low temperature plasma mainly by ablation mechanisms in which electrical energy of the discharge generates a confined arc that radiates heat flux to the surrounding wall. The arc discharge is maintained by the discharge current, which continues to heat the plasma by joule heating over the discharge pulse. The radiative heat transport to the wall deposits energy to the surface and initiates boiling and ejection of the ablated mass into the arc channel. The formation of the plasma is at considerably low temperatures in the range of 1-5 eV, while the plasma is very

dense in the range of 1-10 kg/m^3, which makes the plasma radiate as a blackbody or near blackbody [4, 6]. The plasma formation at such high density builds up the plasma kinetic pressure and drives the plasma to travel out of the open end of the source to an expansion chamber. On the whole, the input arc energy is spent on generation of the plasma, ablation of the sleeve material, heating, dissociation, ionization and acceleration of the ablated material. The heat conduction from the plasma to the wall is an important heat transfer mechanism; however, the heat radiation is the dominant heat transfer mechanism.

Energetic plasma particles, ions, electrons and excited atoms strike the inner wall material and deposit their energy, which causes the ablation of the surface. Therefore, high energy density may shorten the life of the wall material if full energy deposition occurs. However, this is not the case and the heat flux does not reach the surface in full due to the shielding mechanism of the vapor cloud that absorbs a fraction of the incident energy. This has been explained in previous work as a vapor shield mechanism to evaluate the performance of plasma facing components in future fusion tokamak reactors and the relevant applications of ET plasma sources [7-14].

The plasma-surface interaction with a dense near blackbody plasma is illustrated in Figure 2.1, especially for disruption events in future tokamak reactors. The heat flux from the plasma impacts the surface once disruption starts followed by surface ablation and formation of a vapor cloud. The heat flux continues to deposit energy; however, the expanding vapor is absorbing a fraction of the incoming energy. The expanding vapor cloud along with ablated particulates further absorbs the incoming energy, and final expansion ends with the end of the disruption event. The surface suffers ablation and possible melting and, therefore, loses

particles. The final thickness of the material is less than pre-exposed material thickness. The surface is not expected to ablate uniformly, and surface morphology will vary significantly over its entire area. The final thickness removal from the surface, Δx, indicated the net erosion after its exposure to the high heat flux.

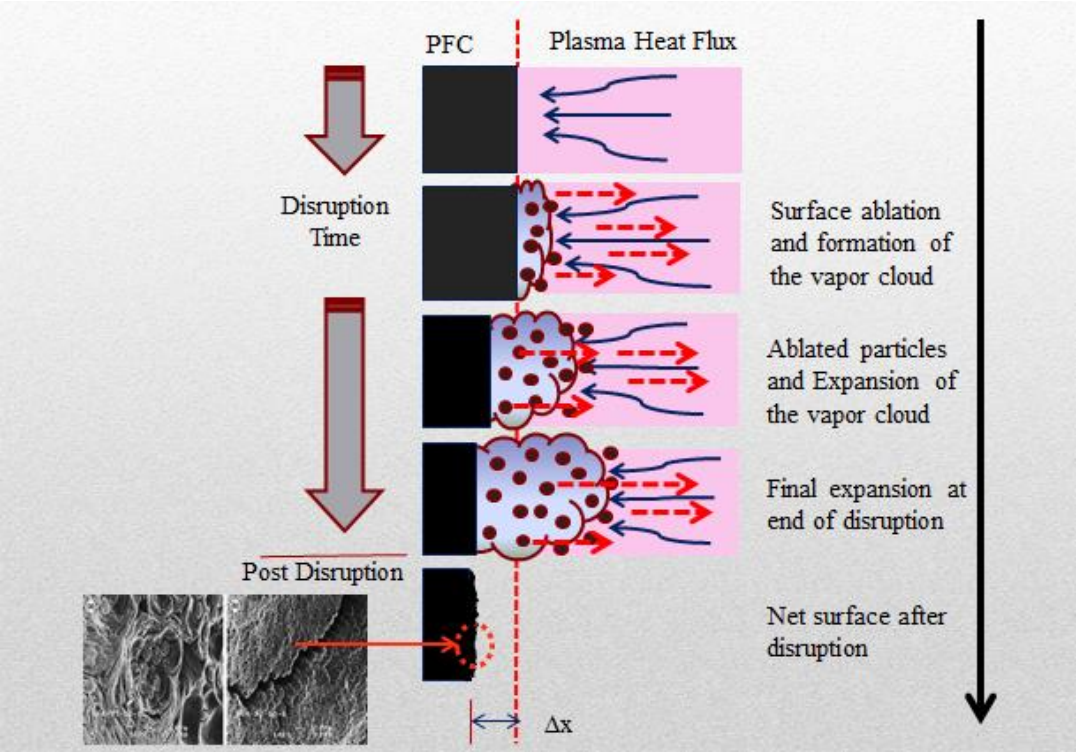

Figure 2.1: Temporal evolution of the plasma-surface interaction showing surface ablation, vapor expansion and the final eroded thickness Δx from the surface.

As ET plasma sources can be used to simulate the high heat flux deposition on plasma facing materials, a better understanding of the plasma parameters in ET plasma sources under various energy transmission fractions is investigated herein. Although there have been a series of theoretical and computational research attempts, the work reported here

forms part of the continuous investigation into high heat flux carried out by ET plasma sources [6-11]. As previously discussed in earlier research, the vapor shield mechanism was suggested to provide a protection to an exposed surface due to the large absorption fraction of the incident energy in the vapor boundary layer [4, 6, 9, 10].

The ablation process of the Lexan insulator as a liner material exposed to high heat flux in an ET plasma source has been analyzed after a series of experiments, and the measured ablation agreed with the theoretical predictions for an energy transmission factor of about 10% through the vapor shield for input discharge energy below 3 kJ. Larger transmission factors were reported in later work on various materials at incident heat fluxes between 2 - 60 GW/m^2 for discharge duration of 100 μs; tested material showed that the transmission factor varies from 10% to 60% and decreases as the heat current increases [4]. In recent work, ETFLOW code calculations were compared to experimentally obtained results of the ablated mass for various heat fluxes measured as total ablated mass versus the peak discharge current of the ET plasma source. These have shown that the ablated mass is in good agreement with code predictions [6]. Interestingly, in the excellent early publication by Ogurtzova et al. in 1971, vapor formation was not considered, and the radiation was an absolute blackbody such that the emissivity integrated over the spectrum was close to unity. However, when their calculations were compared to some experimental work, they noted that the difference was due to the fact that the radiant energy was not an absolute blackbody and the emissivity was less than unity, which was a clear indication of the vapor shield mechanism without using the words ‘vapor shield’ [15]. Several other works considered the formation of the vapor shield layer [4, 6, 7-11, 16-17] and included the melting layer of the

wall material in the analysis. The assumption that part of the incident energy is deposited in the melting phase of the wall material behind the vapor was also considered [9, 10].

2.2 Electrothermal Plasma Theory and Experiments

During a tokamak disruption, much of the thermal energy of the plasma species will be deposited on the plasma facing components, especially on the divertor, resulting in local high heat fluxes that may exceed 100 GW/m^2 over a very short time of 100-1000 μs. The deposition of this high heat flux on the exposed surfaces is sufficient to cause surface ablation and loss of layers of the material's surface. This condition of plasma disruption has been simulated using the NC State University ET plasma facilities PIPE and SIRENS [4, 6-8, 14]. These facilities have been designed to produce high density (10^{23}-10^{27} /m^3) and low temperature (1-5 eV) plasmas generated by ablation of a liner material.

The simulated conditions are closely relevant to expected tokamak disruption conditions; therefore, the use of ET plasma sources serve well as systems adequate to study disruption-like conditions [4]. Plasma facing materials may be selected from carbon materials as tiles on the interior of the vacuum vessel, or beryllium, and metals such as tungsten. It is adequate to select a material with carbon contents to explore the effect of vapor shielding by comparing the computational results to measured values. Many polymers such as Lexan ($C_{16}H_{14}O_3$) have been considered as ablating sleeves in ET capillary plasma sources.

In this study, Lexan ablating sleeves of 9 cm in length and 4 mm in diameter were chosen for computational study for comparison of the results to experimental measurements using a typical Lexan ablator with typical geometry. Figure 2.2 illustrates the general

schematic of the PIPE and SIRENS facilities, in which an ET plasma source is connected to an expansion chamber; it is powered by a pulse power system, and the facility is equipped with diagnostics for discharge current, voltage, and other plasma diagnostics [4]. The open end of the capillary jets the plasma into the expansion chamber at sonic condition, and the plasma is assumed to satisfy local thermodynamic equilibrium state requirements. The data for the PIPE facility is used in this study for comparison with the code calculations.

The capacitor is discharged through the source upon the closing of the spark gap switch. The electrical energy discharged through the source is determined from the difference between the initial and the final capacitor energy $E_{net} = \frac{1}{2} C(V_{initial}^2 - V_{final}^2)$, where C (=340 μF) is the capacitance and $V_{initial}$ and V_{final} are the initial charging voltage and the final residual voltage, respectively. The circuit stray inductance and the energy storage capacitance are input parameters and taken to be 70 nH and 70 μF, respectively. These two parameters will control the length of the pulse generated which range between 100-150 μs as determined by the ETFLOW code [6, 18].

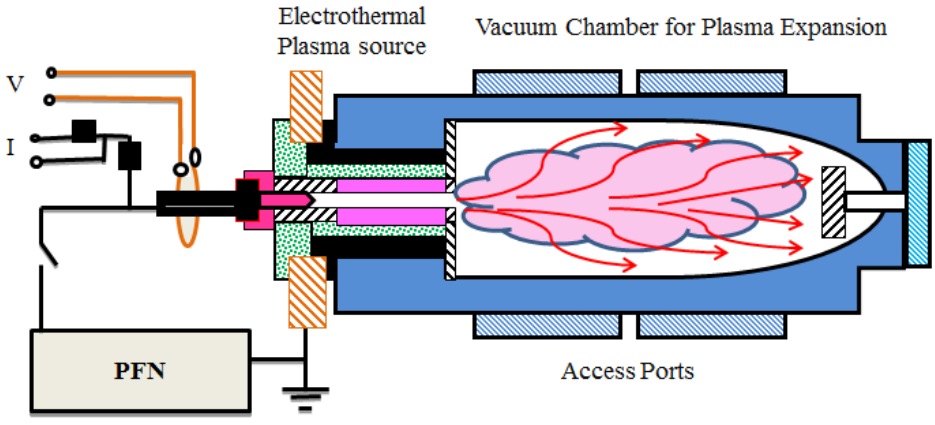

Figure 2.2: Schematic of ET plasma source assembly for PIPE and SIRENS facilities.

Figure 2.3 illustrates the source capillary in which the arc emits radiant energy to the inner wall of the ablating sleeve, followed by ejection of the atoms into the arc channel then dissociation and ionization of the species. The ablating sleeve for each experiment (shot) was weighed before and after the discharge, and the net weight loss was recorded. The discharge current and voltage were measured by a Pearson coil and a capacitively-coupled compensated voltage divider, respectively. The discharge current is the input file to the ETFLOW code, which will calculate the total mass loss for the shot, as well as all other plasma parameters [6].

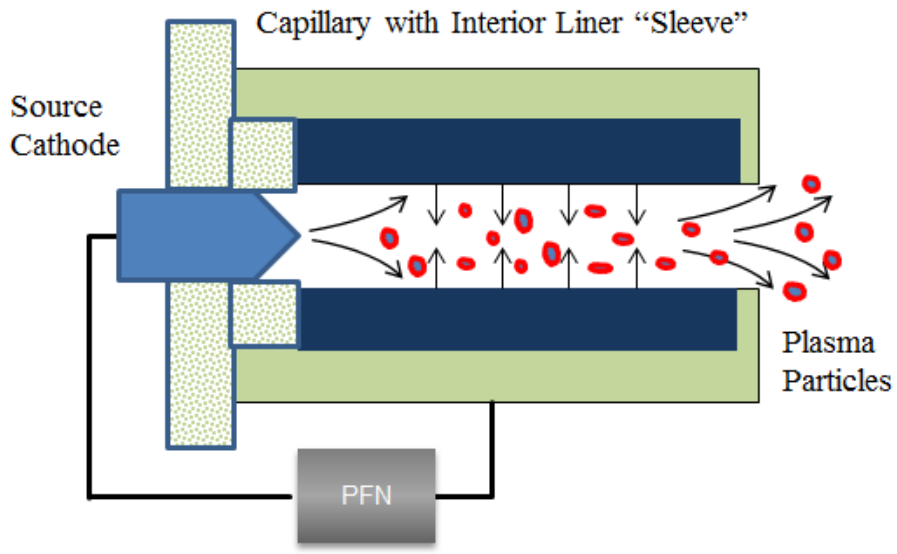

Figure 2.3: Schematic of an arc driven ET plasma source showing the ablation of the wall material.

Signals measured for PIPE shots with input discharge energies ranging between 1-6 kJ provide peak discharge currents that span from 9 kA to 43 kA for a ~100 μs duration. The experiment can operate to deliver 10 kJ input energy into the capillary, thus providing a

maximum of 88.33 GW/m^2 heat flux to the wall. The discharge current increases rapidly after the initiation of the discharge and reaches its peak within ~30 μs. These current traces are used as input in the ETFLOW code in addition to the source geometry and the properties of the ablating material.

Figure 2.4 illustrates the actual shots. It shows peak discharge currents for low and high energy shots and indicates currents as low as ~10 kA and as high as ~45 kA. The experimental mass loss was used in this study to compare to the code calculations. Experimental mass losses are within experimental error of ±10% as a reasonable estimate, though it could rise to ±20% if the ablating sleeve cracks or is forced out of the source for weight measurement.

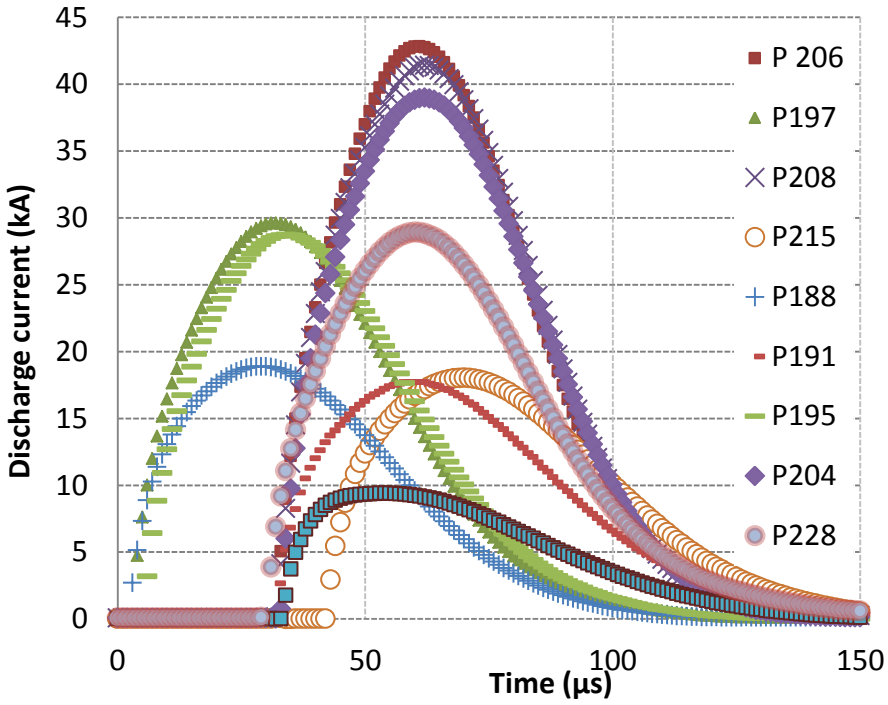

Figure 2.4: Actual discharge currents from experiments performed on the PIPE ET plasma facility.

The heat flux incident on the inner wall of the ablating sleeve during the operation of the PIPE facility for the discharge currents, seen in Figure 2.4, is between 10-50 GW/m^2 , which is spent on the surface melting and ablation of the sleeve material. Nonetheless, if all the incident heat flux is deposited entirely in the sleeve material, extensive ablation of the exposed material surface will extremely shorten its lifetime. However, the actual amount of the ablated material and the corresponding generated plasma parameters will not reflect the full deposition of the incident energy. That is due to the fact that the initial ablated material will form a shielding vapor boundary layer that absorbs part of the incoming heat flux. This was mentioned in the work of Ogurtsova et al [15] when comparing their calculations to experimental data which indicated that the emissivity of the blackbody radiation is less than unity. The radiation heat flux that reaches the wall surface is a fraction of the blackbody radiation emitted from the hot plasma bulk.

Because the vapor shield layer will radiate away some of the deposited energy, the net radiation heat flux $q'' = f\sigma_s(T_P^4 - T_v^4)$ is only a fraction of the difference between the radiation emitted from the plasma core at T_p and the vapor at T_v. The temperature of the vapor shield layer is taken to be the boiling temperature of the ablating sleeve material. The energy transmission factor through the vapor shield boundary layer is given by $f = \rho H_{sub} / \left(P + \rho U + \rho H_{sub}\right)$, where σ_s is the Stefan-Boltzmann constant (5.670 x 10^{-8} W/m^{2}k^4). While the energy transmission factor is a function of the heat of sublimation H_{sub}, plasma internal energy U, plasma pressure P, and ρ is the plasma density [17-22]; however, it has a manual entry into the code such that each code run can be at a selected transmission

factor. The fraction of the energy absorbed by the vapor shield layer is stored as internal energy which causes expansion of the vapor layer against the incoming plasma flux due to the large pressure. Because of their fast development of the vapor layer, the vapor shield for a polycarbonate ablating sleeve is more effective compared with other less ablating materials [4].

2.3 The ETFLOW Code

The system of equations for the ET plasma source is a set of equations that are used to calculate the plasma parameters such as the following: plasma temperature and density, kinetic pressure, plasma velocity, total ablated mass, and plasma conductivity. The ETFLOW is a 1-D, time dependent code that models plasma formation and flow in the ET source and solves the set of the governing equations self-consistently. The code is written in FORTRAN and runs in a VBA environment. An important aspect of the code is its multiple modules including a library of materials, modules that automatically plot the results including axial and temporal graphing, and a module for comparative behavior for different code runs. The basic equations are the conservation of mass, momentum, and energy with the appropriate plasma models and essential plasma equations such as equation of state, ionization, Saha equation, viscosity and electrical conductivity. The set of equations describes the balance of masses, momentum and energy from the formation of the plasma inside the plasma source and through its traveling along the entire length of the plasma source. The details of the governing equations of the ETFLOW code and its developmental history can be found elsewhere [6, 8, 17-20].

In this study, different values of the incident heat flux were incorporated in the ET plasma code (ETFLOW code) by varying the values of the transmission factor f between a minimum of 0.2, this means that 20% of the incident energy reaches the wall, and 80% is absorbed in the vapor boundary layer and its maximum of 1.0, meaning that 100% of the energy is reaching the wall without any absorption in the vapor layer. Code results for Lexan as the ablating sleeve were studied herein at various vapor shielding conditions. A description of the basic equations, continuity, momentum and energy is given here.

The continuity equation is written as:

$$\frac{\partial n}{\partial t} = \dot{n}_{ablation} - \frac{\partial (nv)}{\partial z} \tag{2.1}$$

where $\dot{n}_{ablation}$ is the time rate of change of the number density due to ablation of the material of the inner liner [6, 17].

The momentum equation is written as:

$$\frac{\partial v}{\partial t} = -\frac{1}{\rho}\frac{\partial P}{\partial z} - \frac{1}{2}\frac{\partial v^2}{\partial z} - v\frac{\dot{n}_{ablation}}{n} - \frac{2\tau_w}{\rho R} \tag{2.2}$$

where the first term of the right-hand side of equation (2.2) is the change in velocity due to the axial pressure gradient, the second term is the change in the velocity due to the kinetic energy gradient, the third term is the slowing of the velocity due to the density increase from erosive ablation, and the last term is the velocity loss due to viscous drag along the capillary wall [6, 17].

The energy equation for ablation dominated capillaries is given by:

$$n\frac{\partial U}{\partial t} = \eta J^2 - \frac{2q''}{R} - P\frac{\partial v}{\partial z} + \frac{1}{2}\dot{\rho}_{ablation}v^2 - \dot{n}_{ablation}U - v\frac{\partial (nU)}{\partial z} \tag{2.3}$$

where the first term of the right-hand side of equation (2.3) is the increase in the internal energy due to joule heating and η is the plasma resistivity, the second term is the loss in internal energy due to thermal radiation, the third term is the change in internal energy due to the flow work, the fourth term is the increase in the kinetic energy due to friction from ablation at the wall, the fifth term is the loss in internal energy due to cold ablated material entering the plasma, and the last term is the change in the internal energy due to particles leaving and entering the cell [6, 17].

Details of the complete set of equations, including plasma models for plasma resistivity, friction coefficients, equation of state, viscosity, internal energy, ionization, and Saha equation are given in references 6, 8, 17 and 19. The energy transmission factor is manually entered for each code run to generate the parameters at each selected value, and the code calculations were compared to experimental values to determine the transmission factor. New models are currently under development for the opacity to be coupled to the physics model of the capillary, which will automatically calculate the transmission based on the opacity of the vapor cloud.

2.4 Results and Discussion

A series of experiments have been conducted to study the ablation process of the Lexan polycarbonate ($C_{16}H_{14}O_3$) as an ablating material in a capillary plasma discharge at different discharge energies. The generated plasma was assumed to achieve thermal equilibrium with a homogenous temperature among its ionic species, excited atoms and electrons. For these experiments, the ET source was operated in air at 20 Torr at discharge

energies between 1 to 6 kJ. Discharge currents used in this study are the actual discharge currents of Figure 2.4 to compare the computational results to the measured values of the ablated mass. The solid lines represent the fitted data from the code for the various input currents at each input value of the f factor.

Figure 2.5 illustrates the total mass ablation of the ablative liner sleeve (Lexan) as a function of the peak discharge current. The computationally calculated ablated mass at various values of the vapor shield factor are plotted along with the experimentally obtained ones. The figure shows that the higher the peak discharge current, and hence the higher the input energy, the greater the ablated mass from the sleeve, which is expected as a result of increased heat flux to the ablating surface. The experimental values are with ±10% in magnitude and with a fixed error of ±1 kA in the peak current values. These experimental margins are within the acceptable error ranges for mass loss and peak currents. The mass loss errors account for deviation from the average values including possible errors due to the following: forcing the sample out of the housing insulator, un-recognized micro-breakages and micro-debris lost during the discharge [6]. The fixed error of ±1 kA in the peak current values is due to the flattened peaks. The calculated mass loss for different values of the energy transmission factor is calculated using the ETFLOW capillary plasma code for each corresponding discharge current of the actual experiment.

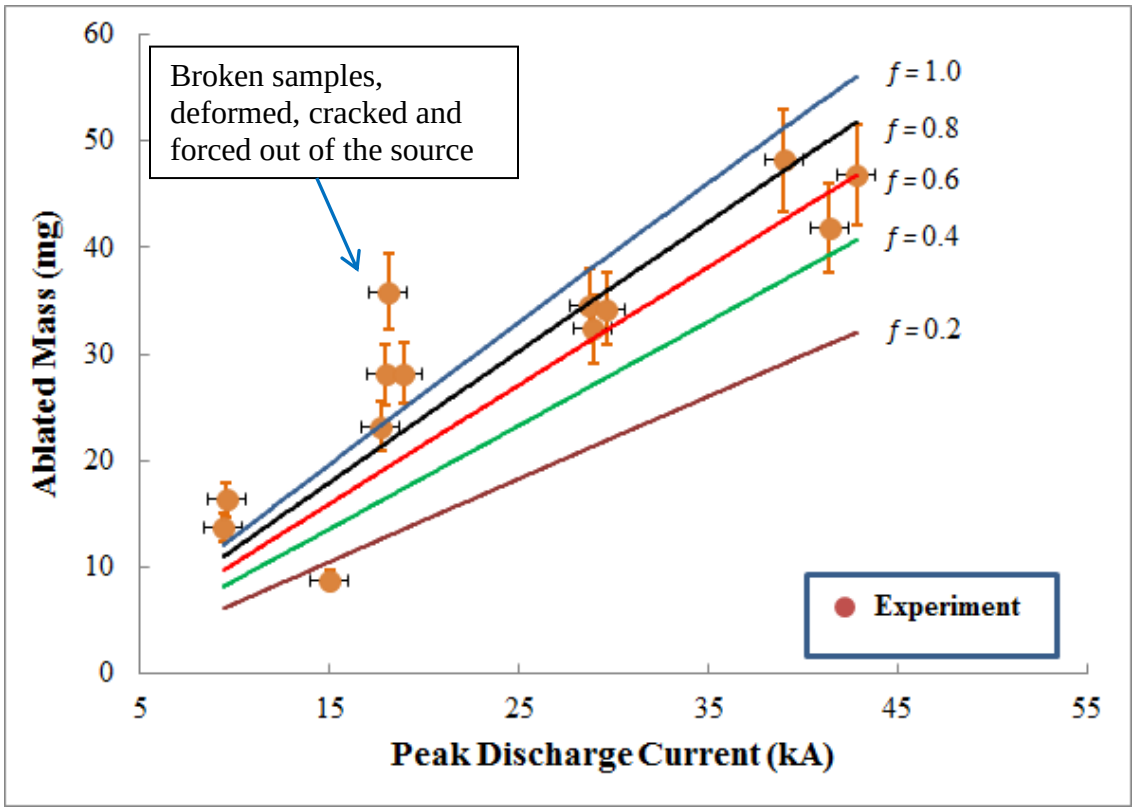

Figure 2.5: Total ablated mass versus peak discharge current showing the experimental values and the calculated mass loss for different values of the vapor shield factor.

The experimental values show that the transmission factor is between f = 0.6 to 0.8 for discharge currents of about 30 kA, indicating that 60-80% of the incident heat flux reaches the surface through the vapor plasma cloud. Therefore, the vapor cloud is optically thick with higher opacity and has absorbed between 20 to 40% of the incident heat flux. At much higher discharge currents above 40 kA, the absorption of the vapor cloud is higher, and the energy transmission factor is between f = 0.4 to 0.8, indicating 20-60% absorption of the incident heat flux into the plasma vapor. At lower peak currents, the transmission factor value tends toward unity, which indicates very low opacity vapor cloud, almost transparent.

The lower current shots may have experienced phase transition instead of direct sublimation, which can be associated with melting and thus increase the amount of mass removal and will not fit with the code results that consider only ablation without melting. The work of Hassanein et al. indicates increased erosion if melting takes place [9, 10]. There was one experimental result below f =0.2 (about f =0.1), but this specific shot suffered from less discharge current into the capillary due to a loop discharge through the main housing that reduced the actual discharge energy. Clearly, the transmission factor is less when the discharge current increases, indicating better effectiveness of the vapor shield at higher incident heat fluxes, which correlates well with previous studies [7-10]. The resulting ablated mass entering the plasma bulk region can be viewed as a supply of plasma density to the plasma initially generated by the arc. As has been shown in Figure 2.5, the thinner the vapor shield layer, the greater the fraction of incident energy that reaches the wall and transfers through the vapor boundary layer. The vapor shield is more effective when the plasma vapor is optically thick and dense such that the absorption of the incident energy is much higher in the vapor cloud, which leaves less energy to reach the wall.

Plasma parameters that were reported in previous work were for the transmission factor of f =1.0, in which all parameters at the capillary exit were reported under the assumption of full energy deposition without the vapor shield effect [6]. The ETFLOW code has been used to re-investigate the exit parameters of the plasma for various values of the transmission factor through the vapor shield. The code results for the peak pressure at the capillary exit as a function of the peak discharge current for different values of the energy transmission factor are illustrated in Figure 2.6. The increase in the peak discharge current

increases the exit pressure for any value of the energy transmission factor through the vapor shield.

When full energy deposition took place, the peak pressure ranged between 0.5×10^8 and 3.8×10^8 Pa for discharge current that peaked between 9.4 and 42.8 kA. However, the increased peak current beyond 40 kA has shown increased effectiveness of the vapor shield and that the energy transmission factor may drop to f =0.4, which in turn reduces the exit pressure to $3.2\text{x}10^8$ Pa, a reduction of about 18% in the exit pressure. If the energy transmission factor drops to a value of f =0.2, the exit pressure would drop by about 30% to $2.7\text{x}10^8$ Pa.

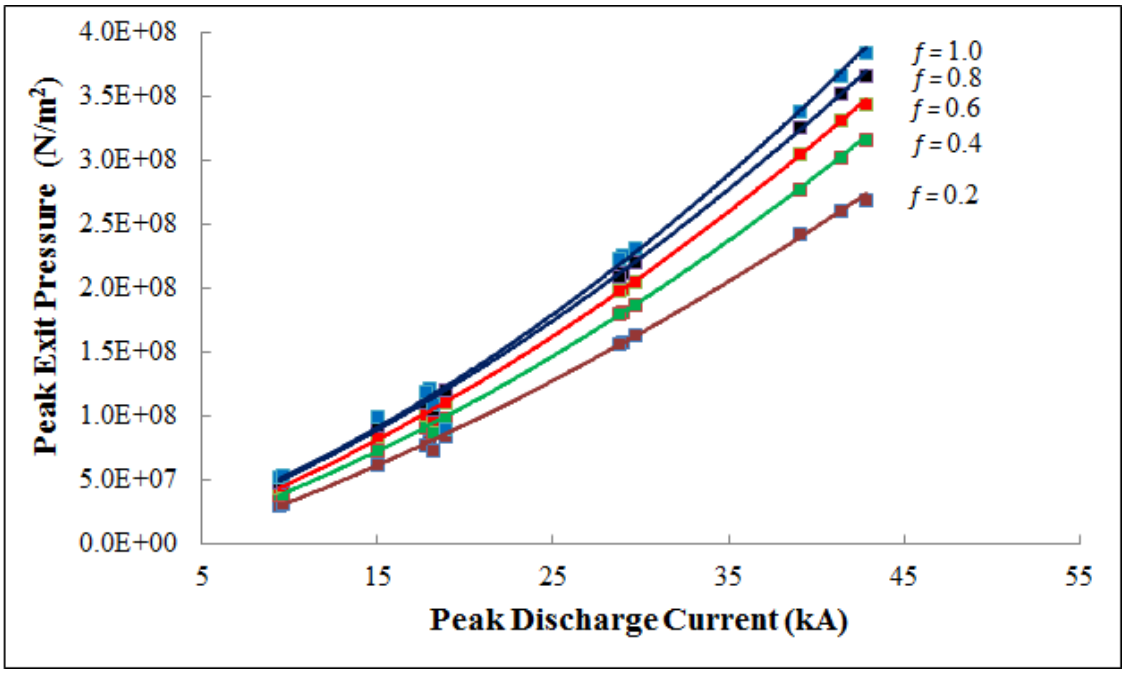

Figure 2.6: Calculated peak plasma pressure at the capillary exit as a function of the peak discharge current for various values of the energy transmission factor.

Figure 2.7 shows the calculated plasma kinetic temperature at the source exit as a function of the peak discharge current. It is clear that the plasma kinetic temperature increases with increased discharge current. The peak plasma temperature at the source exit ranged from 30,926 K (2.66 eV) at a peak discharge current of 42.8 kA and down to 20,195 K (1.74 eV) at a peak discharge current of 9.4 kA when the boundary layer is fully transparent. The peak plasma temperature increases by 12% on average with the vapor shield layer assumed to absorb 40% of the incident energy (if f is set to be 0.6, the dense boundary layer becomes optically thick), and can increase by 30% if the vapor layer expands enough to absorb 80% of the incident heat flux, meaning that most of the heat flux is in the plasma bulk.

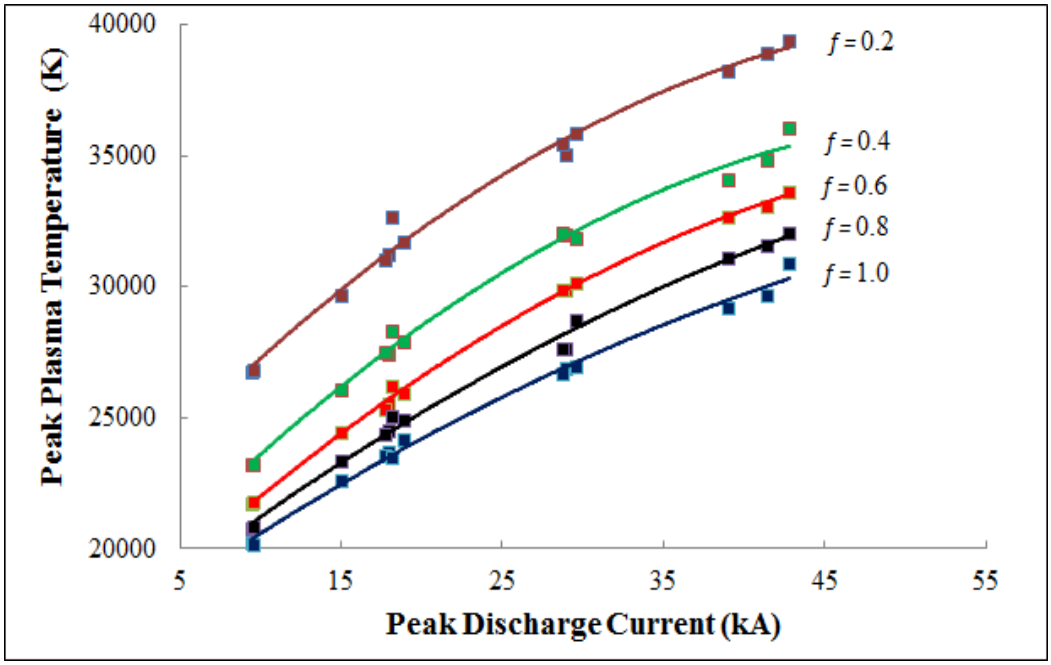

Figure 2.7: Calculated peak plasma temperature at the capillary exit as a function of the peak discharge current for various values of the energy transmission factor.

The radiant heat flux reaching the wall of the inner sleeve is the fraction of the net of the input radiation heat flux from the plasma core and the radiation heat flux emitted out of the thin vapor layer between the plasma core and the ablative capillary wall as given by $q" = f\ \sigma_b\ (T_P^4 - T_v^4)$. In this equation, the full deposition of heat flux to the wall is when the energy transmission factor f =1.0. Figure 2.8 shows the radiant heat flux as a function of the peak discharge current for different values of energy transmission factor. The radiant heat flux at the source exit increases almost linearly with the increase in the magnitude of the peak discharge current and the increase in the energy transmission factor. The radiant heat flux ranged from 9.4 GW/m^2 to 51.5 GW/m^2 for a peak discharge current range between 9.4 kA and 42.8 kA, respectively. The heat flux value calculated by ETFLOW code where f was set to be between 0.2 and 0.6 shows an average of 40% and 20% reduction, respectively, as compared to the case where the vapor layer thickness is zero (fully transparent boundary layer).

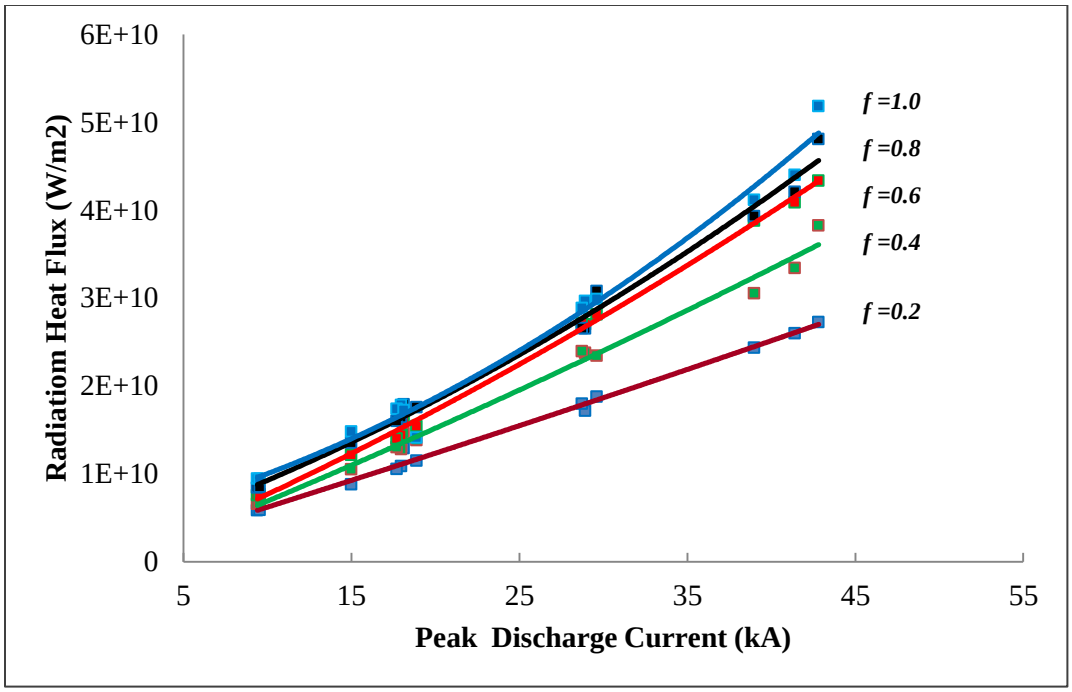

Figure 2.8: Calculated peak radiant heat flux at the capillary exit as a function of the peak discharge current for various values of the energy transmission factor.

The code results for the bulk plasma velocity at the source exit as a function of the peak discharge current is shown in Figure 2.9 in which the exit velocity increases with increased discharge current. The bulk plasma velocity ranged from 4.78 km/s at 9.4 kA to 6.2 km/s at 42.8 kA assuming a full radiation heat flux deposition. For each code run where the energy transmission factor was kept constant so that 40% of the incident heat flux is absorbed by the vapor, it was found that the plasma velocity has only a 5% increase. Further decrease in the transmission factor to about 20% leads to about 15% increase in the plasma exit velocity. The bulk plasma velocity is less sensitive to the change in the efficiency of the vapor shield layer as compared to the other plasma parameters. The increase of the plasma velocity due to the formation of a dense, optically thick vapor layer can be explained by the

lesser effect of the slowing down of the bulk velocity due to less ablated material entering the plasma as stated by momentum equation. It should be noted that the reduction in the velocity while increasing the transmission factors affects the assigning of the Reynolds's number range which determines the drag coefficients and consequently, the plasma flow regime [17].

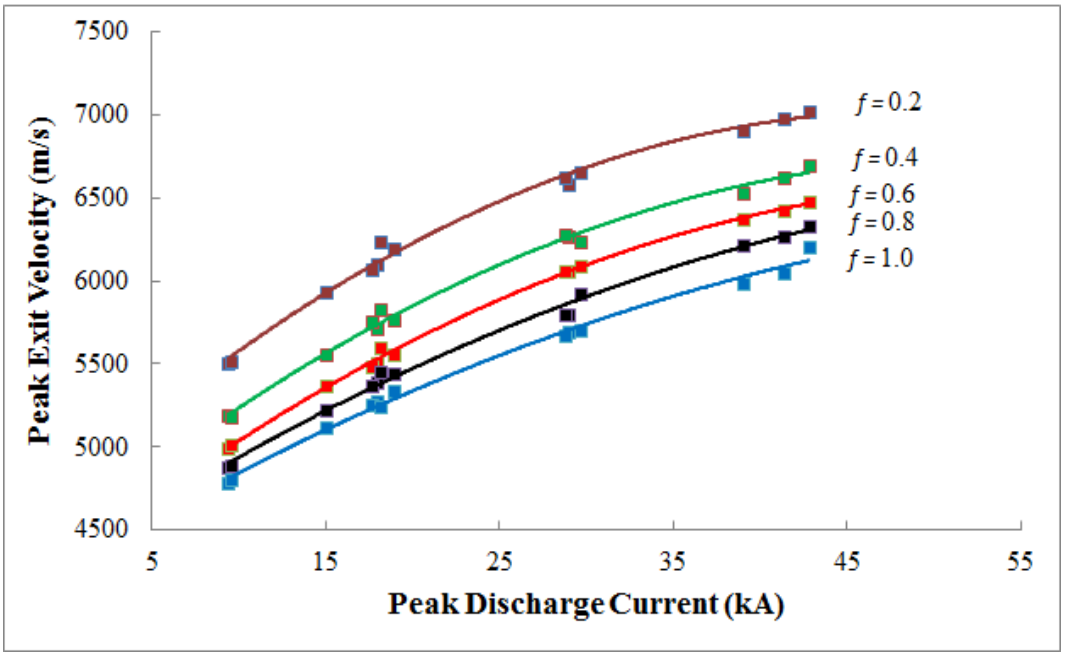

Figure 2.9: Calculated peak bulk plasma velocity at the capillary exit as a function of the peak discharge current for various values of the energy transmission factor.

The ablation velocity is expected to fall with the decreasing energy transmission factor. The ablated material velocity falls from 637.3 m/s to 490.6 m/s if 40% of the incident heat flux is shielded by the vapor at 6.10 kJ input energy. Also, it falls from 439.9 m/s to 347.6 m/s if 80% of the incident heat flux is shielded at 1.09 kJ input energy. The slowing down of the ablation by a factor of 2 may result because of the formation of a vapor shield layer that absorbs 80% of the first wave of the incident energy. Another effect associated

with this result is that if the transmission factor is high enough, the incident heat flux can then melt and ablate more material faster that will diffuse into the plasma bulk [9, 10, 26]. Therefore, the relatively cold entering of the ablated mass will reduce the bulk plasma temperature. This result can explain again the reduction of the plasma temperature with the increase in the energy transmission factor.

2.5 Conclusions

The energy transmission factor has its importance in providing a self-protecting nature when a fraction of the incident energy is absorbed in the vapor layer. This is important for future large tokamak fusion reactors like ITER as a protection against intense heat flux, especially during hard disruptions.

The effect of the boundary vapor layer at the plasma-wall interface in an ET capillary discharge at arc current values between 9.4 to 42.8 kA using Lexan polycarbonate as the ablating liner material has been investigated using ETFLOW code in comparison with experimental results of ablated mass from the PIPE experiment.

The main energy transfer mechanism to the inner wall occurs via radiant energy transport from the near blackbody plasma core. The ablated mass shows that the energy transmission factor is within 0.4 to 0.8 for higher values of the peak discharge currents above 40 kA, which indicates efficient absorption of the incident heat flux into the plasma vapor boundary layer. The dependence of the ablated mass, the plasma pressure, temperature, velocity and radiant heat flux on the variation in the energy transmission factor has been analyzed using various PIPE experimental shots to determine the effectiveness of the vapor

shield layer on these parameters. It has been found that there is a reduction in the plasma temperature and plasma bulk velocity with the increase in the energy transmission factor, while the radiation heat flux, the ablation, and the exit pressure increase as the energy transmission factor increases.

2.6 References

[1] J. Dyvik, J. Herbi, R. Appleton, J. O'Reilly, J. Shin, "Recent Activities in Electro-Thermal Chemical Launcher Technologies at BAE Systems", IEEE Transactions on Magnetics, Vol.43, pp.303–307, January 2007.

[2] T. Edamitsu, H. Tahara, "Experimental and Numerical Study of an Electrothermal Pulsed Plasma Thruster for Small Satellites", Vacuum, Vol. 80, pp. 1223–1228, 2006.

[3] E. Y. Shcolnikov, A. V. Chebotarev, Y. A. Kulikov, A. V. Melnik, and S. V. Volkov, "High Efficiency Electrothermal Accelerator, IEEE Transactions on Magnetics", Vol. 31, pp. 447–451, January 1995.

[4] J. G. Gilligan and M. A Bourham, "The Use of an Electrothermal Plasma Gun to Simulate the Extremely High Heat Flux Conditions of a Tokamak Disruption", Journal of Fusion Energy, Vol. 12, pp.311-316, 1993.

[5] F. Diab, G. M. El-Aragi, G. M. El-Kashef, A. H. Saudy, "Aluminum Surface Analysis After Exposed to Dense Electrothermal Launcher Plasma", Arab Journal of Nuclear Science and Applications, Vol. 46, pp. 204-214, 2013.

[6] A. L. Winfrey, M. A. Abd Al-Halim, J. G. Gilligan, A. V. Saveliev, and M. A. Bourham, "A Study of Plasma Parameters in a Capillary Discharge With Calculations Using Ideal and Nonideal Plasma Models for Comparison With Experiment", IEEE Transactions on Plasma Science, Vol. 40, pp. 843-852, March 2012.

[7] M. Bourham, O. Hankins, O. Auciello, J. Stock, B. Wehring, R. Mohanti, and J. Gilligan, "Vapor Shielding and Erosion of Surfaces Exposed to a High Heat Load in an Electrothermal Accelerator", IEEE Transactions on Plasma Science, Vol. 17, pp. 386-391, June 1989.

[8] M. R. Zaghloul, M. A. Bourham, and J. M. Doster, "Semi-Analytical Modeling and Simulation of the Evolution and Flow of Ohmically-Heated Non-Ideal Plasmas in Electrothermal Guns", Journal of Physics D: Applied Physics, vol. 34, pp. 772–786, March 2001.

[9] A. Hassanein and D. A. Ehst, "Dynamic Modeling of Plasma-Vapor Interactions During Plasma Disruptions", Journal of Nuclear Materials, Vol. 196-198, pp. 679-685, 1992.

[10] A. Hassanein and I. Konkashbaev , "Comprehensive Model for Disruption Erosion in a Reactor Environment", Journal of Nuclear Materials, Vol. 220-222, pp. 244-248, 1995.

[11] S. Jung, D. Andruczyk, D. N. Ruzic, "Laboratory Investigation of Vapor Shielding for Lithium-Coated Molybdenum in Devex", IEEE Transactions on Plasma Science, Vol. 40, pp. 730-734, 2012.

[12] V. Barabash, G. Fediritci, R. Matera, A. R. Raffray, and ITER Home Teams, "Armour Materials for the ITER Plasma Facing Components", Physica Scripta, Vol. T81, PP. 74-83, 1999.

[13] J. M. Linke, T. Hirai, M. Rödig, L. A. Singheiser, "Performance of Plasma-Facing Materials Under Intense Thermal Loads in Tokamaks And Stellarators", Fusion Science and Technology, Vol. 46, pp. 142-151, July 2004.

[14] J. P. Sharpe, B. J. Merrill, D. A. Petti, M. A. Bourham and J. G. Gilligan, "Modeling of Particulate Production in the SIRENS Plasma Disruption Simulator", Journal of Nuclear Materials, Vol. 290-293, pp. 1128-1133, March 2001.

[15] N. N. Ogurtsova, I. V. Podmoshenskii, P. N. Rogoytsev, "Calculation of Parameters of an Optically Dense Plasma Obtained by Discharge Within an Evaporating Wall", High Temperature, Vol. 9, pp. 468-474, 1971.

[16] E. Z. Ibrahim, "The Ablation Dominated Polymethylmethacrylate Arc", Journal of Physics D: Applied Physics, Vol. 13, pp. 2045-2065, November 1980.

[17] J. Hurley, M. Bourham, and J. Gilligan, "Numerical Simulation and Experiment of Plasma Flow in the Electrothermal Launcher SIRENS," IEEE Transactions on Magnetics, Vol. 31, pp. 616–621, January 1995.

[18] A. L. Winfrey, M. A. Abd Al-Halim, A. V. Saveliev, J. G. Gilligan, and M. A. Bourham, "Enhanced Performance of Electrothermal Plasma Sources as Fusion Pellet Injection Drivers and Space Based Mini-Thrusters via Extension of a Flattop Discharge Current", Journal of Fusion Energy, Vol. 32, pp. 371-377, 2013.

[19] J. D. Powell, and A. E. Zielinski, "Capillary Discharge in the Electrothermal Gun", IEEE Transactions on Magnetics, Vol. 29, pp. 591-596, January 1993.

[20] J. G. Gilligan and R. B. Mohanti, "Time-dependent Numerical Simulation of Ablation-Controlled Arcs", IEEE Transactions on Plasma Science, Vol. 18, pp. 190–197, April 1990.

[21] R. B. Mohanti, J. G. Gilligan, and M. A. Bourham, "Time Dependent Simulation of Weakly Nonideal Plasmas in Electrothermal Launchers", Physics of Fluids B: Plasma Physics, Vol. 3, pp. 3046-3052, November 1991.

[22] M. R. Zaghloul, "Improved Modelling of Electrothermal Plasma Source With Radiation Transport", Journal of Physics D: Applied Physics, Vol. 41, pp 1-10 October 2008.

[23] A. Loeb and Z. Kaplan, "A Theoretical Model for the Physical Processes in the Confined High Pressure Discharges of Electrothermal Launchers", Transactions on Magnetics, Vol. 25, pp. 342–346, January 1989.

[24] L. Pekker, "Zero-dimensional Time-dependent Model of High-Pressure Ablative Capillary Discharge for Plasma Thrusters", AIAA Journal of Propulsion Power, Vol. 25, pp. 958–969, August 2009.

[25] K. Kim, "Time-Dependent One-Dimensional Modeling of Pulsed Plasma Discharge in a Capillary Plasma Device", IEEE Transactions on Plasma Science, Vol. 31, pp. 729–735, August 2003.

[26] G. E. Dale and M. A. Bourham, "Melt layer erosion and resolidification of metallic plasma facing components", Proc. 17th IEEE/NPSS Symposium on Fusion Engineering, Vol. 2, pp. 892-895, October 1997.

CHAPTER 3

VAPOR SHIELD MODELS IN HIGH-DENSITY ELECTROTHERMAL PLASMAS AND COMPARISON WITH EXPERIMENTS

Presented in the IEEE ICOPS/Beams, 41st IEEE International Conference on Plasma Science and the 20th International Conference on High-Power Particle Beams, Washington DC, May 25 – 29, 2014, with the title: Vapor Shield Models in Electrothermal Capillary Discharges and Comparison with experiments, Nouf AlMousa and Mohamed Bourham, 2014

Abstract

Radiation transport plays an essential role in electrothermal capillary discharges where the effectiveness of the vapor shield through the evolving ablated layer provides the self-protecting nature and limits surface erosion. Radiant heat flux is the dominant mechanism of energy transfer from the high temperature plasma core to the interior wall of the ablating sleeve inside the capillary. The nature of the flow may tend to be turbulent due to the high velocities (~5km/s) of the generated electrothermal (ET) plasma.

The radiant heat flux incident on the capillary wall is modeled by most researchers as a near-blackbody thermal radiation. However, not all of the incident radiation is transported to the capillary wall due to the development of the vapor cloud that provides the self-shielding mechanism on the plasma boundary layer. Radiation transport through the vapor shield layer has been implemented in this work in the 1-D, time dependent code ETFLOW, which models ET plasma formation and flow in the capillary discharge. In the previous version of ETFLOW, the radiant energy transmission factor (f) through the boundary layer

was set to unity assuming complete energy deposition without any vapor shield effect. Two models of the radiative energy transmission factor were developed and implemented in the code with a switch to run the code with the desired model.

Model 1 treats the radiation transport as it is affected by the variation of the plasma opacity. Based on this model, the evaluation of the vapor shield efficiency depends on the plasma optical thickness and the mean plasma opacity. The optical thickness of the vapor shield is calculated based on the plasma density and thickness. The Rosseland's averaging approximation is used for the calculation of the mean plasma opacity in such ET plasmas. Model 2 defines the *f* factor as the ratio of the energy reaching the capillary wall to the total radiant energy emitted by the plasma. The vapor shielding factor in model 2 is determined by the heat of sublimation, plasma pressure, density, kinetic and internal energies. The code is capable to predict the axial and temporal variation of the transmission factor. Calculations of the transmission factor at each time step and mesh point are used to predict the plasma parameters and the ablated mass with the effectiveness of the vapor shield at the boundary layer. The code predictions, with the implementation of both Models 1 and 2, are used to compare the results with earlier ones and with some experimental data. The inclusion of the vapor shield (VS) modeling produces less deviation from the measured plasma parameters as compared to earlier calculations.

3.1 Introduction

During off-normal events such as hard disruptions in a future tokamak reactor, the plasma facing materials are expected to be exposed to high heat fluxes of up to 100 MJ/m^2

during time scales of 0.1-1 ms. Such high heat fluxes could cause damaging effects due to ablation of the exposed plasma facing surfaces. The exact damage of the exposed surfaces is critical; hence, many theoretical and experimental studies have tested the damage of materials exposed to such high heat fluxes. Material erosion studies can be conducted on laboratory devices that produce a tokomak relevant off-normal heat flux. Examples of devices that generate powerful heat loads are plasma guns, lasers and electron beam facilities [1]. The material erosion data from such experiments show lower ablation rates compared to expected rates under relevant simulated tokamaks off-normal heat flux [2]. For example, data from the VIKA gun experiment predicts ablation rates that are an order of magnitude lower than the estimated values for carbon-based materials in ITER [2]. The decrease in the ablation rate can be explained by the effectiveness of the vapor shield (VS) formation at the plasma-material boundary.

Vapor shielding mechanism results when intense heat fluxes are deposited on solid material surfaces over short heat loading periods, which in turn cause sudden evaporation/sublimation of the exposed material. The continuous evaporation forms a vapor cloud adjacent to the solid surface that expands towards the incoming heat flux, as previously discussed in Chapter 2 and illustrated in Figure 2.1 that shows the temporal evolution of the plasma-surface interaction and formation of the vapor cloud. Hence, the vapor cloud shields the exposed surface from further evaporation by absorbing a fraction of the incoming heat flux.

The exact physics behind the self-shielding mechanism associated with the VS formation have been discussed in many experimental and theoretical studies. In these studies,

modeling was limited to consider the vapor shield as a ratio between the heat flux reaching the surface $q''_{(at\ surface)}$ and the total incoming heat flux $q''_{(from\ plasma\ core)}$ impinging on the surface, $f = q''_{(at\ surface)} / q''_{(from\ plasma\ core)}$, which represents a simple mechanism for vapor shield evaluation [1-5]. The accurate evaluation of the effectiveness of the VS is a key problem in predicting the exact damage of solid materials under the impact of high heat fluxes.

Modeling of the VS effect during plasma material interaction (PMI) with the aim of accurate estimation of material erosion is the goal of this study. The VS is formed under the impact of high plasma density (>>10^{23} /m^3) and low kinetic plasma temperature (<< 100 eV) for the typical range of ET plasmas in confined capillary discharges [1-5]. Such ET plasma is generated using the NCSU ET facilities where the ET source produces fast-raise and intense heat fluxes similar to that expected in off-normal events in future large fusion reactors. These facilities (SIRENS and PIPE) are each composed of an ET plasma source and an expansion chamber. The source section consists of high energy density capacitor, a high-voltage high current spark-gap switch, and a capillary that houses an ablative sleeve. The facilities are equipped with various measuring sensors for discharge current and voltage; detailed description of these facilities are available in the literature [4-7].

In the present work, results from experiments conducted on the PIPE facility are used to compare and validate the proposed VS models. The experiments were carried out using a 340 μF capacitor that delivered between 1-6 kJ of stored energy with discharge currents of 9-43 kA. The corresponding radiant heat flux in these experiments ranges between 10-50 GW/m^2 over a duration of 100-150 μs, which is the same range expected in future large

tokamak fusion reactors. The ablative material used for the capillary lining is a cylindrical tube "sleeve" made of Lexan polycarbonate $[C_{16}H_{14}O_3]_n$, with 9.0 cm in length and 4 mm inner diameter.

The plasma formation within the ET facility and the PMI at the capillary boundaries have been computationally simulated by the ETFLOWVS code, which is a new version of ETFLOW with incorporation of the newly-developed vapor shield models [7]. Since the objective of this study is to investigate the VS formation and its effect on the plasma-facing materials, two different VS models were developed and implemented in the code through different subroutines. The implemented subroutines can run individually, allowing the flexibility of testing the reliability of each VS model.

3.2 Models for Vapor Shielding

As indicated, the first model, Model 1, is based on simulating the radiation transport as it is affected by the variation of the plasma opacity and emissivity. In this model, the calculation of the transmission factor (f) necessitates the evaluation of the VS plasma optical thickness and the mean plasma opacity. For such ET plasma, the Rosseland's averaging approximation is used for the calculation of the mean plasma opacity. The optical thickness of the VS is calculated and has been found to vary with the radiant heat flux and density of the vapor cloud.

The second model, Model 2, defines the transmission factor as the ratio of the energy reaching the capillary wall to the total energy emitted toward the wall by the plasma core. The radiative energy transmission factor is found to be strongly dependent on the plasma

pressure and density, heat of sublimation/evaporation, and the internal energy, and weakly dependent on the plasma kinetic energy.

3.2.1 Vapor Shield Opacity Model "Model 1"

The ideal black body approximation is known to be not accurate enough for modeling kinetic plasma temperatures greater than 1000 K; hence, the near-blackbody, gray body, approximation is adopted in this model. The heat flux emitted by the plasma as gray body is a fraction of the black body radiation depending on plasma emissivity. Therefore, the total heat flux transported to the material surface can be defined as:

$$H_{rad_{gb}} = \varepsilon \; H_{rad_{bb}} \tag{3.1}$$

where ε is the total emissivity coefficient of the plasma that emits as a gray body, $H_{rad_{gb}}$ is the heat flux from the gray body, and $H_{rad_{bb}}$ is the heat flux from black body. The plasma emissivity coefficient is a function of plasma energy, and the values can range between 0 and 1. A new term, defined as plasma absorptivity, which measures the fraction of the energy absorbed by plasma, is required to determine plasma emissivity. The plasma emissivity can be determined by:

$$\varepsilon = 1 - \exp(-\tau_{\omega}) \tag{3.2}$$

where τ_{ω} is the optical thickness of plasma, which is an important radiation transfer parameter that depends on the plasma thickness and the absorption coefficient. The optical thickness can determine how the intensity of radiation will be attenuated as it travels from the surface of the vaporized plasma and along its bath in the vapor shield layer. The plasma is considered optically thin or transparent when the optical thickness is small. For quasi-thermal

transparent plasma, the total emissivity tends to be equal to the optical thickness such that Eq. 3.2 can be re-written as:

$$\varepsilon = \tau_{\omega} \tag{3.3}$$

When the optical thickness is large, the plasma will be optically thick or opaque for radiant heat transport.

ET plasma tends to behave more like a black body with total emissivity increases and tends to be closer to its maximum value due to the nature of such plasma which has high density, is close to local thermodynamic equilibrium (LTE) with isothermal temperature, and has very high optical thickness. This is typical in most ET plasmas where the boundary layer is of higher density compared to the core plasma due to the evolution of additional vaporized mass ablated from the wall surface and forming a thick, dense boundary layer. Consequently, it is suggested in this model that the radiation transport through the boundary layer is an attenuation of the radiant heat flux through an optically thick medium. The mathematical consideration to model radiation attenuation within the optically thick plasma necessitates the evaluation of the optical thickness, which is a function of the characteristic length of the medium and the absorption coefficient.

The characteristic length of the boundary layer, the attenuating medium, can be characterized by the effective beam length (L_{eb}), which is the path length in an isothermal homogeneous medium and results in absorption of radiation equal to absorption by the same medium inside the investigated geometry [8].

In order to accurately determine the effective beam length, a new approach has been developed in this work to relate the effective beam length to the dimension of the region in

which the radiation is attenuated. The width of the boundary layer region can be calculated in the code for each mesh point and each time step based on the density of the optically thick plasma.

On the other hand, the absorption coefficient of the plasma depends on the frequency of multiple absorption processes, which affects the opacity of the plasma. For the aforementioned regime of the investigated ET plasma, the photon absorption mechanisms that take place are the bound-bound, bound-free, and free-free absorption processes. The bound-bound opacity arises when an atom or ion absorbs a photon and becomes excited, causing transition of bound electrons. However, if the absorbed photon has enough energy, the bound electron will be removed, which raises the bound-free opacity. The free-free opacity is mainly due to inverse Bremsstrahlung, which occurs when a photon is absorbed by free electron as it passes by a field of an ion or a neutral atom. Due to the probabilities of all of these attenuation processes, a multi-frequency attenuation coefficient that includes all possible photon absorption processes should be calculated. However, practically during opacity simulation, it is impossible to keep track of all of the attenuation processes' cross sections because they vary in each time step and at each mesh point with plasma state (temperature, density and kinetic pressure) and the geometry of the system.

The complexity of having multiple opacity sources at different possibilities depending on the plasma criteria can be solved by an appropriate averaging of the attenuation coefficient. In other words, this can be achieved by computing a mean opacity that is averaged over all frequencies. The Rosseland mean opacity is the most commonly applied approach to find the mean opacity of optically thick ET plasma that met the LTE condition

[8-10]. The simple expression for one group Rosseland mean opacity (χ_{av}) as a function of the frequency-dependent absorption coefficient (χ_v) can be written as:

$$\frac{1}{\chi_{av}} = \int_0^\infty \frac{1}{\chi_v} G'(u)\, du \tag{3.4}$$

In this expression the mean opacity is weighted by a weighting function $G'(\alpha)$ given by [12]:

$$G'(u) = \frac{15}{4\pi^4} \frac{u^4 e^{-u}}{(1-e^{-u})^2} \tag{3.5}$$

Where the integration variable u is given by:

$$u = \frac{hv}{kT} \tag{3.6}$$

where u is the ratio between the photon energy and thermal energy.

3.2.2 Vapor Shield Energy Ratio Model "Model 2"

A different way to determine the efficiency of the VS is based on the numerical quantification of the transmission factor. In this approach, the transmission factor is determined from the ratio between the two heat fluxes: the heat flux that causes the material erosion (evaporation) to the total heat flux radiated by the plasma core. To determine the heat flux that penetrates the VS layer and causes material erosion, assumptions on the main erosion mechanism should be made. In this case the incident thermal radiation is assumed to be high enough to directly sublime the impacted material, followed by dissociation and ionization. The relationship between the dissociation energy E_D and the sublimation energy (H_{sub}) is expressed in the following form:

$$E_D = m_p H_{sub} \tag{3.7}$$

where m_p is the atomic mass of the constituent atoms. In addition to the sublimation energy, other resources can determine the total energy of the plasma species, the density of the evaporated material (ρ) and the kinetic pressure of the plasma (P). Hence, the transmission factor is calculated according to the previous definition of heat fluxes and can be written as [7-9]:

$$f = \frac{\rho\, H_{sub}}{P + \rho\, H_{sub} + \rho\, U} \tag{3.8}$$

The internal energy is due to the sublimation energy, the ionization potential ($\bar{I}$), and the thermal motion ($1.5\, KT\, (1 + \bar{Z})$), and for ideal plasma can be expressed as [7-10]:

$$U = 1.5\, KT\, (1 + \bar{Z}) + \bar{I} + H_{sub} \tag{3.9}$$

where $\bar{Z}$ is the average charge state.

Additionally, the kinetic energy of plasma species can contribute to the total energy emitted by the plasma bulk, and a modification can be applied to include the kinetic energy in the transmission factor equation, which can be written as:

$$f = \frac{\rho\, H_{sub}}{P + \rho\, H_{sub} + \rho\, U + \frac{1}{2}\, \rho\, v^2} \tag{3.10}$$

It is obvious from Eq. 3.10 that the introduction of the kinetic energy into the denominator of the transmission factor leads to lower energy transmission factor; hence, less heat flux will reach the surface, resulting in a prediction of less ablation. Overall, the decrease of the ratio between the heat flux that reaches the eroding surface to the total incident heat flux from the plasma core indicates better vapor shielding effect with the inclusion of the plasma kinetic energy.

3.3 Results and Discussion

Results from ETFLOWVS code based on the developed VS models are presented in this section. ETFLOWVS code is used to model the behavior of the ET plasma flow as well as the erosion of the plasma facing material with the effect of the vapor shield. For a given ET source geometry and initial discharge parameters, the code calculates the initiation and the flow of the plasma along the axial direction of the source. Thus, the code calculates the plasma temperature, heat flux, density, pressure, ablated mass, and velocity with detailed calculation of the number density of electrons, ions (up to second ionization) and the neutrals at each time step and spatial step. The input discharge current in the code is experimentally measured and taken from the experimental facility PIPE. The detailed composition and the plasma species distribution are determined from a subroutine for solving a linearized Saha equation. Based on the concentrations of the plasma particles, a subroutine for a linearized equation of state is solved to adequately determine the thermodynamic properties of the generated plasma inside the ET source.

The resulting set of linear differential equations with the appropriate boundary conditions is solved using Newton's method of finite difference approximation [11]. The mesh spacing and time step values were chosen to optimize the computational run time and the accuracy of calculations. The bulk plasma parameters are computed for each mesh point at each time step and are manipulated at the next time step to find the solution for new plasma parameters as time progresses.

Figure 3.1 is the same figure previously shown in Chapter 2 (Figure 2.4), which represents the shapes of the discharge current used in this study where all current pulses are

the actual discharge currents recorded from experiments conducted on the facility. Although the code can generate any form of discharge current with any desired peak and pulse length, , it is an advantage to use experimentally measured currents instead of artificially generated current profiles. This choice avoids discrepancy between computational and experimental results that may arise from employing negotiable theoretical models and simplifying assumption that might not perfectly fit the physics of the case study. The selected discharge currents peak between 9-43 kA over a discharge duration of 100-150 μs for a discharge arc voltage range between 1-5 kV. These shots were also validated between the code and the measurements of the total ablated mass; therefore, their selection for the study is adequate and beneficial for the evaluation of the new vapor shield model. The ETFLOWVS code reads the input file of the discharge current and runs the case for the selected sleeve material. The material data in this case study is Lexan polycarbonate ($C_{16}H_{14}O_3$), which is automatically imported with its parameters from the material library that is built in ETFLOWVS code.

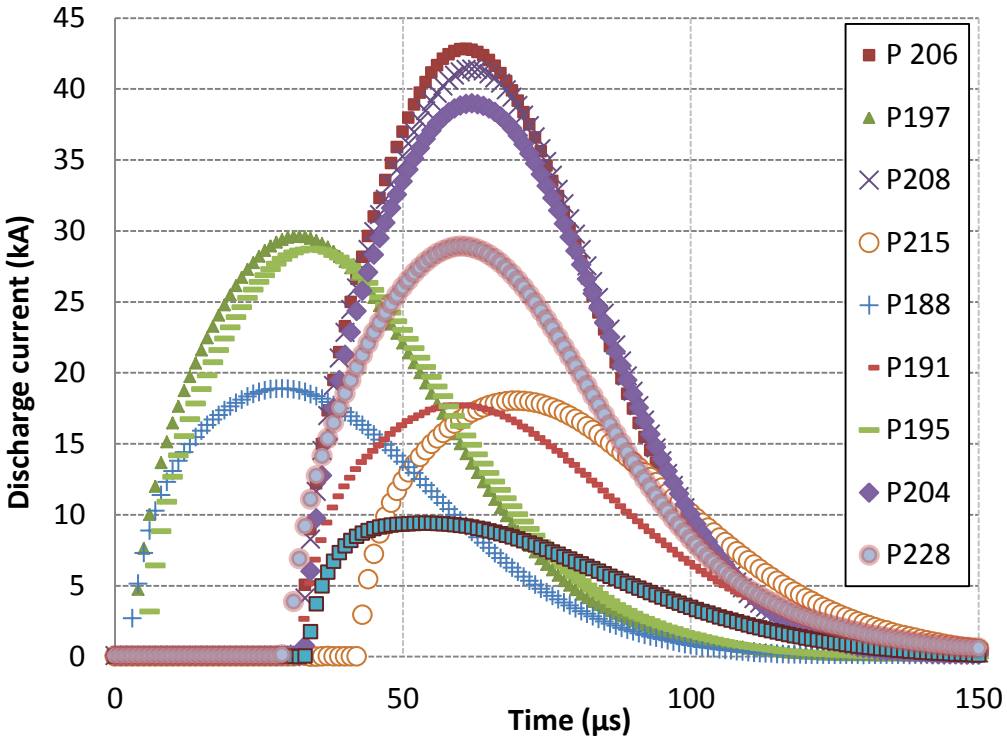

Figure 3.1: Discharge current traces as recorded from shots performed on the PIPE ET plasma facility.

Four test cases have been run using the developed vapor shield models, and the results are compared to the experimentally measured ablated mass as available measured data. The four test cases are cases that used Model 1 "opacity model", Model 2 "ratio model", modified Model 2 "ratio with kinetic energy" and a fully transparent vapor shield where the transmission factor equals unity.

Figure 3.2 shows the measured total ablated mass as a function of the peak discharge current as recorded from the actual PIPE shots. The energy discharged during the shots for this study has been classified to three regimes: low, medium, and high discharge energy. Figure 3.2 shows a comparison between the calculated total ablated mass using various VS

models and the experimentally measured values. There is a strong dependence of the total ablated mass on the magnitude of discharge current because any increase in the discharge current results in an increase in the radiant heat flux from the core plasma regardless of the adopted VS model. The dependence on the peak value of the discharge current follows the same trend for the measured total ablated mass. The non-vapor shield calculations overestimate the total ablated mass compared to the experimentally measured values. This can be explained by the assumption that the entire radiant heat flux from the plasma core is deposited on the exposed surface without any vapor shielding.

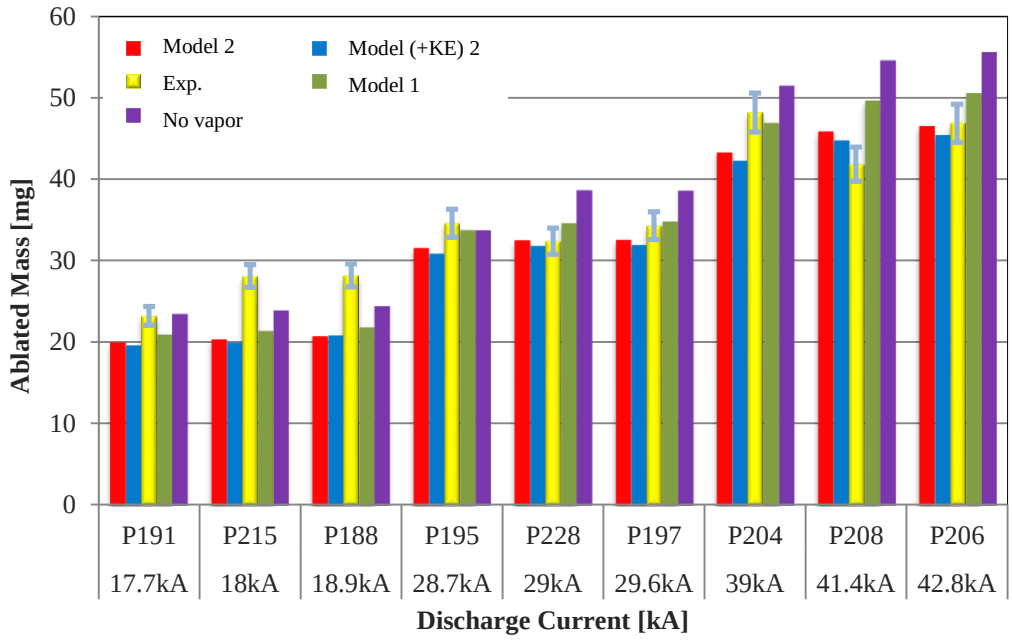

Figure 3.2: Total ablated mass as a function of the peak discharge current.

Increased overestimation is observed towards the higher discharge current range, suggesting that there is an increase in the vapor shield efficiency as the incident radiant heat

flux increases. Furthermore, Figure 3.2 also shows that the total ablated mass calculated by the developed VS models lie within the range set by the margin of error of 10% of the measured ablated mass. However, in the lower current range, both VS models predicted values are lower than the measured ones and fall out of the defined error margin. As previously mentioned in Chapter 2 (Figure 2.5) the off normal behavior of some low energy shots was due to broken, fragmented, cracked and deformed samples and the possibility of forcing the sample outside the source inner tubing. Excluding the low current shots, there is a good agreement between experimental and simulation data by using the developed VS models.

Figure 3.3 shows the code results for the plasma's total density as calculated by the various VS models. The assumption of no vapor shield (f=1) indicates the highest density as it is attributed to the full energy deposition on the surface without vapor shield. The both models show less plasma density as a result of less ablation due to the vapor shield effectiveness. The ratio model with the inclusion of the kinetic energy shows the lowest density, which shows that the plasma density decreases by about 20.5% on average when using this model. The opacity model result falls between the ratio model and the no vapor shield model, with about an 8.5% decrease in the plasma density. It indicates that the opacity is an attenuation effect, as modeled by an exponential decay model, and that the developed boundary layer is determined by the boundary layer thickness. Of importance is that the model assumed a mean opacity that is averaged over all frequencies. From all models, vapor shield provides a self-protecting mechanism to the surface.

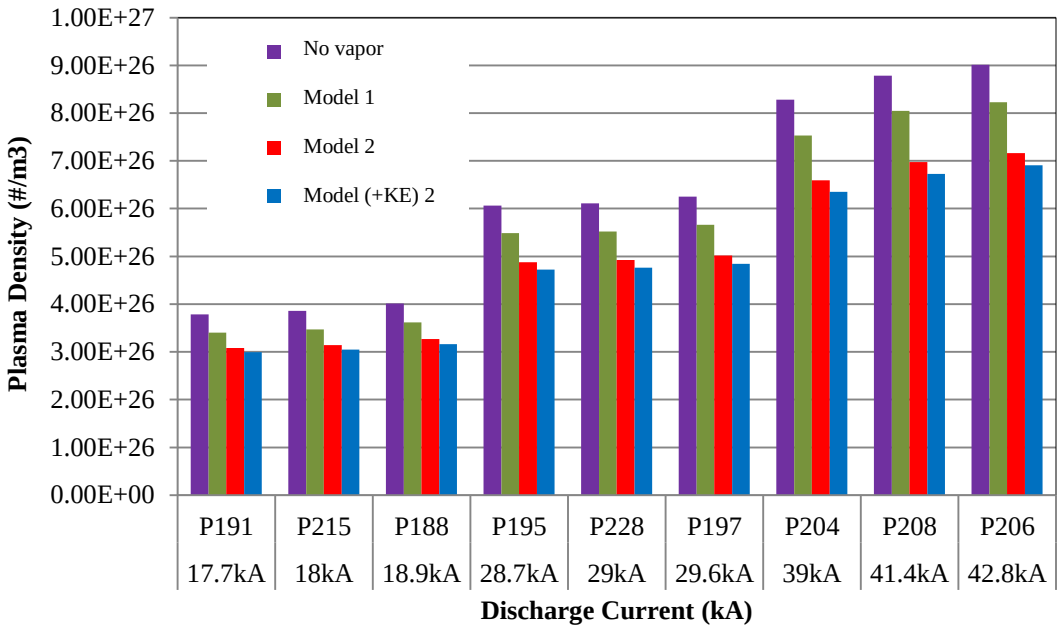

Figure 3.3: Plasma density as a function of the peak discharge current for all VP models.

Figure 3.4 compares the plasma pressure results using the different VS models. The pressure is determined by the equation of state $P = nkT(1+\bar{Z})$ where n is the plasma number, kT is the plasma kinetic temperature and $\bar{Z}$ is the average charge state [12, 13]. Accordingly, the pressure results are expected to influence by the plasma density results. However, a modification to the equation of state to account for the long-term Coulomb interactions necessitates the addition of pressure correction term $\Delta P = kT / 24\pi\lambda_D^3$ where λ_D is the Debye length; hence, the equation of state is modified to $P + \Delta P = \sum nkT$ which takes into consideration such pressure corrosion [7, 12-15].

Results of the Model 1 "opacity model" suggests that the developed optically thick vapor layer results in a pressure reduction of 4.3% compared to non-vapor shield calculations

whereas, Model 2 shows an average of 12.5% reduction in the pressure. As seen in Figure 3.4, the effect of the plasma species' kinetic energy on the plasma pressure is small for low current ranges; however, the effect becomes more pronounced with the increase in the magnitude of the discharge current.

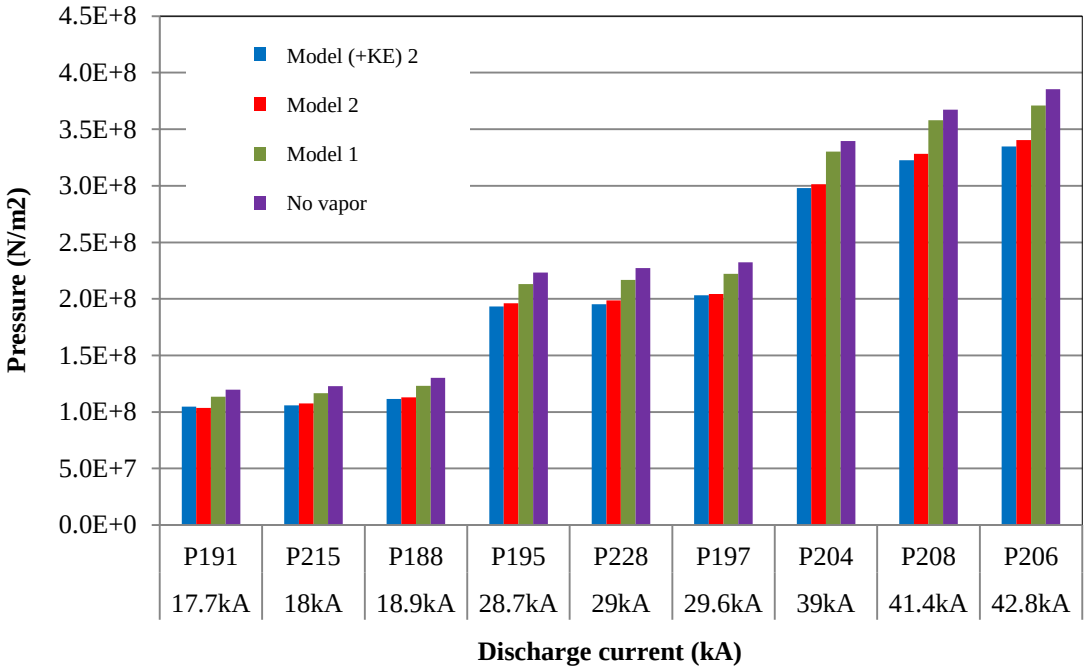

Figure 3.4: Plasma pressure as a function of the peak discharge current for all VS models.

Unlike the plasma density and pressure, the plasma bulk velocity decreases compared to the case where no VS formation is taking place, which is an expected result regardless of which vapor shield model was adopted [15]. As seen in Figure 3.5, Model 1 "opacity model" results in higher velocity values than that without vapor shield, almost 1%, which indicates that the optically thick vapor layer does not seem to strongly affect the bulk plasma motion. On the other hand, Model 2 "ratio model" predicts plasma velocities that are over 5% greater

than those in absence of VS. Comparing Model 2 "ratio model" calculations with and without kinetic energy consideration has shown that the inclusion of the plasma kinetic energy results in a better vapor shielding effect. This can be attributed to the effect of allowing the kinetic energy of the impinging plasma species to contribute to the total incident power density, which slightly decreases the transmission factor, meaning that higher shielding can be provided by the boundary layer. Therefore, the accumulating vapor layer occupies a thicker boundary layer, and, therefore expands toward the plasma bulk which then gradually accelerates the plasma bulk towards the ET source exit.

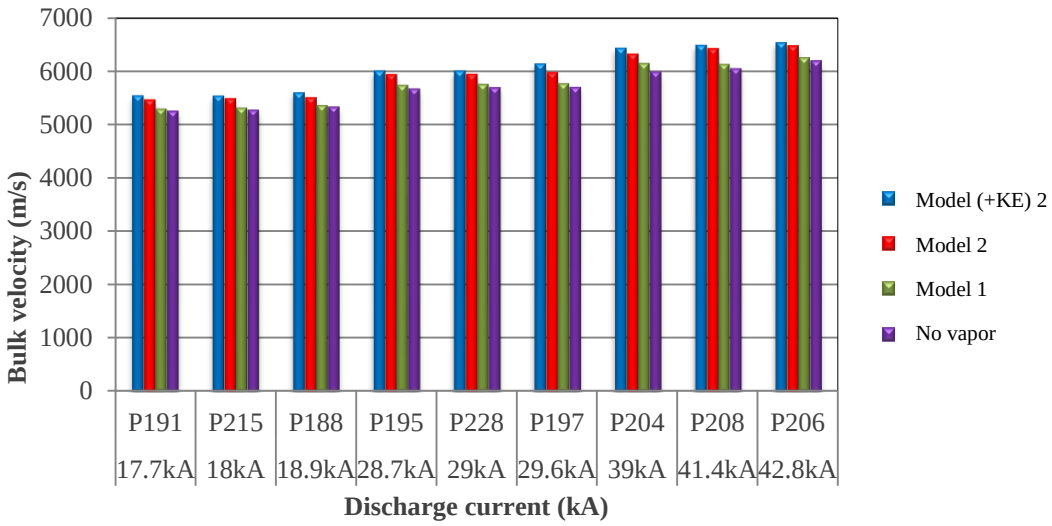

Figure 3.5: Plasma bulk velocity as a function of the peak discharge current.

In the subsequent section, shot number P228 has been chosen to further investigate the vapor shield parameters as a sample ET shot; however, similar trends would be expected in the rest of the shots. This shot was chosen because it represents the mid-range discharge

energy among all shots presented in this study. It is also of a record that it is a clean experimental shot with ablated mass that matches the simulation values calculated by both models.

All above calculations by the proposed VS models differ in the way the transmission factor is calculated based on the modeling of the VS evolution. Figure 3.6 shows the temporal evolution of the transmission factor for an incident discharge current that peaks at 29 kA as predicted by ETFLOWVS vapor shield models.

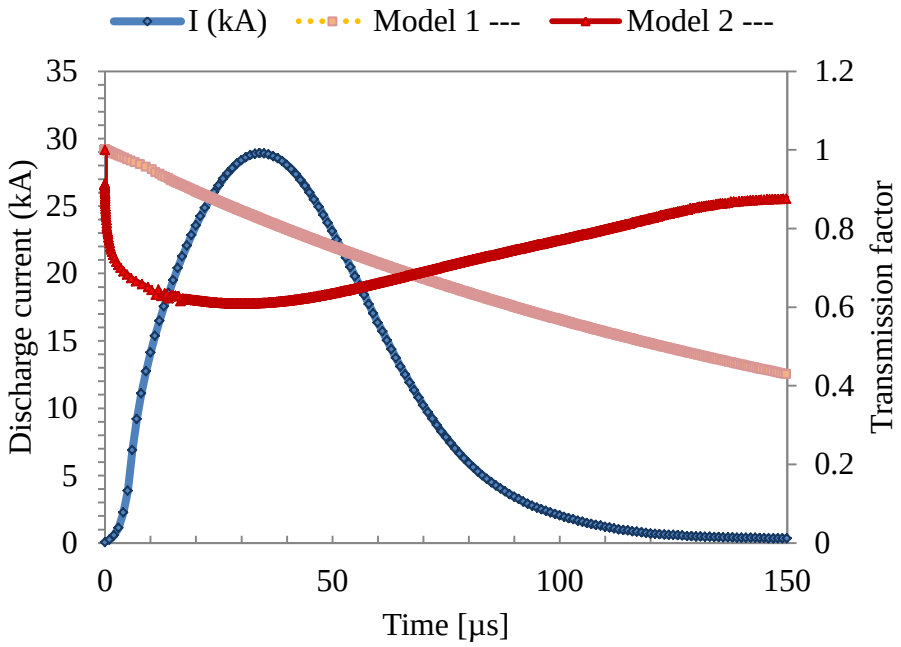

Figure 3.6: Temporal evolution of the transmission factor for an incident discharge current that peaks at 29 kA.

The temporal behavior of the plasma parameters, temperature, density, heat flux and pressure, follow the temporal behavior of the discharge current. This, consequently, implies that the time variation of the deposited energy and the evolved VS layer on the exposed

surface forces a temporal variation in the energy transmission factor, and therefore, in the boundary layer behavior. Based on the theory adopted by Mode l "opacity", an optically thick VS forms and builds up on the surface due to the exposure to the incident high heat flux from the plasma core. As a result, the transmission factor exponentially decreases over the course of energy deposition despite the after-peak decreasing current and input power. This is caused by the formation of the optically thick boundary as the opacity of the boundary layer plays a significant role to exponentially attenuate the transmission of the incoming radiant heat flux from the photons and plasma particles.

However, the predicted temporal evolution by Model 2 "ratio" of the transmission factor is completely different. As per this model, the transmission factor drops rapidly from its initial value of unity as the deposited discharge energy increases up to its peak. Soon after the beginning of the discharge, the transmission factor reaches a minimum value of 0.6. For the rest of the 120 μs discharge time; the transmission factor gradually increases to about 0.9 due to reduced plasma heat flux as the input power decreases. Also, as seen in Figure 3.6, the transmission factor follows an inverse profile of the typical temporal evolution of the discharge current as predicted by this model.

Figure 3.7 supports the earlier findings in regard to radiation attenuation by optically thick vapor shield. The effective thickness of the boundary layer has a great impact on the transmission factor as shown on Figure 3.7. The effective thickness increases as thicker boundary layer accumulates over the exposed surface. The increasing thickness strongly indicates stronger attenuation of the transmitted radiant heat flux through the boundary layer.

As mentioned earlier, the attenuation in this model accounts for all possible radiation absorption processes upon the formation of the optically thick boundary layer. The transmission factor exponentially decays to a minimum value despite the cooling down of the bulk plasma at the end of the discharge.

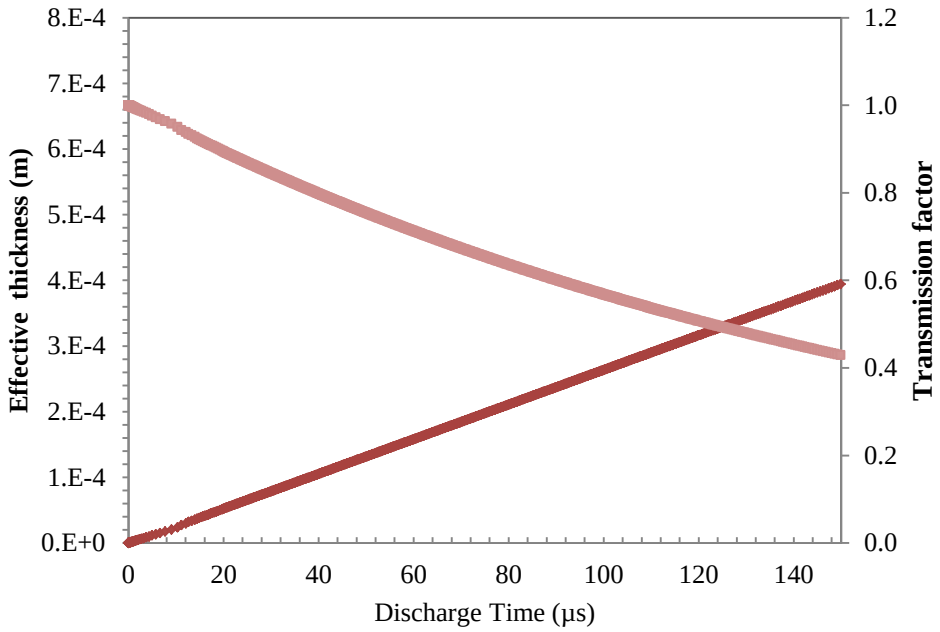

Figure 3.7: Effective thickness of the boundary layer and the transmission factor as functions of discharge time.

The values of the transmission factor as a function of the discharge current is shown in Figure 3.8. The transmission factor drops exponentially with the increase in the magnitude of the discharge current. For Lexan polycarbonate material, it varies from 0.65 to 0.56 for the discharge current range between 15 and 45 kA. The data in Figure 3.8 indicates better shielding by the VS with the increase in the input power and, consequently, the increase in the incident radiant heat flux. This is primarily due to the increased sublimed material that forms the absorbing boundary layer.

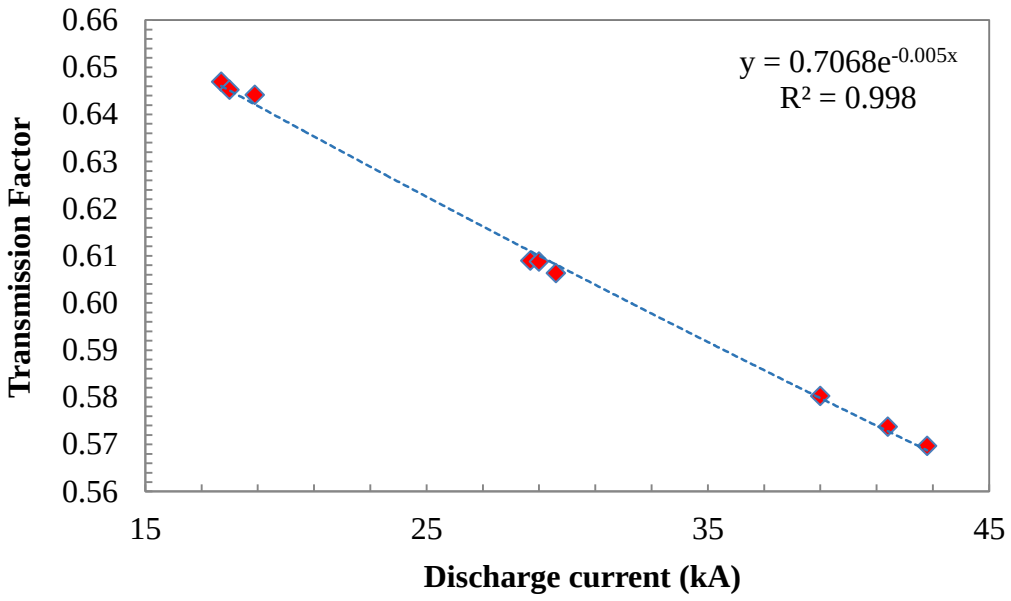

Figure 3.8: The transmission factor value as a function of the discharge current.

3.4 Conclusions

Calculations of the transmission factor at each time step and mesh point have been conducted with the ET code ETFLOWVS to predict the plasma parameters at the capillary exit and the mass ablated from the capillary inner wall. The code predictions were used to compare the results of two newly-developed vapor shield models with earlier ones and with experimental data of mass ablation from an ET source. The inclusion of the vapor shield modeling produces less deviation from the measured ablated mass as compared to earlier calculations. However, the plasma bulk has higher exit velocities by including the vapor shield effect. The calculation done by using Model 1, the opacity model, has shown that the energy transmission factor through the vapor shield for Lexan varies with the peak discharge current. The calculations done by using Model 2, the ratio model, suggested that the optical thickness of the vapor shield varies with the incident radiant heat flux. Code results for Lexan polycarbonate indicate a transmission factor of 0.65 to 0.56 for the discharge current range between 15 and 45 kA, which confirms a reduction in the energy reaching the surface as the initial energy deposition from the plasma core increases. This self-protecting mechanism is an essential mechanism in protecting the surface from incoming high heat flux, a protection that all tested models are providing. The essential vapor shield mechanism is of important applicability in future fusion tokamak reactor where plasma facing materials are expected to suffer from high heat flux deposition.

3.5 References

[1] A.Hassanein and I. K. Konkashbaev, "Disruption Simulation Experiments and Extrapolation to Reactor Conditions", Proc. 20th Symposium on Fusion Technology (SOFT-20), pp. 1-7, Marseilles, France, 7-11 September, 1998.

[2] A. Hassanein, G. Federici, I. Konkashbaev, A. Zhitluknin, and V. Litunovsky, "Materials Effects and Design Implications of Disruptions and Off-Normal Events in ITER", Fusion Engineering and Design, Vol. 39-40, pp. 201-210, 1998.

[3] N. N. Ogurzowa, I. V. Podmoshenskii, and P. N. Rogovtsev, "Calculation of the Parameters of an Optically Dense Plasma Obtained by a Discharge with an Evaporating Wall", High Temperature , Vol. 9, pp. 430-435, 1971.

[4] J. Gilligan, M. Bourham, O. Hankins, W. Eddy, J. Hurley and D. Black, "Vapor Shield Protection of Plasma Facing Components Under Incident High Heat Flux", Journal of Nuclear Materials, Vol. 196-198, pp. 596-601, 1992.

[5] M. Bourham, O. Hankins, O. Auciello, J. Stock, B. Wehring, R. Mohanti, and J. Gilligan, "Vapor Shielding and Erosion of Surfaces Exposed to a High Heat Load in an Electrothermal Accelerator", IEEE Transactions on Plasma Science, Vol. 17, pp. 386-391, 1989.

[6] W. Oberle, I. Stobie, M. Del Guercio, K. White, M. Bourham, and J. Gilligan, "Summary of Experimental Efforts to Determine Plasma-Augmented Burn Rates for Solid Propellants", Army Research Laboratory, Adelphi, MD, ARL-TR-782, Final Report, June 1995.

[7] L. Winfrey, M. A. Abd Al-Halim, J. G. Gilligan, A. V. Saveliev, and M. A. Bourham, "A Study of Plasma Parameters in a Capillary Discharge With Calculations Using Ideal and Nonideal Plasma Models for Comparison With Experiment", IEEE Transactions on Plasma Science, Vol. 40, pp. 843-852, 2012.

[8] J. D. Powell and A.E. Zielinski, "Capillary Discharge in the Electrothermal Gun," IEEE Transactions Magnetics, vol. 29, pp. 591–595, 1993.

[9] J. Hurley, M. Bourham, and J. Gilligan, "Numerical Simulation and Experiment of Plasma Flow in the Electrothermal Launcher SIRENS", IEEE Transactions on Magnetics, vol.31, pp.616-621, 1995.

[10] J. G. Gilligan and R. B. Mohanti, "Time-Dependent Numerical Simulation of Ablation-Controlled Arcs", IEEE Transactions on Magnetics. Vol.18, p. 190-197, 1990.

[11] H. C. Hottel and A. F. Sarofim, Radiative Transfer, McGraw-Hill, New York, 1967.

[12] Y. B. Zel'dovich and Y. P. Raizer, Physics of Shock Waves and High-Temperature Hydrodynamic Phenomena, Vol. 1, Academic Press, New York and London, 1966.

[13] H. G. Griem, "High-Density Corrections in Plasma Spectroscopy", Physical Review, Vol.128, pp.997-1003, 1962.

[14] M. R. Zaghloul, "Improved Modelling of Electrothermal Plasma Source With Radiation Transport", Journal of Physics D: Applied Physics, Vol. 41, pp 1-10 October 2008.

[15] N. AlMousa, L. Winfrey, J. Gilligan, and M. Bourham, "Radiative Heat Transport Through Vapor Plasma for Fusion Heat Flux Studies and Electrothermal Plasma Sources Applications", Journal of Nuclear Energy Science & Power Generation Technology, Vol. 3, pp. 1-7, January 2014.

CHAPTER 4

ELECTROTHERMAL PLASMA SOURCE SIMULATION OF FUSION REACTORS CRITICAL COMPONENTS EROSION

Presented in the 67th Gaseous Electronics Conference (GEC), Raleigh NC, November 3 – 7, 2014, with the title: Simulation of the Vapor Shield Effect on Plasma Facing Materials under Tokomak-like Disruption Conditions, Nouf AlMousa and Mohamed Bourham, 2014.

Abstract

Hard disruptions are expected in large-scale tokomaks where the critical interior components of the reactor are exposed to strong radiant high heat fluxes that result in surface melting and evaporation. These plasma-facing components (PFCs) are essentially the divertors, first wall, limiters and RF antennae. As described in previous chapters, a boundary layer will form at the plasma-surface interface and forms a vapor shield layer that absorbs a fraction of the incident heat flux that protects the PFCs from further erosion/melting. The mechanism of vapor shielding was previously discussed in Chapter 2 where an illustration of the time evolution of the process was shown to indicate that a reduction of the net surface erosion takes place. Chapters 3 also showed that two essential models of the vapor shield can be adopted to determine the value of the energy transmission factor *f* through the vapor shield. The ratio model describes the transmission factor as a ratio between the actual heat flux reaching the ablating surface to the total incident heat flux from the plasma. The models of Chapter 3 are implemented in the ETFLOW code; however, only the ratio model will be used in this chapter. The code has been used to calculate the erosion under disruption-like

conditions relevant to ITER for power density of 55 GW/m^2 over 180 μs. The energy transmission factor through the vapor shield f was found to be strongly dependent on the materials' properties, plasma pressure, and density but weakly dependent on the plasma internal and kinetic energies. Calculations of f at each time step and mesh point are used to predict the total ablated mass. The code predictions are used to estimate the erosion rate and erosion thickness for selected PFMs. High-Z PFMs have been proven to suffer higher ablation rate as compared to low-Z PFMs. However, the erosion in units of material thickness indicates that the erosion thickness of the highest Z PFMs (tungsten) is less than that of the lowest Z PFMs (beryllium). Detailed comparisons of the erosion behavior and properties of PFMs are presented.

4.1 Introduction

During hard disruptions in large scale tokomaks and expected elevated disruption severity, high heat flux and high energy plasma particles hit the machine plasma facing components (PFCs), which results in erosion of these critical components. The plasma flow in some large scale tokomaks (like ITER) has pulse duration longer than 100 μs and heat flux of up to 100 MJ/m^2. Under such short and intense high energy density conditions, the PFCs suffer melting and evaporation of a thin layer of its surfaces. The vapor plasma boundary layer will be formed at the ablating surfaces, and this vapor acts as a shield that protects the PFCs from further erosion. A further increase in the vapor plasma shield thickness should come as a result of increased incident heat and particle fluxes. Based on earlier publications,

the scenario of the vapor shield formation suggests that this process has strong time dependence [1-6].

The direct deposition of the high energy density carried by plasma particles on the PFCs is immediately followed by melting and vaporization of the exposed surfaces. It should be noted that the direct deposition occurs at the first instant without any vapor shield present. However, the initial wave of the vaporized material forms a thin layer of vapor plasma between the PFCs surface and the incoming plasma flux. As disruption time goes on, further heating and evaporation of the PFC's surface is taking place and the vapor shield expands toward the incoming plasma flux [1-6]. The energy of the incoming plasma particles will be partially absorbed by the vapor shield layer; thus. less heat flux will reach the PFCs surface. Once the incoming energy is deposited in the vapor shield layer, the radiant energy transport becomes the primary mechanism by which energy is transferred to the eroding surface [1-6]. The continuous deposition of the incoming energy eventually raises the temperature of the vapor; hence, the vapor plasma decreases the re-radiated heat flux to the PFCs. The heat flux of such plasmas is primary from black body spectrum photons of the dense plasma core.

Early investigations considered a steady state vapor shield that has constant spatial and temporal properties adjacent to the eroded surfaces [1-3]. Further studies have shown the existence of an effective radiating shielding region due to partial deposition of the incident heat flux [4-6]. Reported experiments and modeling on carbon-based materials, insulators, and composites have shown how the vapor shield absorbs a large fraction of the incident high heat loads and minimized surface erosion [1, 2].

Computational studies using electrothermal (ET) plasma capillary sources are used in this study since experimental invaginations are inflexible to be conducted on large scale fusion devices. Simulations using small scale disruption-like experiments, such as the SIRENS and PIPE facilities were used to evaluate the vapor shielding formed from PFCs candidate materials [1-4, 7, 8]. The usefulness of the small experimental devices is the ability to simulate the typical conditions of high heat loading in ITER and to evaluate the damage of the PFCs during disruption [1, 2, 7, 8]. The SIRENS "**S**urface **I**nteraction **R**esearch **E**xperiment at **N**orth Carolina **S**tate" has been extensively used to simulate disruption like conditions [1, 2]. SIRENS was capable of producing high heat fluxes of up to 100 GW/m^2 from high density energetic plasma particles (10^{23}-10^{28} m^{-3}) for 100-200 μs duration. The early modeling of such experiments was in a 0-D, time dependent ZEUS code [9], followed by an upgrade to a 1-D, time dependent ODIN code [10], with a series of upgrades until the developed version of the ETFLOW code [3] and the recent ETFLOWVS [11]. Disruption simulation experiments performed on the plasma source facility SIRENS were used for validation of ETFLOW computational results.

4.2 Plasma Ablation Model

ETFLOW has been successful in simulating the ablation process in the ET plasma experiments SIRENS and PIPE. It predicted the erosion of material surfaces with good agreement with the experimental data previously obtained on the SIRENS facility. However, by fitting the plasma parameters calculations to the measured values, it was clear that the numerically calculated ablation values are scattered within 12-24% of the experimentally

measured ones. The over prediction of the ablation and erosion calculations is suggested to be due to using a fixed transmission factor or assuming f = 1, which means full energy deposition without vapor shield effect. In addition, the accuracy in the experimental data is within 10-20% due to the experimental conditions, sample streaks, micro-cracking, and accuracy within few micrograms of weight measurements. The f =1 condition overestimates the ablation calculations because the heat flux reaching the surface is exactly the same as the incident heat flux with full deposition. Simulation with inclusion of vapor shield indicates that part of the incident heat flux is absorbed by the vaporized wall material through the vapor shield mechanism [3, 4, 11].

In this study, radiation transport with vapor shield model has been conducted on candidate PFMs for selected PFCs of fusion reactors such as beryllium, carbon, and boron carbide as low-Z materials and tungsten and molybdenum as high-Z materials. The "ratio" model with inclusion of the kinetic energy $f = \rho H_{sub} / \left(P + \rho U + \rho H_{sub} + 0.5 \rho v_z^2 \right)$ has been used in this study. More details of the basic equations of ETFLOW code and its developmental history can be found elsewhere [3, 4, 10, 11]. As discussed in Chapter 3, the plasma pressure for an ideal plasma is given by $P = nkT(1 + \bar{z})$, and the implementation of the pressure correction term to account for the long-term Coulomb interactions $\Delta P = kT / 24\pi\lambda_D^3$ is incorporated in the code to modify the equation of state to $P + \Delta P = \sum nkT$. The ablation rate ρ_a is given by $\rho_a = \dfrac{2\rho\ \Delta q}{r_p \left(P + \rho U \right)}$, which represents the rate at which the plasma density increases because of the ablation of surface, where ρ is the

plasma density, P is the pressure, U is the internal energy, and Δq is the heat flux on the surface. The temporal variation of the energy transmission factor f and the ablation rate are predicted by the code. In the calculations, radial heat conduction is neglected, and only radiative heat transport to the surface is considered.

4.3 Results and Discussion

The set of computational runs were conducted using the ETFLOW code with an input current file peaking to about 40 kA within 30 μs of the discharge (Figure. 4.1), which has a total pulse length of 180 μs, providing 6.51 kJ discharge energy. The pulse tail after 120 μs is the current decay with minor values as the capacitor discharges its full stored energy.

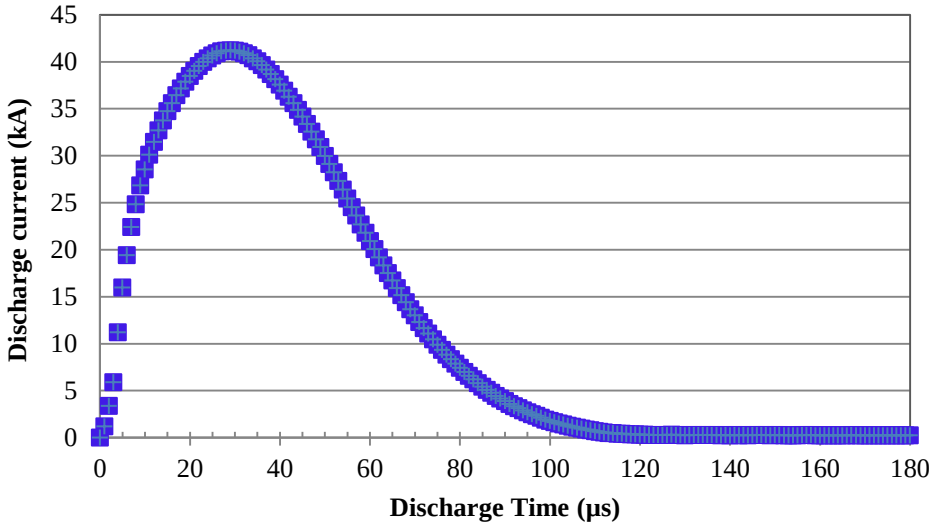

Figure 4.1: Input discharge current for ETFLOW calculations.

The other main input parameters needed in ETFLOW are the source geometry and the material parameters. The chosen source geometry is cylindrical capillary 9.0 cm in length

and 4 mm in diameter, which is typical in the SIRENS and PIPE facilities [1-4, 7-11], with a total inner exposed surface area of 11.304 cm^2. The material properties are listed in a material library in a module built in the code and includes atomic, electrical, thermal, and thermodynamic properties. The code subroutines access the material library and pull the required data for the material of interest.

Any material or variety of PFMs can be used as input material in the ETFLOW code including metals, insulators, composites, or even energetic materials. The choice in this study is based on the importance of specific materials for use in future tokamak fusion reactors. The code was run for tungsten and molybdenum as high-Z refractory metals for the divertor, carbon and beryllium as low-Z materials for first wall tiles, and boron carbide as carbon-based ceramic material also for first wall liners. For the selected 40 kA peak current input file, the corresponding heat flux peaks to 55 GW/m^2 as shown in Figure. 2, which has a similar shape to the current pulse.

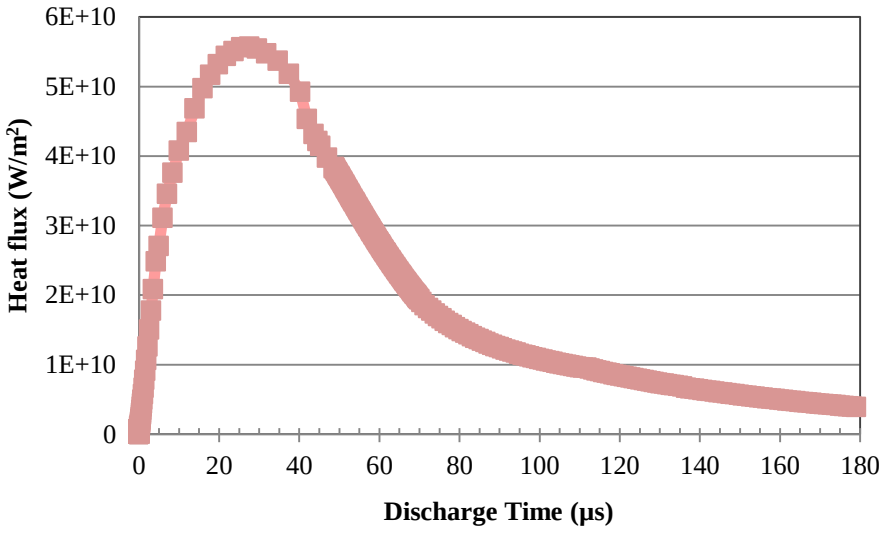

Figure 4.2: Time history of the plasma radiant heat flux.

Figure 4.3 shows the temporal evolution of the energy transmission factor for the selected five PFMs. Comparing the temporal change in the heat flux (Figure 4.2) to the transmission energy factor profile (Figure 4.3), one can see that the transmission factor decreases as the incident heat flux increases. The increase in the radiant heat flux incident on the material surface during a disruption event results in an increased vaporization and formation of a thicker vapor shield; hence less radiative heat flux to the PFM surface due to photon attenuation through the vapor shield.

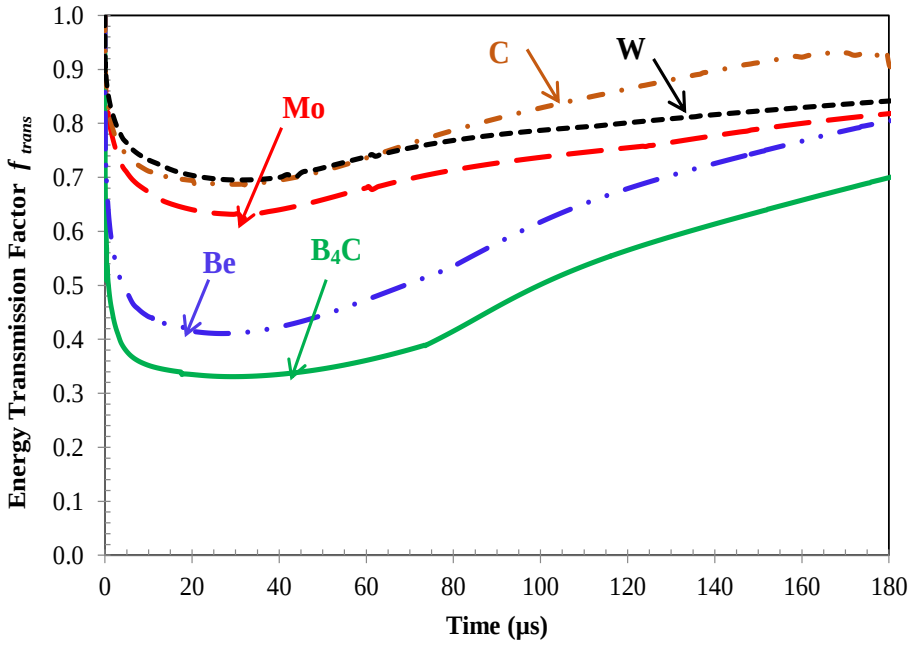

Figure 4.3: Temporal evolution of the energy transmission factor for different PFMs.

The increase of the incident energy and the radiant heat flux cause the sudden early drop in the transmission factor. At the initiation of the discharge, the energy transmission factor is equal to 1; meaning that full energy deposition occurs due to the non-existence of the vapor shield. As the plasma energetic particles first hit the PFC surface, vaporization of the material immediately follows. The vaporized material accumulates and forms a thin shield layer in front of the PFC wall. Upon the formation of the vapor shield layer, part of the incoming energy is absorbed by the vapor shield, and the rest will hit the PFC surface. This explains the drop in the f value as the heat flux rises to its peak of about 55 GW/m^2. The transmission factor drops to a peak of 0.71 for W, 0.68 for C, 0.63 for Mo, 0.41 for Be and 0.33 for B_4C. The inflection point of the transmission energy factor curves occurs at around 30 μs, which corresponds to the time of maximum heat flux. After this time, the transmission factor profile begins to flatten out and rise as the incident heat flux drops. This happens because the incoming heat flux decreases, and less heat flux reaches the PFM surface; therefore, less eroded mass is being removed from the surface. As a result, less vaporized PFM particles contribute to the vapor shield layer buildup. As time goes on, further decrease in f value suggests that more vapor is produced; therefore, less heat flux reaches the PFC surface. However, this leads to a decrease in the vapor shield density, and as a result, less shielding is expected. The shielding efficiency continues to decrease as the energy transmission factor through the vapor shield increases. Later in time, the transmission factor increases to a maximum of 0.9 but never returns to unity. Although radiant heat flux decays in time as the input energy decreases after the peak, the transmission energy factor shows slower increase during the rest of the disruption time. Such slight increase is due to a

sufficient attenuation at the beginning of disruption, which effectively shielded the PFM surfaces even after stopping a high fraction of the incident heat flux. It is also important to couple the temporal behavior of the energy transmission factor to the temporal ablation. An explanation of the flattened profile of f at the later time could be the profile of the PFM temporal ablation as seen in Figure. 4.4.

Figure 4.4 shows a comparison between the ablation of PFMs per unit area (kg/m^2) for the same incident heat flux (55 GW/m^2). As seen in the figure, the ablation exhibits similar trends for all materials, a large increase in the early disruption time followed by a flattening out after the time of peak heat flux. This is due to the sharp decrease of the f factor which is followed by a slow increase after the peak time. High-Z materials show higher ablation, while low-Z materials exhibit lower mass removal per unit area.

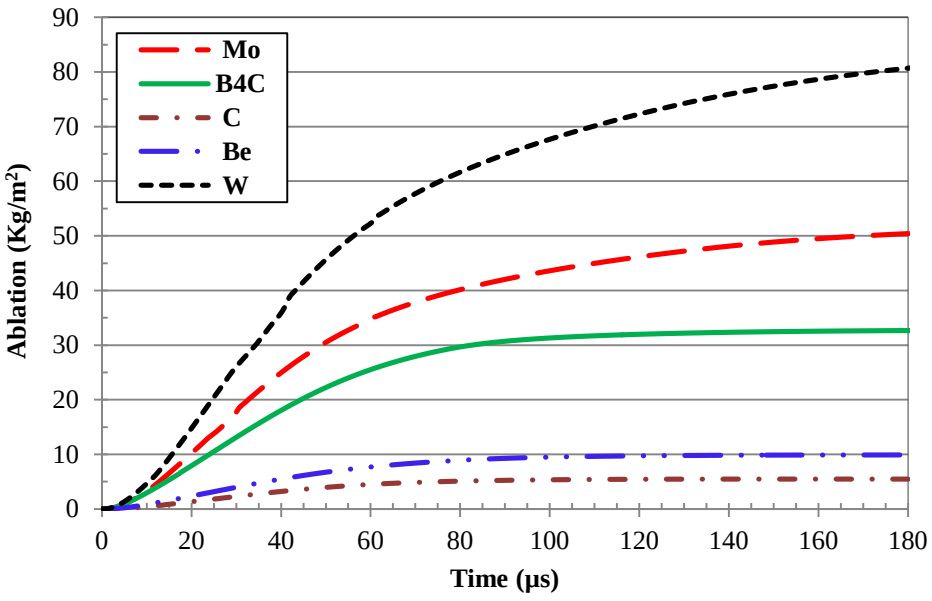

Figure 4.4: Temporal ablation of plasma facing materials under 55GW/m^2 radiant heat flux.

The time evolution of the incident heat flux is quite similar to the ablation rate (mg/ μs), but the ablation rate decays slower, which can be seen in Figure 4.5. It is clear that for early disruption time, the ablation rate sharply increases up to the time at which the heat flux peaks. During disruption, high heat flux incident on the PFM surface releases the surface atoms or molecules, ionizes, and transports them towards the plasma. The higher the heat loads, the higher the ablation rate and the more ablated material. The decrease in the radiant heat flux results in lowering the ablation rate. The eroded mass, and the ablation depth, can be estimated from the ablation rate.

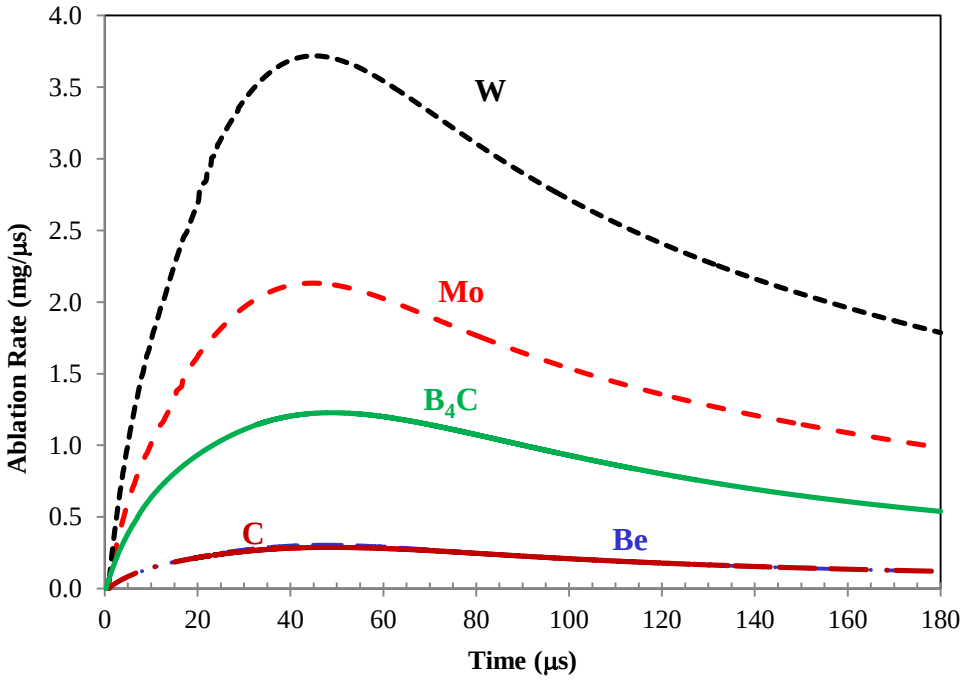

Figure 4.5: Ablation rates of plasma facing materials under 55GW/m^2 radiant heat flux.

The erosion thickness (depth from the surface) as a function of time is illustrated in Figure. 4.6 for radiant heat flux of 55 GW/m^2 for beryllium, carbon, tungsten, molybdenum, and boron carbide. As predicted by ETFLOW, the erosion thickness is found to be strongly

time dependent for the first 60-70 μsec followed by a flat profile for the rest of the disruption time. The sharp initial increase in the erosion thickness is due to the direct deposition of the incident heat flux, and the subsequent flat profile is due to the vapor shield effect. The erosion depth shows less eroded thickness for high-Z materials because such materials have higher molar mass, atomic density, and vaporization/sublimation energies.

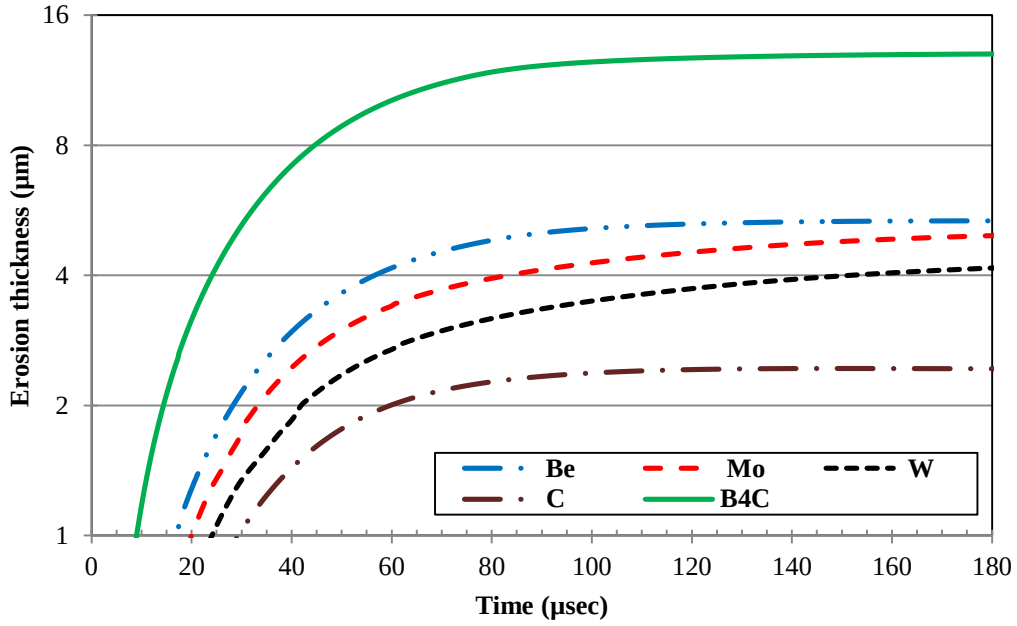

Figure 4.6: Erosion thickness of plasma facing materials under 55GW/m^2 radiant heat flux.

Table 4.1 summarizes the calculations of the ablation and erosion thickness for a disruption time of 180 μs. In all cases, there is approximately 0.55 kJ/cm^2 deposited onto the plasma facing material. The ablation thickness was obtained from the difference of the final and initial radius of the capillary geometry. The ablated mass calculations were taken per unit area of the internally-exposed capillary surface.

Table 4.1 1-D erosion calculations for incident heat flux of 55 GW/m^2 over 180 µsec.

PFM	Molar mass g/mol	Heat of sublimation kJ/mol	Density g/cm^3	Ablated mass[(1)] mg	Erosion Thickness[(2)] µm
Be	9.01	291	1.84	9.86	5.34
C	12.01	711.28	2.26	5.44	2.42
Mo	95.94	664	10.28	51.83	4.99
W	183.85	851	19.25	84.26	4.21
B_4C	55.25	557.39	2.52	32.73	13.03

[(1)] Ablated mass per unit area (cm^2) of PFC, [(2)] Assuming uniform eroded layer

The results of the low-Z PFM are summarized in the following:

Carbon has been used in many tokomaks as PFM. It is the preferred material for areas that suffer from direct hit by disruption like dump targets, baffles and dome. Carbon is a good candidate for its low z number and high sublimation temperature. The carbon net erosion thickness after deposition 55 GW/m^2 over 180 µsec is calculated to be about 2.5 µm. The eroded mass from a unit area cm^2 leaving such erosion thickness is about 5.5 mg. The minimum average ablation rate of 0.103 mg/cm^{2}µsec is observed also for carbon, which verifies the earlier findings regarding low carbon erosion.

Beryllium is the material of PFC in some tokamaks such as the Joint European Torus (JET) as the tiling material in the main reactor chamber [12]. It is preferred compared to carbon for its lower-Z number, which results in lower radiative power loss. The estimated beryllium eroded layer would be about 5.3 μm thick where the removed mass from a unit area (1.0 cm^2) of beryllium is 9.8 mg. The eroded mass and the thickness are almost double that of carbon, which results from the lower heat of sublimation of beryllium. Also the low melting point of beryllium (1250 C^o) leads to severe melting during disruption. Overall, the low radiation losses were the main requirement to apply low-Z plasma facing materials.

Boron carbide has relatively low heat of sublimation, which explains the high erosion thickness of about 13 μm where the removed mass is predicted to be 32.73 mg from a unit area. Although the ablated mass of boron carbide is a factor of 6 greater than that of carbon, the boron carbide erosion thickness is only a factor of 3 greater than carbon due to the higher density of boron carbide.

However, other requirements for optimizing the plasma performance in fusion devices can't be fulfilled by low-Z material. The relatively high erosion thicknesses is an example of the poor low-Z PFM as it shortens the PFC lifetime and increases the need of PFC exchange. To fulfill the need of the material that withstands the high heat loads and energetic particle fluxes, tungsten is proposed as a favored material for divertor plate [13]. The main advantage of tungsten is due to its heavy atom. It is used in high erosion areas in divertors such as vertical targets, dump targets and wings [13]. Another example of high-Z plasma facing material is molybdenum which is considered to be a good choice as a first-wall material [14, 15]. Modeling of the erosion of high-Z PFM has shown that the predicted

eroded mass of tungsten (84.26 mg) is about twice that of molybdenum (51.83mg). However, because tungsten has higher density, erosion thickness of tungsten (4.21μm) is about 20% less than that of molybdenum (4.99 μm).

4.4 Conclusions

Due to the difficulties of performing an experimental test on a fusion test reactor, a computational evaluation of plasma facing materials was conducted using the ETFLOWVS code, which simulates typical conditions of plasma interaction with materials and tokamak disruption events. Simulation was conducted considering a power density of 55 GW/m^2 as the radiant high heat flux incident on the material surface for a disruption time of 180 μsec. Five materials are considered as PFM: beryllium, carbon, boron carbide, molybdenum and tungsten. The erosion of all PFMs is almost linear with time for $t < 70\,\mu sec$. After this time, the eroded material seems sufficient to form a vapor layer that can effectively shield the PCM's surface from further erosion. Calculations of ablation rate of PFM were carried out to identify the tolerable ablated mass of the exposed PFC surfaces. High-Z materials suffer higher ablation rates compared to low-Z materials. However, the erosion in units of material thickness indicates that the erosion thickness of the highest Z-number material (tungsten) is less than that of the lowest Z-number material (beryllium). All calculations in this study were based on the influence of the vapor shield layer being taken into account to accurately estimate the mass losses of the PFMs.

4.5 References

[1] M. Bourham, O. Hankins, O. Auciello, J. Stock, B. Wehring, R. Mohanti, and J. Gilligan, "Vapor Shielding and Erosion of Surfaces Exposed to a High Heat Load in an Electrothermal Accelerator", IEEE Transactions on Plasma Science, Vol. 17, pp. 386-391, 1989.

[2] J. G. Gilligan and M. A Bourham, "The Use of an Electrothermal Plasma Gun to Simulate the Extremely High Heat Flux Conditions of a Tokamak Disruption", Journal of Fusion Energy, Vol. 12, pp.311-316, 1993.

[3] A. L. Winfrey, M. A. Abd Al-Halim, J. G. Gilligan, A. V. Saveliev, and M. A. Bourham, "A Study of Plasma Parameters in a Capillary Discharge With Calculations Using Ideal and Nonideal Plasma Models for Comparison With Experiment", IEEE Transactions on Plasma Science, Vol. 40, pp. 843-852, 2012.

[4] N. AlMousa, L. Winfrey, J. Gilligan, and M. Bourham, "Radiative Heat Transport Through Vapor Plasma for Fusion Heat Flux Studies and Electrothermal Plasma Sources Applications", Journal of Nuclear Energy Science & Power Generation Technology, Vol. 3, pp. 1-7, 2014.

[5] A. Hassanein and D. A. Ehst, "Dynamic Modeling of Plasma-Vapor Interactions During Plasma Disruptions", Journal of Nuclear Materials, Vol. 196-198, pp. 679-685, 1992.

[6] A. Hassanein and I. Konkashbaev , "Comprehensive Model for Disruption Erosion in a Reactor Environment", Journal of Nuclear Materials, Vol. 220-222, pp. 244-248, 1995.

[7] G. E. Dale and M. A. Bourham, "Melt layer erosion and resolidification of metallic plasma facing components", Proc. 17th IEEE/NPSS Symposium on Fusion Engineering, Vol. 2, pp. 892-895, 1997.

[8] J. P. Sharpe, B. J. Merrill, D. A. Petti, M. A. Bourham and J. G. Gilligan, "Modeling of Particulate Production in the SIRENS Plasma Disruption Simulator", Journal of Nuclear Materials, Vol. 290-293, pp. 1128-1133, 2001.

[9] J. G. Gilligan and R. B. Mohanti, "Time-dependent Numerical Simulation of Ablation-Controlled Arcs", IEEE Transactions on Plasma Science, Vol. 18, pp. 190–197, 1990.

[10] J. Hurley, M. Bourham, and J. Gilligan, "Numerical Simulation and Experiment of Plasma Flow in the Electrothermal Launcher SIRENS," IEEE Transactions on Magnetics, Vol. 31, pp. 616–621, 1995.

[11] N. AlMousa and M. Bourham, "Vapor Shield Models in Electrothermal Capillary Discharges and Comparison with Experiments", IEEE ICOPS-Beams 2014, Paper 1251, Washington DC, May 25–29, 2014.

[12] M. Keilhacker and the JET Team, "Overview of Results from the JET Tokamak using a Beryllium First Wall", Physics of Fluids, Vol. 2, pp.1291-1299 , 1990.

[13] R. Neu et al., "Plasma Wall Interaction and its Implication in an all Tungsten Divertor Tokamak", Plasma Physics and Controlled Fusion, Vol. 49, pp. B59–B70, 2007.

[14] D. A. Pappas, B. Lipschultz, B. LaBombard, M.J. May and C.S. Pitcher, "Molybdenum Sources and Transport in the Alcator C-Mod tokamak", Journal of Nuclear materials, Vol. 266-269, pp. 635-641, 1999.

[15] B. Lipschultz, D.A. Pappas, B. LaBombard, J.E. Rice, D. Smith and S.J. Wukitch, "A study of Molybdenum Influxes and Transport in Alcator C-Mod", Nuclear Fusion, Vol. 41, pp.585-596, 2001.

CHAPTER 5

ABLATION BEHAVIOR AND MELT-LAYER EROSION OF PLASMA FACING COMPONENTS DUE TO INTENSE HIGH HEAT FLUX FROM THERMAL QUENCH PHASE OF TOKAMAK PLASMA DISRUPTION

Published in the Proc. IEEE 26th Symposium on Fusion Energy (SOFE'15), Austin, TX, 31 May – 4 June 2015, Nouf AlMousa, John Gilligan and Mohamed Bourham, with the title: Models and Simulation for Divertor Erosion Following Plasma Disruption in Tokamak Reactors, 2015.

Abstract

Thermal quench phase of tokamak plasma disruption is considered a serious severity in the operation of future magnetic fusion reactors like ITER. Hard disruptions affect plasma facing components (PFCs) causing ablative erosive behavior with direct evaporation or mixed melting and vaporization. Such abnormal event limits the lifetime of PFCs and increases the need for maintenance and their replacement. During a disruption, energetic plasma particles and photons deposit their energy on the PFCs with high heat fluxes of up to several GW/m^2 over a short time of 0.1-1.0 ms. It has been shown, theoretically and experimentally, that the deposited energy by plasma particles and radiant heat flux vaporizes the surface of the PFCs; however, metallic PFCs, such as tungsten and molybdenum, may suffer severe surface melting-layer erosion. The boundary layer developed by vapor or melts provides shielding mechanisms, specifically vapor shield, melt-layer shield or mixed

melting/vapor shield. This boundary layer absorbs a fraction of the incoming heat flux in the dense and optically thick boundary layer, which significantly decreases the erosion. The net heat flux deposition should be accurately calculated to determine the effectiveness of the boundary layer in shielding the surface of the PFC. Vapor and droplet formation and their associated shielding effect have been investigated in this work to assess the difference between a developed boundary layer from only vapor or melt layer or the mixed vapor-melt layer with possible ejection of molten droplets away from the surface. Fully self-consistent erosion models are developed and implemented in the electrothermal ETFLOW code in a new version ETFLOW-Boundary Layer (ETFLOW-BL) to model the PFCs' response and their erosive behavior under high heat fluxes closely similar to expected ones in future fusion large tokamaks.

5.1 Introduction

Fusion reactors are expected to deposit high heat fluxes on the interior of the reactor vessel, specifically the plasma-facing components (PFCs), during hard disruptions and thermal quench phases. Events such as hard disruption and edge-localized modes (ELMs) are off-normal events in tokamaks and may deliver transient heat flux up to 100 MJ/m^2 deposited in PFCs over a short heat loading time over a period of 0.1-1.0 ms. Surface ablation, defined as direct surface vaporization, produces particulates in the form of aerosol expanding into the vacuum vessel. However, other phenomena such as melting and blowing-off can also take place from the high energy deposition ion metallic surfaces like the divertor, limiters and first

wall. Such extremely high heat flux conditions on the PFCs shorten their lifetimes and will require frequent replacement of such components.

A definition of the various erosion losses of plasma facing materials (PFMs) could result from sublimation, vaporization, loss of melt layer and additional blown off material, micro and macro cracking, spallation, or a mix of these mechanisms [1-6]. While several erosion-causing mechanisms can be responsible for surface damage of PFCs, the most damaging impact on the metallic PFCs are vaporization and melt layer erosion [3-5]. Of particular interest is the damage to the armor materials of PFCs in tokamak fusion reactors on the first wall tiles, limiters and divertor cassettes where the most intense flux strikes. Metallic PFMs such as beryllium and tungsten are materials of interest proposed for the International Thermonuclear Experimental Reactor (ITER) [7-10]. Multi-boundary layers could be evolving for the deposition of the high heat flux on the plasma facing components, resulting in evaporation and melting and possible ejection of aerosol and molten particulates into the tokamak vessel. The initial wave form of plasma energy carried by photon radiation and energetic plasma particles forms a vapor cloud adjacent to the exposed surface [1-6].

Ablation/melting layers can provide self-protecting nature to the surface due to shielding mechanisms that result from absorbing a fraction of the incoming energy into these layers. This unique mechanism partially shields the solid structure of PFCs from further erosion. However, the continuing incoming photon radiation that penetrates the vapor cloud causes further vaporization of the exposed surface which provides additional vapor-shielding [4-6, 11]. Melting effect becomes significant for metallic armors for melt layer erosion, slipping, molten particulates ejection, melt layer shielding mechanism and partial evolution

into vaporization. Extensive theoretical and experimental studies have been conducted on the erosion behavior of metallic PFCs and have shown evidence of melting of the exposed surfaces under disruption like conditions [5, 12-14].

The short and intense disruption events within a few microseconds (~100μs) at high heat fluxes in the 100 GW/m^2 range can cause immediate vaporization, and the PFC surface will sublime without melting. However, for longer plasma disruption events and lower heat fluxes (<100 GW/m^2), melting can be eminent due to the longer heat loading period, which raises the temperature of the exposed surface beyond the melting point. Consequently, a melt layer will develop on the solid surface behind the vapor layer. A thicker melt layer is expected since the evaporation point is greater than that of melting; therefore, more melting is expected. The thickness of the melt layer is one or two orders of magnitude greater than that of the vapor cloud as shown by recent theoretical calculations [5, 6, 12-15]. Though a melt layer can provide a shielding mechanism that protects the PFCs similar to that of the vapor shield, the melt layer is not stable and can contribute more to surface erosion [5, 14]. Several mechanisms may contribute to the instability of the melt layer during a disruption event such as gravitation, mechanical vibration, surface tension, vapor cloud pressure, and plasma momentum. These forces along with other forces act on the interface between the vapor and melt layer which result in a loss of a thin layer of liquid surface [4, 5, 12, 13]. Though several mechanisms may be responsible for the melt layer loss, experimental studies have emphasized the significant effect of the melt splashing mechanism on the PFCs erosion [5, 11, 15]. Melt splashing is mainly attributed to the formation of bubbles and their boiling

in the melt layer and force ejection of liquid drops that diffuse into the plasma flow [4, 12, 14].

Early studies on the erosion of PFCs and their lifetime were mainly based on the sublimation of the materials under intense high heat fluxes without consideration to melting and focused solely on the ablative behavior of the surfaces to evaporate once disruption takes place [1-4, 16]. However, recent designs of tokamak reactors that favor the use of metallic PFCs raise attention to serious concerns regarding melting and its associated complications. Therefore, the most recent studies on the PFCs' performance under disruption-like conductions are based on both melting and evaporation [14, 17].

Performing melt and vapor layer studies under induced disruptions in tokamak experimental facilities is difficult; therefore, small scale relevant experiments can simulate such typical conditions, as well as computational experiments [11, 12-18]. Various high heat flux experimental facilities can be used to simulate typical expected tokamak disruption conditions such as electron and particle beam sources, intense infrared heaters, plasma guns and electrothermal (ET) plasmas from capillary discharge [1, 5, 11, 15, 16]. A particle beam source and IR heaters are reliable tools to examine a wide range of expected heat flux in ITER [15]; however, coaxial plasma guns and ET capillary plasma sources are reliable tools to simulate the extreme high heat flux conditions for erosion of plasma facing components under disruption-like conditions with relevance to the effect of both melt and vapor boundary layers [1, 11, 13]. Several of ITER divertor studies have considered tungsten or tungsten alloys as a choice armor material [7-10, 16-17]. However, other materials such as molybdenum, beryllium and graphite are also considered.

5.2 Theoretical and Computational Models

This study focuses on investigating the erosion of metallic PFCs due to high heat flux deposition during a hard disruption. Evaluation of PFC erosion and consequently their lifetime is a critical issue for tokamak design and from economical and safety points of view. Therefore, it is essential to evaluate the erosion behavior and the corresponding shielding effect of the eroded metallic PFCs under disruption like conditions. Both evaporation and melt layer loss are considered in this study. A computation model has been developed to simulate the effect of disruption events on the erosion of metallic PFCs. In this model, the source of the high heat flux is taken from two laboratory experiments at NC State University (SIRENS and PIPE), which are ET plasma capillary discharge sources [1, 5, 19, 20].

PIPE and SIRENS generate low temperature (1-5 eV), high density plasma (10^{23}-10^{27} /m^3), and high heat flux (10-100 GW/m^2). The intense heat flux is also fast-rise, which makes it similar to heat fluxes expected in ITER. The computational code ETFLOW-BL, a modified version of ETFLOW [20], is used in this study. The modification included models for melt layer, melt ejection and splashing, opacity and vapor shield. Theoretical predictions are provided for different materials for a heat flux relevant to the range of heat fluxes expected in ITER during hard disruptions. The ET plasma sources are designed to generate high heat flux plasma. Figure 5.1 shows a schematic diagram of the ET plasma source where a detailed description of such experiments can be found elsewhere [1, 5, 9, 19, 20].

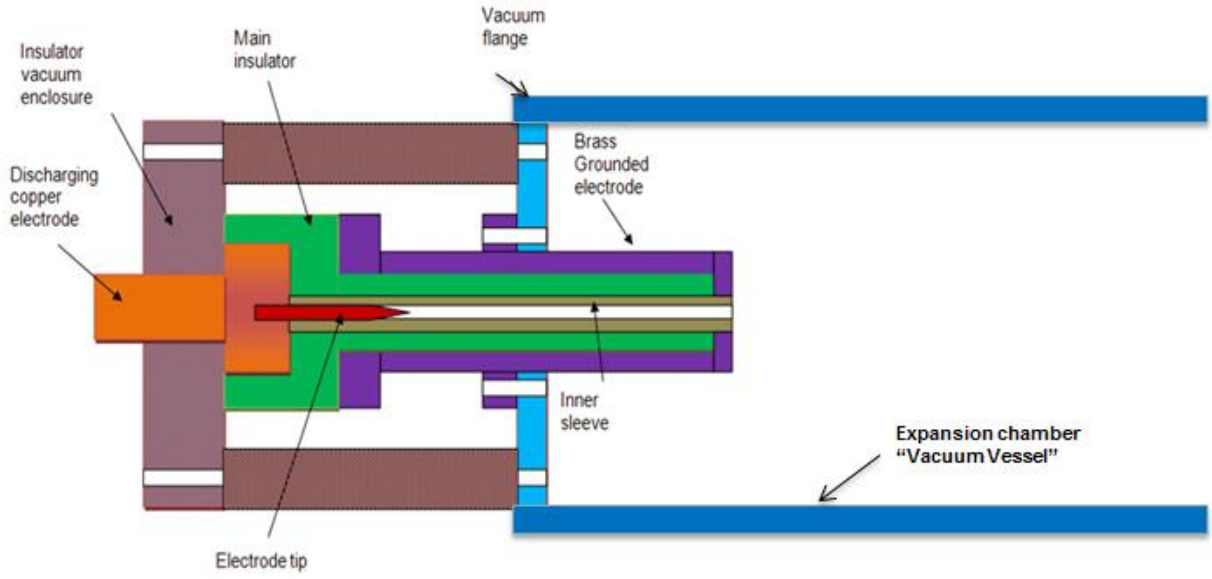

Figure 5.1: Schematic drawing of the NC State University ET facility

The highly energetic plasma is generated within the capillary in the ET source section, which operates under ablation-controlled arc regime. In this study tungsten, molybdenum, and beryllium were chosen as metallic liner materials for the source capillary. The intense heat flux is directed outwards from the plasma bulk toward the capillary liner. The early stage of the direct deposition of the high heat flux on PFCs will cause a sudden ablation by the sublimation of the exposed surfaces. After this initial energy deposition, continuous incoming radiant heat flux results in a dense vapor layer that appears adjacent to the exposed surface. The vapor layer provides the PFCs with a self-shielding mechanism that essentially depends on the emissivity of the vapor formed from exposed surface material. This shielding effect results in the absorption of a fraction of the incoming radiant heat flux [3, 12]. Therefore, only a fraction of the incoming heat flux can penetrate the vapor layer and hit the solid wall. The heat flux is primarily from near black body spectrum photons

described by Stefan–Boltzmann law. Hence, the net radiant heat flux to the PFCs can be modeled by a fraction of the black body radiation emitted by the plasma at temperature T_P that incident on a material of vaporization temperature T_v, which is given by:

$$H_{rad} = f\varepsilon_b\left(T_p^4 - T_v^4\right) \tag{5.1}$$

where H_{rad} is the net radiant heat flux, f is the transmission factor which is the fraction at which the incident heat flux transmitted through the vapor layer, and ε is Stefan–Boltzmann constant. Although significantly reduced by the evolving vapor layer, the net heat flux reaching the exposed surfaces can diffuse into the metallic solid surface and raise its temperature to the melting point, which in turn forms a melt layer on the top of the PFC. As shown in Figures 5.2 and 5.3, in some ET shots where metallic materials were used, droplets from splattered melt layer were ejected and observed at the test sample surfaces [5].

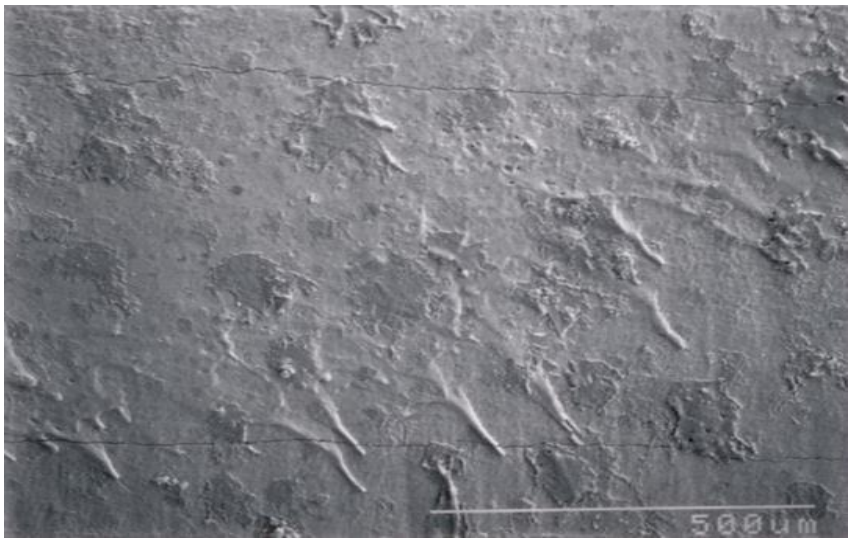

Figure 5.2: Photograph of tungsten surface after a 4 kJ ET discharge showing the runoff of melt layer.

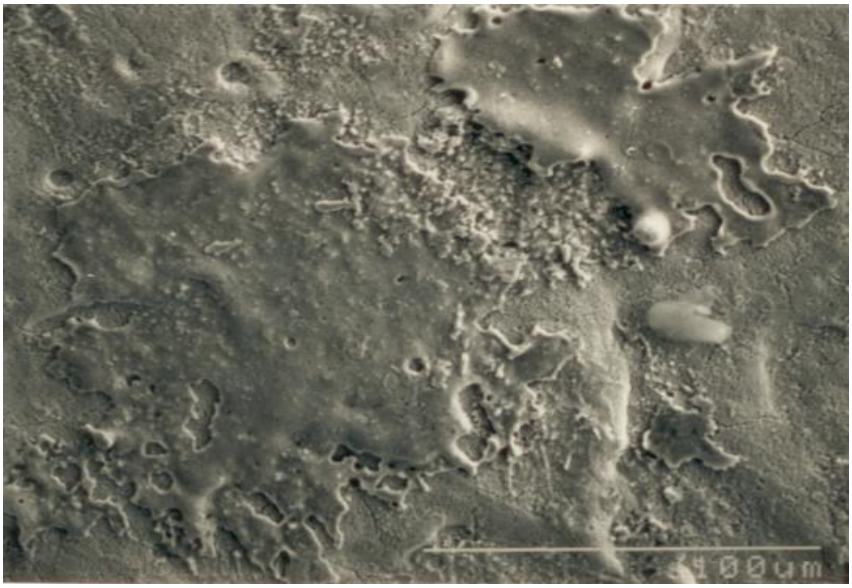

Figure 5.3: Photograph of tungsten surface after a 4 kJ ET discharge showing the evidence of melt layer re-solidified on the surface.

The melt layer can exist during a simulated disruption experiment as shown in Figures 5.2 and 5.3; however, direct sublimation may take place at higher discharge energies, and surface ablation may be eminent. Figures 5.4 (molybdenum) and 5.5 (steel) illustrate the ablative surfaces on which direct evaporation took place without melting.

Figure 5.4: Photograph of molybdenum surface after a 6 kJ ET discharge showing surface ablation due to direct sublimation.

Figure 5.5: Photograph of steel surface after a 6 kJ ET discharge showing surface ablation due to direct sublimation.

Although both vapor and melt layers may exist on the metallic PFCs' boundary, one is likely thicker than the other, depending on the duration of the exposure to the high heat flux. Theoretical studies show that the longer the disruption time, the deeper the net heat flux penetrates into the solid surface, which results in a thicker melt layer [5, 12].

With the existence of a melt layer, the heat flux equation must be modified to account for conduction, melting, evaporation and radiation [21] and can be expressed as:

$$H_{rad} = -k(T_v)\frac{\partial T}{\partial r} + \rho(T_v)\, L_v\, v(T_v) + f\varepsilon(T_P^4 - T_v^4) \qquad (5.2)$$

where k is the thermal conductivity of the melt layer, ρ is the material density, L_v is the material heat of evaporation, and $v(T_v)$ is the velocity of the receding surfaces. Heat flux equations for vaporization and melting cases, Eq. 5.1 and Eq. 5.2, have been implemented in the original version of the ETFLOW code, which is detailed in Reference 13 and Reference 20, to formulate the ETFLOW-BL code.

Based on the previously explained mechanism of melt layer loss that leads to melt layer droplet ejection and splashing, an erosion model due to melt layer splashing, based on the work of Hassanein et al [4, 12, 21], is implemented in ETFLOW-BL code. The code interface allows the user to run the simulation with or without melting and with or without splashing. However, the default erosion mechanism in all possible cases is the direct sublimation of the PFCs. This is a useful feature that allows one to compare different case studies on various PFCs' erosion mechanisms. Also, it allows the user to test the individual effect of each erosion mechanism and to combine all the mechanisms into an entire overview of PFC erosion.

To accurately estimate the melt layer loss due to splashing, it is essential to calculate the velocity of which splashing wave is moving v_s, which can be expressed as [2]:

$$v_s = \frac{H_{rad}}{(q_m + C_v T_v)} \tag{5.3}$$

where q_m is the material heat of fusion and C_v is the material specific heat. The splashing velocity is strongly material dependent, and it also depends on the magnitude of the incident heat flux. Based on Eq. 5.3, the melt-splatter eroded mass m_s can be estimated using the following expression:

$$m_s(t) = \frac{2\rho_v v_s \Delta t \Delta V}{r_p} \tag{5.4}$$

where r_p is the plasma radius. Knowing the splattered melt mass and the splattered melt volume allows estimation of the splattered melt depth (h_s). The calculation of h_s is based on the assumption that the intensity of the radiant heat flux is uniformly distributed over the exposed PFC surface.

The erosion rates due to both processes can be readily obtained from the temporal variation of the eroded depth. Based on this definition, the erosion rate can be written as:

$$R_{i=m,s,v} = \frac{dh_i}{dt} \tag{5.5}$$

where i stands for the different erosion processes: melting, vaporization, or splashing.

The ETFLOW-BL code has all the basic set of equations of ETFLOW, namely conservation of mass, momentum, energy and the plasma equations, equation of state, dissociation and ionization, Saha equation, ideal and nonideal plasma electrical conductivity models, and friction coefficients [13, 20]. Modifications include the effect of the vapor and

melt layers formation and splash-splattering model. The ETFLOW-BL code solves the set of equations self-consistently in a time dependent fashion which allows the user to monitor the erosion of the exposed surfaces as disruption time progress. Also, the code has been developed to predict the total eroded mass and erosion thickness at the end of the disruption cycle.

5.3 Results and Discussion

The ETFLOW-BL code has been developed to simulate plasma-material interaction within ET plasma sources. ET facilities are capable of generating plasma with high heat flux and power density that are relevant to those expected in ITER during disruption events [1, 5, 6]. The materials under study are tungsten, molybdenum and beryllium. The choice of such metallic PFCs was motivated by the current design of ITER [22-24]. For comparison purposes, a unified incident heat flux is considered to be a fast-rise pulse that peaks at around 30 μs over about 200 μs duration. Figure 5.6 illustrates the heat flux profile and the discharge current trace under specific experimental plasma discharge conditions taken from the PIPE ET plasma experiment. The charging potential provides about 4 kJ of discharge energy, which corresponds to a peak discharge current of about 30 kA over an average discharge period of 200 μs, delivering a peak heat flux of 38 GW/m^2. Based on this heat flux profile, the erosion calculations are evaluated by ETFLOW-BL code for different materials of interest.

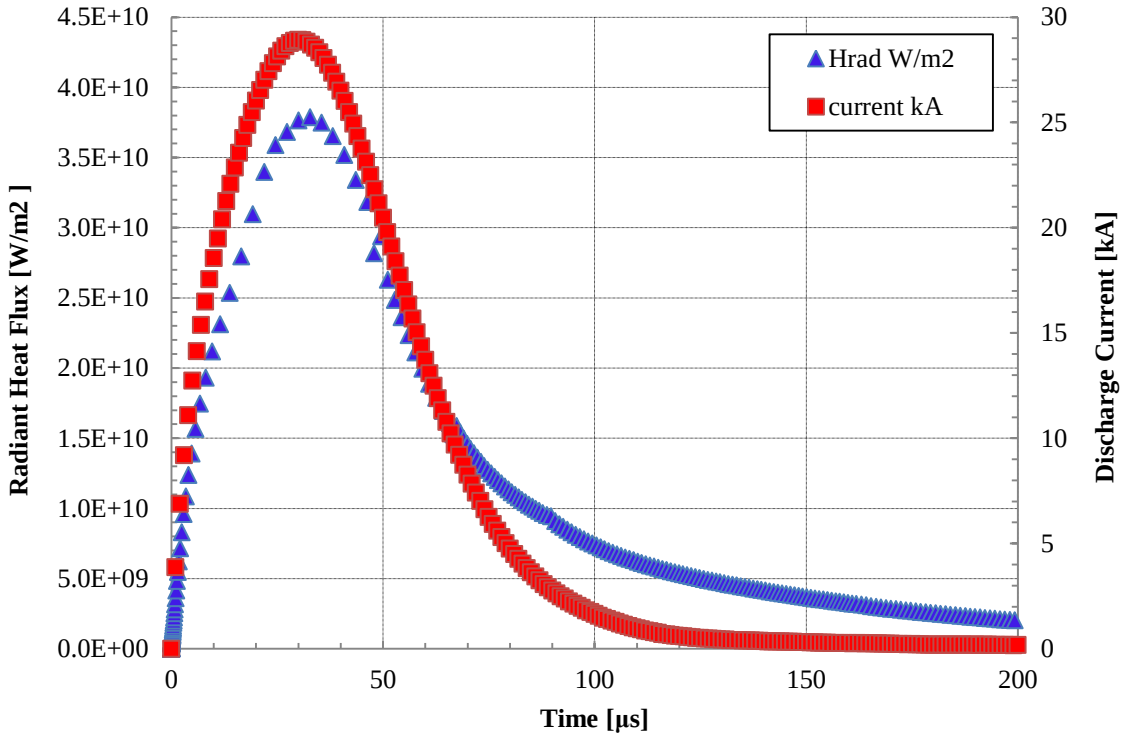

Figure 5.6: Heat flux and discharge current as a function of the discharge time.

Total mass loss for tungsten due to vaporization, melting, and splashing are shown in Figure 5.7. The total mass loss due to vaporization only emphasizes the shielding of the vapor layer as it achieves less total mass loss. In this study, for modeling purposes, the vaporized material is considered to be an optically thick layer that attenuates the incident photon radiation as it penetrates the vapor layer, and hence it minimizes the net total mass loss. From a previous study on the vapor shield effect of PFCs, it was found that up to 60% of the incident heat flux can be absorbed by the vaporized tungsten layer [6, 13].

In the case of melting where melt layer is stable and confined, and consequently no melt layer loss takes place, the melt layer may provide additional shielding that protects the exposed material. This explains the slight decrease of the total mass loss compared to the individual shielding effect of the vapor layer. If part of the melt layer were splattered due to the possible multiple forces and instabilities, then the total mass loss increases due to the removal of liquid droplets.

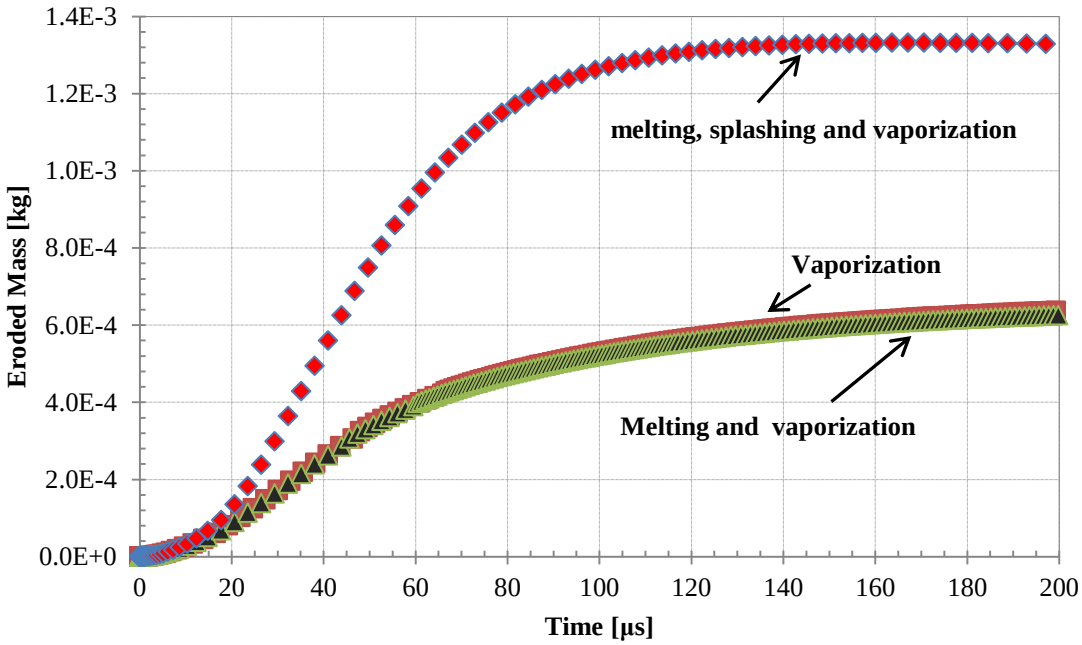

Figure 5.7: Total eroded mass of tungsten.

The erosion of tungsten as a function of the incident heat flux is illustrated in Figure 5.8 which shows the total eroded mass with and without consideration of splattering/splashing. With the effect of splattering/splashing, the erosion increases by a factor of 2.5 at the highest heat flux and a factor of 2.0 at the lowest, indicating an increased erosion effect at higher heat fluxes. While it appears that the erosion increases linearly with

increased heat flux; however, a power law has a better fit to the data according to studies on scaling laws [25, 26].

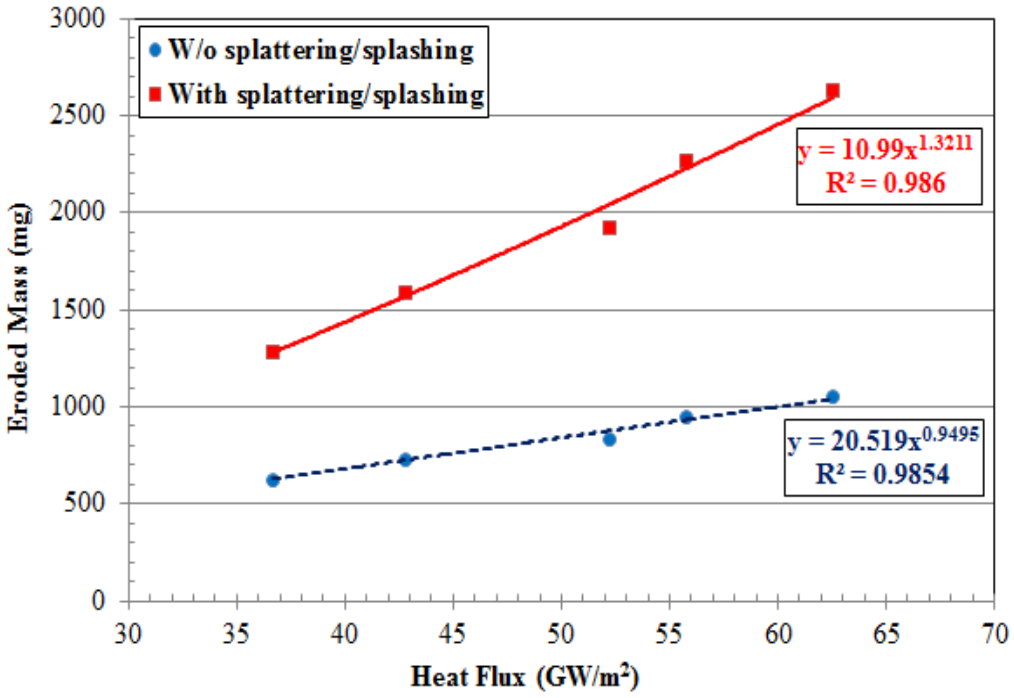

Figure 5.8: Erosion of tungsten with and without splattering/splashing as a function of the incident heat flux.

The effect of splattering/splashing, which is material and heat flux dependent, can be seen from the splashing/splattering velocity as a function of time (as shown in Figure 5.9) for the 4 kJ discharge with 38 GW/m2 heat flux. The splashing/splattering velocity peaks in 10 μs with 26.44 m/s as the highest velocity for tungsten, 24.09 m/s for molybdenum and 19.32 m/s for beryllium.

Figures 5.10 and 5.11 show the erosion rates caused by vaporization and melt layer splashing/splattering, respectively. For early disruption time, erosion rate increases as the incident heat flux increases up to its maximum value of 38 GW/m2 then decreases for the rest of the disruption time; both erosion rates decrease as the deposited power density decrease.

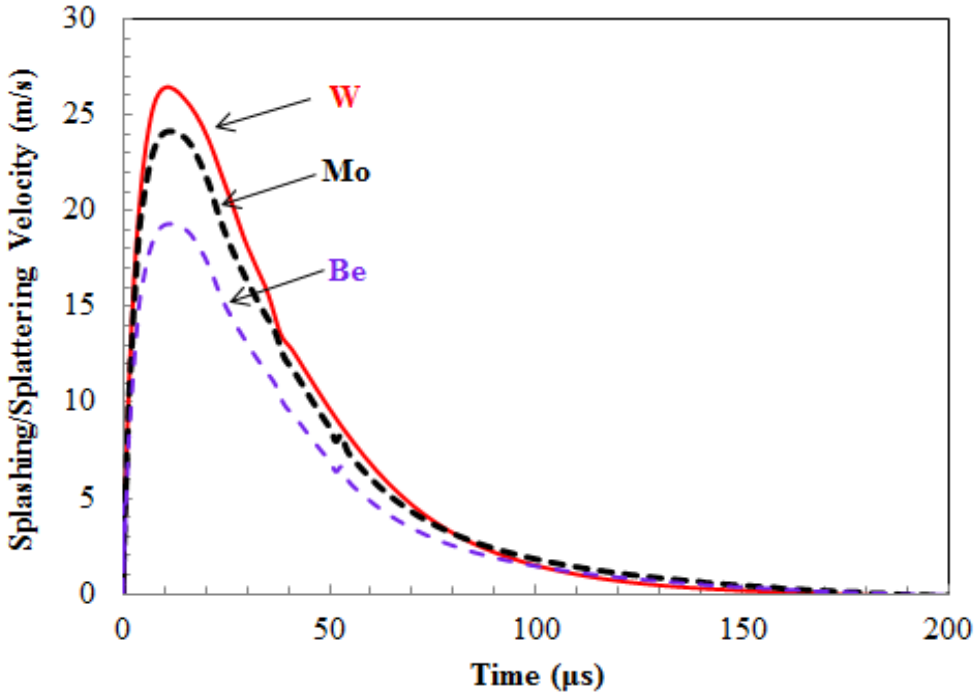

Figure 5.9: Splashing/splattering velocity of tungsten, molybdenum and beryllium as a function of time.

Also, as shown in Figure 5.10, tungsten exhibits a relatively higher vaporization rate of about 7 mg/μs at the peak heat flux. For beryllium, the ablation rate has much lower values compared to tungsten and molybdenum.

Figure 5.11 clearly shows the differences in the melting rates of the materials under investigation. The erosion rate due to melting has strong dependence on splashing/splattering velocity and the melting threshold of the exposed materials. Because of these factors, the tungsten erosion rate due to melt layer loss is the highest among the tested PFCs. The erosion rate due to vaporization and melt layer loss for beryllium is less than those of heavier metals like tungsten and molybdenum.

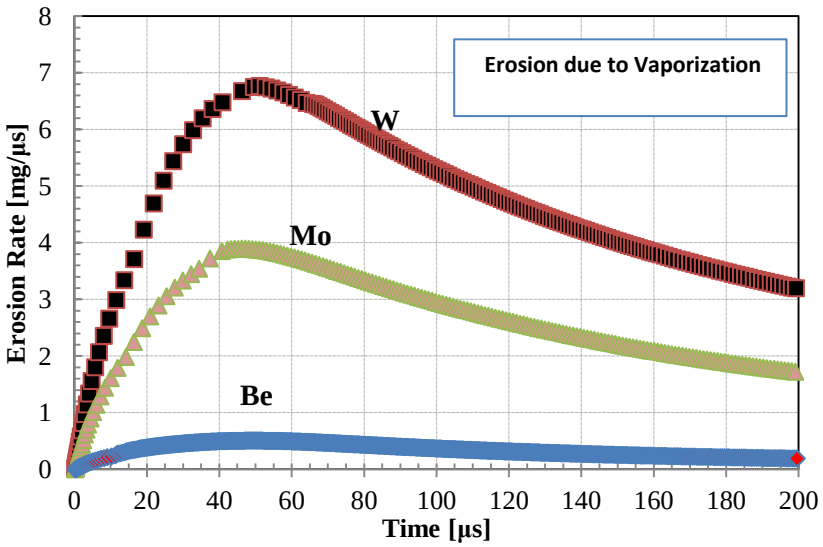

Figure 5.10: Erosion rate due to vaporization only.

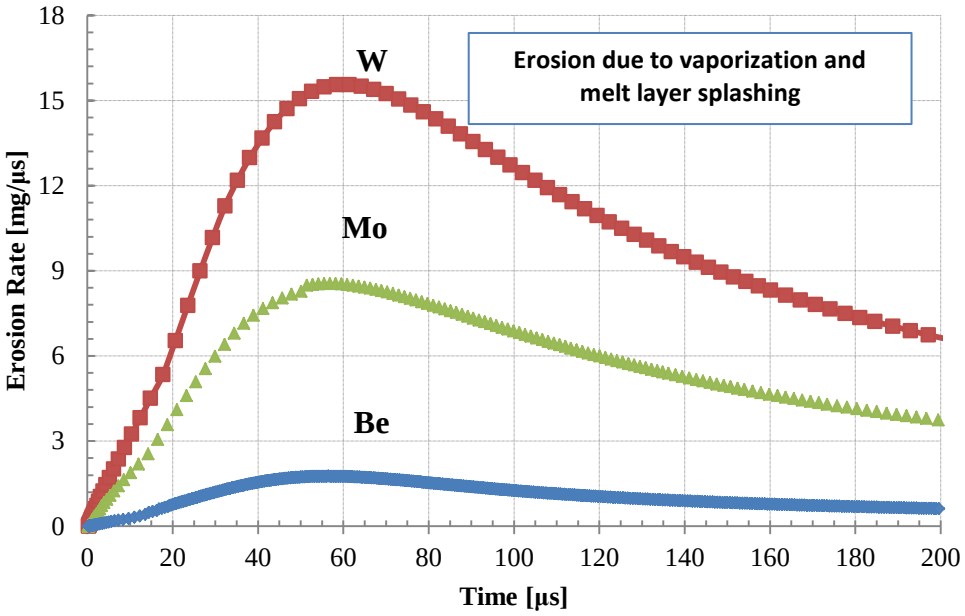

Figure 5.11: Erosion rate due to vaporization and melt layer splashing.

Based on the disruption simulation with the aforementioned conditions, the eroded thickness is estimated for each case: vaporization with or without melting and with or without splashing; and the total eroded thickness for the selected PFCs are reported in Table 5.1, with vaporization included in all cases.

Table 5.1: Erosion parameters for a 750 J/cm^2 plasma disruption.

Material	Melting	Splashing	Total eroded mass (mg)	Total eroded thickness (μm)
W	no	No	58.188	24.066
W	yes	No	57.079	23.608
W	yes	Yes	115.763	47.879
Mo	no	No	30.920	23.947
Mo	yes	no	30.335	23.494
Mo	yes	yes	65.407	50.657
Be	no	no	3.345	14.414
Be	yes	no	3.198	13.780
Be	yes	yes	10.845	46.725

The comparison between the total eroded mass and total eroded thickness for a specific material highlights a noteworthy fact. The high eroded mass of heavy metals such as tungsten and molybdenum are caused by their high specific density and does not necessarily convert into high erosion thickness. Hence, under the same disruption conditions, tungsten and molybdenum show less eroded thickness as compared to their own high eroded mass.

The set of experiments previously conducted on the NC State University ET facility on pure arc cast molybdenum have shown an eroded thickness of 1.0077 μm/GW.m^{-2} for an incident heat flux of 33 GW.m^{-2}; hence, the erosion thickness is 33.254 μm, while for pure sintered molybdenum, the erosion was 0.9502 μm/GW.m^{-2}, which translates to 31.36 μm [27]. These experimental results are higher than the code results of about 23-24 μm without considering splashing. However, they are less than the splashing results from the code. This may be attributed to the precision in measuring the mass difference of the samples, as well as resolidification effect, which is not considered in the code. It is also noted that previous

experiments on various metallic surfaces have shown resolidification on tungsten such that its net erosion appeared to be negligible [3, 5, 27]. However, the erosion rate of tungsten in another set of experiments was 0.91μm/GW.m^{-2}, which translates to 29.7μm [28]. This experimental result is comparable to the calculated values of about 24μm with inclusion of melting but less than the values if splashing would be included. This is due to the code does not take into account the possible resolidification of the molten material.

5.4 Conclusion

Plasma facing components suffer from high heat fluxes during hard disruptions and thermal quenching. Assessment based solely on surface vaporization indicates less erosion when compared to inclusion of melting and splashing and splattering. Inclusion of melting and splashing has shown a factor of 2 higher erosion rates (mg/μs) for tungsten and molybdenum, and a factor of about 3.5 for beryllium.

It is concluded that the addition of melting to vaporization does not result in much change in the total erosion; for example, tungsten ablation due to only vaporization is 58.188 mg and drops to 57.079 mg with melting included. However, splashing increases total erosion to 115.763 mg, which is almost a factor of 2 higher than vaporization only or vaporization and melting. For beryllium, it is 3.345 mg for only vaporization, 3.198 mg with melting, but it is 10.845 mg with splashing, which is almost a factor of 3.5 higher than vaporization or vaporization with melting. Splashing forces the melt layer to splatter which results in much removal from the surface.

5.4 References

[1] J. G. Gilligan and M. A. Bourham, "The use of an electrothermal plasma gun to simulate the extremely high heat flux conditions of a tokamak disruption", Journal of Fusion Energy, vol. 12(3), pp.311-316, 1993.

[2] A. Hassanein, A. Konkashbaev, and I. Konkashbaev, "Erosion of melt layers developed during a plasma disruption," Proc. 18th Symposium on Fusion Technology, August 22-26, 1994, Karlsruhe, Germany, vol.1, p. 223, 1994.

[3] J. G. Gilligan, M. A. Bourham and W. C. Tucker, "Effect of disruption on plasma-facing components", Proc. 16th IEEE/NPS Symposium on Fusion Energy, SOFE'95, Champaign, IL, 30 Sep-5 Oct 1995, vol.1, pp.424-429, 1995.

[4] A. Hassanein , V. Belan, I. Konkashbaev, L. Nikandrov, V. Safronov, A. Zhitlukhin, and V. Litunovsky, "Modeling and simulation of melt-layer erosion during a plasma disruption," Journal of Nuclear Materials, vol. 241-243, pp. 288-293, 1997.

[5] G. E. Dale and M. A. Bourham, "Melt layer erosion and resolidification of metallic plasma facing components", Proc. 17th IEEE/NPSS Symposium on Fusion Engineering (SOFE'97), vol. 2, pp. 892-895, 1997.

[6] J. R. Echols and A. L. Winfrey, "Ablation of fusion materials exposed to high heat flux in an electrothermal plasma discharge as a simulation for hard disruption", Journal of Fusion Energy, vol. 33(1), pp. 60-67, 2013.

[7] G. Janeschitz, K. Borrass, G. Federici, Y. Igitkhanov, A. Kukushkin, H. D. Pacher, G. W. Pacher, and M. Sugihara, "The ITER divertor concept", Journal of Nuclear Materials, vol. 220-222, pp, 73-88, 1995.

[8] M. Roedig, W. Kuehnlein, J. Linke, M. Merola, E. Rigal, B. Schedler, and E. Visca, "Investigation of tungsten alloys as plasma facing materials for the ITER divertor", Fusion Engineering and Design, vol.61-62, pp. 135-140, 2002.

[9] G. Federici, P. Andrew, P. Barabaschi, J. Brooks, R. Doerner, A. Geier, A. Herrmann, G. Janeschitz, K. Krieger, A. Kukushkin, A. Loarte, R. Neu, G. Saibene, M. Shimada, G. Strohmayer, and M. Sugihara, "Key ITER plasma edge and plasma–material interaction issues", Journal of Nuclear Materials, vol. 313-316, pp, 11-22, 2003.

[10] J. Roth et al., "Recent analysis of key plasma wall interactions issues for ITER", Journal of Nuclear Materials, vol. 390-391, pp, 1-9, 2009.

[11] J. T. Bradley, J. M. Gahl and P. D. Rockett, “Diagnostics and analysis of incident and vapor shield plasma in PALADIS I, a coaxial deflagration gun for tokamak disruption simulation”, IEEE Transactions of Plasma Science, vol. 27(4), pp. 1105-1114, 1999.

[12] A. Hassanein, “Prediction of material erosion and lifetime during major plasma instabilities in tokamak devices,” Fusion Engineering and Design, vol. 60, pp. 527–546, 2002.

[13] N. AlMousa, L. Winfrey, J. Gilligan, and M. Bourham, “Radiative heat transport through vapor plasma for fusion heat flux studies and electrothermal plasma sources applications”, Journal of Nuclear Energy Science & Power Generation Technology, 3:1 (2014) 1000116.

[14] G. Miloshevsky and A. Hassanein, “Stability and erosion of melt layers developed on plasma facing components of tokamaks,” Nuclear Fusion, vol. 54 , 8pp., 2014.

[15] M. Seki, S. Yamazaki, A. Minato, T. Horie, Y. Tanaka, and T. Tone, “A simulated plasma disruption experiment using an electron beam as a heat source Journal of Fusion Energy, vol. 5, pp. 181–189, 1986.

[16] M. Roedig, W. Kuehnlein, J. Linke, M. Merola, E. Rigal, B. Schedler and E. Visca, “Investigation of tungsten alloys as plasma facing materials for ITER divertor”, Fusion Engineering and Design, vol. 61-62, pp. 135-140, 2002.

[17] G. Federici, A. Loarte and G. Strohmayer, “Assessmwent of erosion of the ITER divertor targets during type I ELMs”, Plasma Physics and Controlled Fusion, vol.45(9), p.1523, 2003.

[18] R. B. Mohamti, J. G. Gilligan and M. A. Bourham, “Edge exposure of poloidal divertor target plate tiles”, Fusion Science And Technology, vol. 30(3P1), pp. 2789-299, 1996.

[19] J. P. Sharpe, B. J. Merrill, D. A. Petti, M. A. Bourham and J. G. Gilligan, “Modeling of particulate production in the SIRENS plasma disruption simulator”, Journal of Nuclear Materials, vol/ 2990, pp. 1128-1133, 2001.

[20] L. Winfrey, M. Abd Al-Halim, J Gilligan, A. Saveliev, and M. Bourham, “A study of plasma parameters in a capillary discharge with calculations using ideal and nonideal plasma models for comparison with experiment,” IEEE Transactions of Plasma Science, vol. 40(3), pp.843-852, 2012.

[21] A. M. Hassanein, “Simulation of plasma disruption induced melting and vaporization by ion or electron beam,” Journal of Nuclear Materials, vol. 122 and 123, pp. 1453-1458, 1984.

[22] A. R. Raffray, G. Federici, V. Barabash, H. D. Bacher, H. W. Bartels, A. Cardella, R. Jakeman, K. Ioki, G. Janeschitz, R. Parker, R. Tivey and C. H. Wu, "Beryllium application in ITER plasma facing components", Fusion Engineering and Design, vol. 37(2), pp. 261-286, 1997.

[23] V. Barabash, G. Federici, R. Matera, A. R. Raffray and ITER Home Team, "Armour materials for the ITER plasma facing components", Physics Scripta, vol. T81, pp.74-83, 1999.

[24] ITER Divertor, https://www.iter.org/mach/divertor

[25] P.P. Vergara, "Development of scaling laws for electrothermal plasma sources with geometry variables", M.S. thesis, Dept. Nuclear Engineering, North Carolina State University, Raleigh, March 2013.

[26] M. A. Abd Al-Halim and M.A. Bourham, "Characterization of short intense pulsed electrothermal plasma capillaries for use as fusion and launchers heat flux sources", Journal of Fusion Energy, vol.33, pp.258-263, 2014.

[27] M.A. Bourham, O.E. Hankins, J.G. Gilligan, J.D. Hurley and J.R. Earnhart, "Comparative study of component erosion for electromagnetic and electrothermal launchers", IEEE Transactions on Magnetics, vol. 29(1), pp.1107-1112, 1993.

[28] M.A. Bourham, J.G. Gilligan, M.L. Huebschman, D. Lianos and P.D. Aalto, "Review of components erosion in electric launchers technology", IEEE Transactions on Magnetics, vol. 31, pp.678-683, 1995.

CHAPTER 6

CONCLUSIONS AND FUTURE WORK

An electrothermal (ET) plasma code was developed to simulate the formation and flow of plasma in the NC State University ET plasma facilities PIPE and SIRENS and evaluation of the effect of the boundary layer at the plasma-material interface. The developed models take into account the mechanisms by which the material evolved from the exposed surfaces by melting, melt layer splashing, and evaporation or direct sublimation. The shielding effects associated with the aforementioned erosion mechanisms are melt layer and vapor shielding.

The effect of the boundary vapor layer at the plasma-wall interface in an ET capillary discharge with discharge arc current between 9.4 to 42.8 kA using Lexan polycarbonate as the ablating liner material has been investigated using the ETFLOW code in comparison with experimental results of ablated mass from the PIPE experiment. The ablated mass shows that the energy transmission factor is within 0.4 to 0.8 for higher values of the peak discharge currents above 40 kA, indicating efficient absorption of the incident heat flux into the plasma vapor boundary layer. The dependence of the ablated mass, the plasma pressure, temperature, velocity and radiant heat flux on the variation in the energy transmission factor has been analyzed using various PIPE experimental shots to determine the effectiveness of the vapor shield on these parameters. It has been found that there is a reduction in the plasma temperature and plasma bulk velocity with the increase in the energy transmission factor,

while the radiant heat flux and the exit pressure increase as the energy transmission factor increases.

New vapor shield models have been developed and implemented in the ETFLOW code. The new code, ETFLOWVS, calculates the transmission factor using either the "Opacity" model or the "Ratio" model at each time step and mesh point to predict the plasma parameters at the capillary exit and the mass ablated from the capillary inner wall. The inclusion of the vapor shield modeling produces less deviation from the measured ablated mass as compared to earlier calculations. However, the plasma bulk has higher exit velocities by including the vapor shield effect. The calculation done by using the opacity model has shown that the energy transmission factor through the vapor shield for Lexan polycarbonate material varies with the peak discharge current. The calculations done by using the ratio model suggested that the optical thickness of the vapor shield varies with the incident radiant heat flux. Code results for Lexan polycarbonate indicate a transmission factor of 0.65 to 0.56 for the discharge current range between 15 and 45 kA, which confirms a reduction in the energy reaching the surface as the initial energy deposition from the plasma core increases. This self-protecting mechanism is an essential mechanism for reducing surface erosion from incoming high heat flux.

Because of the difficulties of performing an experimental test on a fusion test reactor, a computational evaluation of plasma facing materials was conducted using the ETFLOWVS code. Simulation was conducted considering a power density of 55 GW/m^2 as the radiant high heat flux incident on the material surface for a disruption time of 180 μsec. Five materials are considered as PFM; beryllium, carbon, boron carbide, molybdenum and

tungsten. The erosion of all PFMs is almost linear with time for $\tau<70\mu s$. After this time, the eroded material seems sufficient to form a vapor layer, which can effectively shield the PCMs' surface from further erosion. Calculations of ablation rate of PFM were carried out to identify the tolerable ablated mass of the exposed PFC surfaces. High-Z materials suffer higher ablation rates compared to low-Z materials. However, the erosion in units of material thickness indicates that the erosion thickness of the highest-Z material (tungsten) is less than that of the lowest Z-material (beryllium).

A melt and splattering/splashing model was developed and implemented in the ETFLOW-BL code to include the effect of melting and splashing on the erosion of plasma facing materials. Inclusion of melting and splashing has shown about a factor of 2 higher erosion rates (mg/μs) for tungsten and molybdenum and a factor of higher than 3 for beryllium. It is concluded that the addition of melting to vaporization does not result in much change in the total erosion; for example, tungsten ablation due to only vaporization is 58.188 mg and drops to 57.079 mg with melting included; however, splashing increases total erosion to 115.763 mg, almost a factor of 2 higher than vaporization only or vaporization and melting. For beryllium, it is 3.345mg for only vaporization and 3.198 mg with melting, but it is 10.845 mg with splashing, which is almost a factor of 3 higher than vaporization or vaporization with melting. Splashing forces melt layer to splatter which results in much removal from the surface. The set of experiments previously conducted on the NC State University ET facility on pure arc cast molybdenum have shown an eroded thickness of $1.0077\mu m/GW.m^{-2}$ for an incident heat flux of 33 $GW.m^{-2}$; hence the erosion thickness is 33.254μm. However, for pure sintered molybdenum, the erosion was $0.9502\mu m/GW.m^{-2}$,

which translates to 31.36μm. These experimental results are higher than the code results of about 23-24μm without considering splashing. However, they are less than the splashing results from the code. This may be attributed to the precision in measuring the mass difference of the samples or the re-solidification effect, which is not considered in the code. It is also noted that previous experiments on various metallic surfaces have shown re-solidification on tungsten such that its net erosion appeared to be negligible. However, the erosion rate of tungsten in another set of experiments was 0.91μm/GW.m^{-2}, which translates to 29.7μm. This experimental result is comparable to the calculated code values of about 24μm with the inclusion of melting but less than the values if splashing would be included, which may be attributed to resolidification of the molten material.

Several important items are suggested for future work, among which is the consideration of the radial effects in the code and the inclusion of heat conduction. On the other side, axial radiation transport is expected to reduce the net radiant heat flux at the eroded surface as lateral radiation escapes out of the boundary layer. Additionally, an inclusion of a magnetic field on the ET source would result in additional magnetization of the vapor cloud and may enhance the effectiveness of the vapor shield. The modeling of the higher range of radiant heat flux attenuation through the optically thick boundary layer necessitate more in-depth investigation of the plasma optical characteristics and the use of multi-group opacities rather than an averaged single group to improve the accuracy of the model.

Another important modification would be to consider the resolidification with respect to the angle of heat flux deposition on metallic PFMs, which is an important factor when modeling the PFMs erosion under simulated disruption like conditions. Although melt-layer splashing is experimentally demonstrated to be the main melt-layer splashing mechanism, the evolution of hydrodynamic instabilities within the melt layer may eject more liquid droplets and increase the melt layer loss and should be taken into consideration. However, detailed measurements and spectroscopy of radiant heat flux under reactor disruption-relevant conditions are recommended to conduct more realistic simulation of erosion behavior of PFMs in nuclear fusion reactor environment.